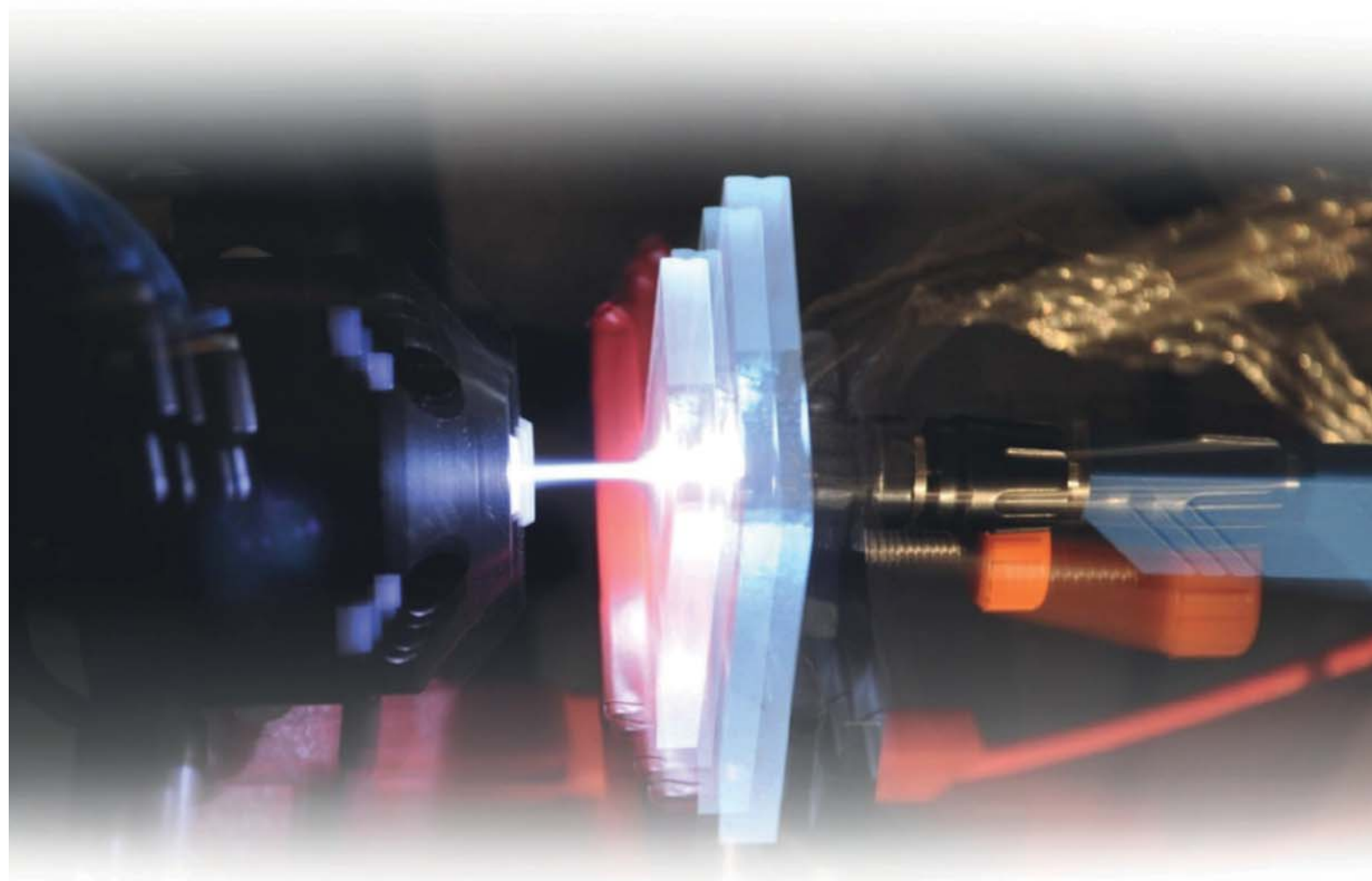


Christoph Gerhard

Atmospheric Pressure Plasma-Assisted Laser Ablation of Optical Glasses

Atmosphärendruckplasma-unterstützte
Laserablation optischer Gläser



Cuvillier Verlag Göttingen
Internationaler wissenschaftlicher Fachverlag



Atmospheric Pressure Plasma-Assisted Laser Ablation of Optical Glasses





Atmospheric Pressure Plasma-Assisted Laser Ablation of Optical Glasses

Dissertation

to be awarded the degree

Doctor rerum naturalium (Dr. rer. nat.)

submitted by

Christoph Gerhard
from Lich

approved by the Faculty of Natural and Materials Science,
Clausthal University of Technology

Date of oral examination:
7th of August 2014



Bibliografische Information der Deutschen Nationalbibliothek

Die Deutsche Nationalbibliothek verzeichnet diese Publikation in der Deutschen Nationalbibliografie; detaillierte bibliografische Daten sind im Internet über <http://dnb.d-nb.de> abrufbar.

1. Aufl. - Göttingen : Cuvillier, 2014
Zugl.: (TU) Clausthal, Univ., Diss., 2014

Chairperson of the Board of Examiners
Prof. Dr. Winfried Daum

Chief Reviewer:
apl. Prof. Dr. Wolfgang Maus-Friedrichs

Reviewer:
Prof. apl. Prof. Dr. Wolfgang Viöl

Dissertation Clausthal 2014
D 104

© CUVILLIER VERLAG, Göttingen 2014
Nonnenstieg 8, 37075 Göttingen
Telefon: 0551-54724-0
Telefax: 0551-54724-21
www.cuvillier.de

Alle Rechte vorbehalten. Ohne ausdrückliche Genehmigung des Verlages ist es nicht gestattet, das Buch oder Teile daraus auf fotomechanischem Weg (Fotokopie, Mikrokopie) zu vervielfältigen.

1. Auflage, 2014

Gedruckt auf umweltfreundlichem, säurefreiem Papier aus nachhaltiger Forstwirtschaft.

ISBN 978-3-95404-826-7
eISBN 978-3-7369-4826-6



There is good reason to believe that the impact of photonics in the 21st century will be as significant as electronics was in the 20th, or steam in the 19th.

David J. Sainsbury
13th of July 2006





Foreword

This work represents a cumulative dissertation and includes several recently published research articles originating from the author's doctoral project. For purposes of a consistent embodiment and a consecutive classification, the reference citation style, the figure and table captions as well as the equation numberings were adapted to the format of the entire document. The references cited in the particular articles are integrated in a collective reference section.





Abstract

Atmospheric Pressure Plasma-Assisted Laser Ablation of Optical Glasses

In the present work, two different approaches for atmospheric pressure plasma-assisted ablation of optical glasses were investigated. For sequential plasma-assisted ablation, the glasses were plasma pre-treated prior to laser ablation. Here, a hydrogenous process gas was applied in order to initiate a plasma-chemical surface modification. It was shown that relevant optical properties and in particular the transmission characteristics of the investigated glasses were modified as a result of such pre-treatment. Several underlying mechanisms were determined: (i) the formation of suboxide layers close to the glass surface, (ii) the implantation of hydrogen into deeper regions of the glass bulk material and (iii) surface roughening due to the plasma pre-treatment. As a result, an enhanced coupling of incoming laser irradiation during subsequent ablation was achieved. This effect allowed a significant reduction of the laser ablation threshold as well as an improved machining quality, i.e. a higher contour accuracy and a reduced surface roughness of the ablated area. For simultaneous plasma-assisted ablation, the laser beam was guided coaxially to an argon plasma beam in order to benefit from plasma-physical interactions. Due to an additional energy transfer by the plasma during ablation, the ablation rate was notably increased. It was further shown that the plasma beam used for this simultaneous process effects the smoothing of rough optical glass surfaces. The combination of the investigated approaches thus allows providing a novel integrated plasma-assisted ablation process for the micro structuring of optical devices of high quality.

keywords:

atmospheric pressure plasmas, optical glasses, hybrid laser ablation





Kurzzusammenfassung

Atmosphärendruckplasma-unterstützte Laserablation optischer Gläser

In der vorliegenden Arbeit wurden zwei unterschiedliche Ansätze zur Atmosphärendruckplasma-unterstützten Laserablation optischer Gläser untersucht. Zur sequentiellen plasmaunterstützten Ablation wurden die Gläser vor der Laserablation plasmabehandelt. Dabei kam ein wasserstoffhaltiges Prozessgas zum Einsatz, um eine plasmachemische Oberflächenmodifikation zu initiieren. Es wurde gezeigt, dass relevante optische Eigenschaften und insbesondere das Transmissionsverhalten der untersuchten Gläser durch eine solche Plasmavorbehandlung modifiziert wurden. Mehrere dem zugrunde liegende Wirkmechanismen wurden bestimmt: (i) die Bildung von Suboxidschichten nahe der Glasoberfläche, (ii) die Implantation von Wasserstoff in tiefere Bereiche des Volumensmaterials des Glases und (iii) eine Oberflächenrauung durch die Plasmavorbehandlung. Als Folge davon konnte eine verbesserte Einkopplung einfallender Laserstrahlung während der anschließenden Laserablation erreicht werden. Dieser Effekt ermöglichte sowohl eine signifikante Verringerung der Laserablationsschwelle als auch eine Verbesserung der Bearbeitungsqualität, d.h. eine erhöhte Formtreue und eine Verringerung der Oberflächenrauheit der ablatierten Fläche. Zur simultanen plasmaunterstützten Ablation wurde der Laserstrahl coaxial zu einem Argonplasmastrahl geführt, um plasmaphysikalische Einwirkungen auszunutzen. Als Folge eines zusätzlichen Energieeintrags durch das Plasma während des Ablationsprozesses wurde die Ablationsrate beträchtlich gesteigert. Es wurde zudem gezeigt, dass der für diesen simultanen Prozess verwendete Plasmastrahl eine Glättung rauer optischer Glasoberflächen ermöglicht. Die Kombination der untersuchten Ansätze erlaubt somit die Bereitstellung eines neuartigen geschlossenen plasmaunterstützten Ablationsprozesses zur Mikrostrukturierung hochqualitativer optischer Komponenten.

Schlagworte:

Atmosphärendruckplasmen, optische Gläser, Hybrid-Laserablation





Contents

1 Introduction and Motivation.....	001
2 State of the Art and Research.....	003
2.1 Interactions of atmospheric pressure plasmas with glasses.....	003
2.2 Interactions of laser irradiation with glasses.....	009
3 Experimental Setups, Materials and Methods.....	017
3.1 Experimental setup for sequential plasma-assisted ablation.....	017
3.2 Experimental setup for simultaneous plasma-assisted ablation.....	018
3.3 Investigated glasses.....	019
3.4 Measurement methods.....	022
3.4.1 Microscopic measurement methods.....	022
3.4.2 Spectroscopic measurement methods.....	023
4 Plasma Treatment of Optical Glasses.....	025
4.1 Plasma pre-treatment for sequential ablation.....	025
4.2 Plasma treatment during simultaneous ablation.....	045
5 Sequential Plasma-Assisted Laser Ablation.....	057
6 Simultaneous Plasma-Assisted Laser Ablation.....	083
7 Discussion.....	093
8 Summary and Outlook.....	097
References.....	101
Table of Symbols and Abbreviations.....	111
Acknowledgements.....	115
Appendix.....	117
A - Curriculum Vitae of the Author.....	117
B - Statutory Declarations (<i>Eidesstattliche Erklärungen</i>).....	118





Introduction and Motivation

Nowadays, optical micro components and systems represent key devices for a number of daily-used convenience goods and apparatuses such as multimedia terminals, safety devices and medical equipment. For instance, micro lenses and optical systems are required for fibre couplers in telecommunication applications, CD and DVD players, micro cameras for safety monitoring or park assistance assemblies as well as endoscopes and fibrescopes in medical engineering. Besides, such devices have outstanding relevance for research and industry and contribute to the development of novel techniques and processes. In this context, micro lens arrays for laser beam shaping by optical homogenisers or micro optical monitoring systems for industrial vision, logistics planning and traffic management shall be mentioned exemplarily amongst a number of micro-optical, optoelectronic and opto-mechanical components and systems.

In this context, fused silica has become one of the most important materials in modern optical technology. This medium stands out due to a number of advantageous properties such as a low coefficient of thermal expansion, a high chemical resistance, a low dispersion and a high transmission in the ultraviolet (UV) wavelength range. However, the use of further optical glasses with differing indices of refraction and dispersion characteristics becomes crucial for the realisation of optical systems with high image quality and colour fidelity. As an example, the combination of both crown and flint glasses allows the correction of chromatic aberrations. The simplest example for such a combined optical system is an achromatic lens where chromatic correction is realised for two selected wavelengths.

For structuring and patterning optical glasses with structures in the range of some microns to some tens of microns, different techniques such as lithography or reactive ion etching can be applied. However, referring to complexly-shaped required surface forms, laser micro structuring is the preferable method. Here, UV lasers are usually used in order to overcome the high transmission and to benefit from the short laser wavelength for the realisation of (sub)micro structures. However, such techniques are partially limited due to the high required fluence for initialising ablation. In order to increase the coupling of laser energy into the highly-transmittive glass surface, hybrid laser ablation methods can be used. Here, absorbing layers are applied to the surface. Such techniques thus allow a significant decrease in the laser ablation threshold. However, the use of chemicals as well as time-consuming final cleaning procedures can become necessary in order to remove residues of the particularly used absorbing substance. In addition, comparatively low ablation rates are obtained by some of the existing techniques, resulting in poor process efficiency.



Against this background, novel hybrid laser ablation techniques for machining optical glasses are presented in the present work. These hybrid techniques are based on atmospheric pressure plasmas, which were introduced to classic laser ablation processes. This combination was chosen due to the fact that atmospheric pressure plasma sources feature a high efficiency, stability and reliability. Depending on the used process gas, a number of technically usable plasma properties such as a certain defined chemical, physical and electrical activity can furthermore be generated. Two different strategies, sequential and simultaneous plasma-assisted ablation, were investigated. Regarding sequential plasma-assisted ablation, the glass surfaces are pre-treated by chemically reactive hydrogenous atmospheric pressure plasmas before laser ablation. Such pre-treatment allows a significant modification of the optical properties, giving rise to an increase in absorption. In contrast to existing hybrid ablation techniques, the absorbing layer is thus generated directly within the bulk material to be ablated. This effect is utilised in order to improve the energy coupling of incoming laser irradiation into the pre-treated glass surface. In addition to this sequential process, a simultaneous plasma-assisted ablation method, based on a chemically inert process gas, is presented and discussed. Here, the laser ablation process is assisted by plasma-physical interactions. With respect to pure laser ablation, both investigated hybrid techniques allow a significant improvement of laser machining results and a considerable saving of laser energy. Owing to the adaptivity of the used plasma sources, the presented plasma-assisted ablation methods can easily be adapted to almost any existing industrial laser source by flanging the particular plasma nozzle.

Enhanced laser-based structuring of optical glasses is of notable interest for manufacturers of optical components and systems, laser micro machining facilities and users of such systems. The aim of the present work is thus to provide a description of novel approaches as well as an understanding of the underlying mechanisms for highly-efficient and versatile laser ablation methods for micro structuring of transparent silicon dioxide-based optical media.



State of the Art and Research

In this chapter, basic interactions and mechanisms of both atmospheric pressure plasmas and laser irradiation with glasses are described. First, an overview on established and lab-scale methods for atmospheric pressure plasma-induced etching, cleaning and activation as well as the particularly underlying mechanisms and effects is given. Second, the principles of laser interaction with glassy bulk material, laser ablation and the influence of the laser pulse duration on the ablation process are introduced. Finally, the most common hybrid methods for laser ablation of transparent media are presented.

2.1 Interactions of atmospheric pressure plasmas with glasses

Atmospheric pressure plasmas (APP) have achieved significant importance in a number of different fields of application. As the main advantage, no cost-intensive vacuum chamber and equipment, which would limit the dimension of work pieces, are required. This enables the integration of APP into large-scale industrial processes such as hybrid APP-assisted welding or joining. Owing to the low gas temperature of dielectric barrier discharge (DBD) plasmas, temperature-sensitive materials such as plastic sheets and lumbers [ben04] can be processed by this special type of APP. It is also suitable for the treatment of human tissue [mar12] for medical applications such as wound healing, disinfection [emm13] and microbial decontamination [ehl11]. Due to a comparatively low effective depth of action of approximately some tens to hundreds of nanometres, plasma processes are generally near-surface impacting. Depending on the plasma parameters, i.e. for example the plasma power, the process gas and, as the case may be, precursors, a number of different surface effects can be realised. Besides surface reduction, activation by the plasma-induced formation of functional groups [kog04] and wrinkling, surface oxidation and passivation [dah12] shall be mentioned. Such effects can be used in order to increase the surface adhesion of different substrates such as polymers [bel12] and glasses [shu12].

Atmospheric pressure plasma etching of glasses

In a number of applications such as micro-structuring of semiconductors, scribing integrated electric circuits by mask projection techniques and correction of micro-optics, reactive ion etching (RIE) techniques [lee99, nus97] are well-established production methods. For this dry etching process, the particular work pieces are placed within a vacuum chamber and exposed to a high-energy ion beam. However, direct plasma etching of glasses and glassy materials can also be achieved at atmospheric pressure by the use of reactive process gases and gas mixtures. Such methods are usually referred to as reactive atomic plasma technology (RAPT[®]) and have recently gained in importance for precision machining applications such as etching of micro channels and structures or

space-resolved aspherisation and polishing of optically operative surfaces. In general, such techniques require the use of fluorochemical compounds (MF_x) as process gas as shown schematically in figure 2.1.

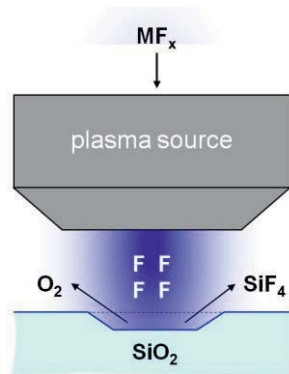


Fig. 2.1: Functional principle of reactive plasma etching

Here, etching is accomplished by chemical reactions of both fluorine (F) and silicon dioxide (SiO_2) to gaseous silicon tetrafluoride (SiF_4) and gaseous dioxygen (O_2) according to



In 1998, *Jeong et al.* reported on etching of fused silica using an atmospheric pressure plasma jet at room temperature (293 K). This rotation-symmetric jet source was driven by 13.56 MHz radio frequency (RF) at a power of 500 W. The used process gas was a mixture of helium (He [97%]), oxygen (O_2 , [1%]) and tetrafluoromethane, a.k.a. carbon tetrafluoride (CF_4 [2%]), where the helium flow rate was 51 litres/minute (slm). The distance between the plasma jet nozzle outlet and the fused silica samples was 5 mm. Using this configuration, fused silica was etched at an etch rate R_{etch} of 1.5 $\mu\text{m}/\text{minute}$ [jeo98].

Smoothing and precision correction of optical surfaces made of fused silica by an atmospheric pressure plasma jet source was introduced by *Schindler et al.* in 2005. Here, the plasma was microwave-excited with a microwave power of some hundreds of watts. In this case, reactive species were generated from the process gas, a composition of argon (Ar), sulfur hexafluoride (SF_6) and nitrogen (N_2). As a result, material removal was achieved by fluorine-induced reactions with fused silica and the formation of gaseous silicon tetrafluoride (SiF_4). Volume etch rates up to some 10 $\text{mm}^3/\text{minute}$ were obtained [sch05a].

Another etching process for fused silica applying an atmospheric-pressure pulsed remote plasma jet built up of two plane-plate electrodes was presented by *Iwasaki et al.* in 2006. The samples were placed 5 mm below the plasma jet nozzle outlet. As process gas, a mixture of Ar and CF_4 was used where the flow rates amounted to 0.24 slm for Ar and 0.06 slm in the case of CF_4 . Experiments were performed for different plasma pulse repetition rates f_{rep} in the range from 5 to 20 kHz. It was shown that the etch rate was strongly depending on the pulse frequency where higher pulse frequencies resulted in higher etch rates with a maximum value of approximately 130 nm/minute at



$f_{rep} = 20$ kHz. When adding O_2 to the process gas, this value was increased up to 400 nm/minute whereas the addition of water vapour (H_2O) resulted in an even higher etch rate of 8 $\mu\text{m}/\text{minute}$. Based on the characterisation of the plasma volume that was performed by the use of ion attachment mass spectrometry (IAMS), this water-induced significant increase in ablation rate was considered to be due to the generation of hydrogen fluoride (HF) from CF_4 and H_2O [iwa06].

The dependency of the etch rate on the process gas composition during atmospheric pressure plasma etching of fused silica was also observed by *Oh* et al. in 2010. Experiments were performed using a remote plasma jet source based on a DBD. Here, the electrode configuration was a multiple pin-to-plate setup, driven by a frequency of 20 to 40 kHz at a plasma power of 4 kW. The considerations were mainly focussed on the influence of the process gas mixture, consisting of nitrogen (N_2 [30 to 80 slm]) and nitrogen trifluoride (NF_3 [0.2 to 1 slm]), on the resulting etch rate. Further, the impact of different additives, i.e. helium (He), Ar and O_2 , each at a flow rate of 0.2 to 1 slm, was investigated. For this purpose, fused silica samples were placed on a motorised linear stage at a distance of 2 mm from the plasma source outlet. During the experiments, the sample traverse speed was 0.25 metres/minute. It was shown that the maximum etch rate was obtained for a medium flow rate of N_2 (60 slm) and a high NF_3 flow rate (1 slm) which was explained by the resulting high fluorine atomic density caused by the high plasma density within this given process gas composition. The addition of He and Ar effected a further increase in etch rate by an additional increase of the fluorine density as a consequence of *Penning* ionisation and dissociation processes¹. Further, the etching process was amplified for higher pulse repetition rates. The maximum etch rate was found to amount to approximately 323 nm/scan at a traverse speed of 0.25 metres/minute [oh10].

Apart from fused silica, plasma etching at atmospheric pressure can also be achieved in the case of other glasses. Etching of Ultra Low Expansion (ULE[®]) glass from Corning, Inc. by applying an inductively coupled plasma (ICP) jet at atmospheric pressure with an effective area of approx. 314 mm² was presented in 2006 by *Fanara* et al. The plasma source was run at powers ranging from 1250 to 1500 W. The process carrier gas was Ar, which was nourished by NF_3 (10 to 20%). Here, a volume etch rate up to 0.55 mm³/second was achieved. It was shown that the reactive gas concentration is rather of importance than the applied plasma power. Further, the etch rate is not influenced by thermo-chemical effects [fan06a].

A further interesting application of atmospheric pressure plasma sources in terms of the machining of glassy materials was presented by *Al-Shamma'a* et al. in 2002. Here, cutting of fibre glass mats with a thickness of 2 mm was achieved using an atmospheric microwave plasma jet. The microwave frequency was 2.45 GHz and the microwave power amounted to 3 kW. As process gas, Ar at a flow rate of 10 slm was applied. After cutting the samples at a traverse speed of 10 mm/second, no singeing of the cutting edges was observed [als02].

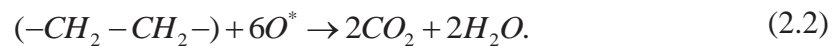
¹ Basically, *Penning* ionisation describes an ionisation process resulting from the interaction of excited atoms or molecules and neutral molecules and atoms [pen27].



Atmospheric pressure plasma etching is also applied for other silicon-based materials that are commonly used in the manufacture of optical components of high precision. As an example, figuring and polishing of silicon carbide (SiC) with atmospheric pressure plasma jets using a process gas mixture containing CF₄ was reported by *Wang et al.* in 2006 [wan06] and *Arnold and Böhm* in 2012 [arn12]. Such technique was also applied in order to polish optical components made of pure silicon (Si) as presented by *Zhang et al.* in 2008 [zha08a,zha08b].

Atmospheric pressure plasma cleaning of glasses

Atmospheric pressure plasma has a high potential for cleaning glass surfaces by the removal of organic contaminations, which are adsorbed due to common environmental conditions [lan18]. Here, the main contaminations are hydrocarbons (C_xH_y, where $x < y$). A number of different mechanisms can be utilised for plasma-induced cleaning since generally plasma provides radicals, ozone (O₃), negative and positive ions, free electrons and a certain amount of ultraviolet irradiation and thermal impact. As an example, hydrocarbons can be removed chemically when applying O₂ as plasma process gas. By the plasma discharge, O₂ is dissociated to excited, radical oxygen atoms (O^{*}) and subsequently reacting with surface-adherent hydrocarbons according to



Beyond chemical cleaning, physical cleaning can be achieved using inert process gases due to ion bombardment and electron sputtering. Such cleaning is of specific interest for medical and biological applications as for example for preparing object holders for microscopic analysis or for plasma-sterilisation of injection needles or surgery devices [che10].

The removal of carbonic contaminations from glass surfaces by atmospheric pressure plasma cleaning was presented by *Shun'ko and Belkin* in 2007. According to the experimental setup as described by the authors, the plasma source was a capacitively coupled DBD plasma jet, driven at 13.56 MHz radio frequency and a power of 300 W. As process gas, O₂ (2%) was admixed to the carrier gas, Ar (98%), where the gas flow velocity was approximately 6 m/s. By such treatment of glass substrates, which were placed about 10 mm below the plasma source nozzle outlet, efficient cleaning as confirmed by a rapid increase in the sample wettability by a factor of approximately 8 was achieved after a plasma treatment duration t_{plasma} of merely one second [shu07].

Comparable results were reported by *Iwasaki et al.* in 2008 applying a multiple nozzle jet atmospheric pressure plasma source based on a glow discharge. This plasma source was operated at a voltage of 10 kV and a frequency of 60 Hz. Using a gas mixture of Ar (99%) and O₂ (1%) at a flow rate of 15 slm, the contact angle on glass substrates was reduced from approximately 50° to approximately 8° after a plasma treatment duration of 23 ms [iwa08a]. This reduction in contact angle was stated to be due to the removal of organic contaminants from the sample surfaces. In further work, the authors confirmed this assumption by X-ray photoelectron spectroscopic (XPS) analysis of plasma cleaned glasses. For this purpose, plasma treatment was performed using a planar DBD jet, driven at a frequency of 40 kHz and a power of 300 W. As process gas, a



mixture of N_2 and O_2 was applied, where the particular flow rates were 40 slm (N_2) and 0-0.08 slm (O_2), respectively. The working distance from the plasma source outlet to the glass sample surface was 5 mm. The presented change in chemical composition of the sample surface as determined by XPS showed a high correlation with the measured contact angles, where a decrease in the percentage of carbon implicated a decrease in contact angle. Based on these findings, the authors showed that oxygen-based species such as ozone or radicals have a remarkably higher impact on the glass cleaning efficiency than nitrogen species [iwa08b]. The maximum cleaning efficiency was found for an O_2 admixture of 0.03% to the carrier gas, N_2 . Here, carbon was reduced by a factor of approximately 1.6; the contact angle was 8-times lower with respect to untreated glass.

In 2008, *Buček* et al. reported on atmospheric pressure plasma cleaning of glass using a diffuse coplanar surface barrier discharge (DCSBD) source. Here, a thin plasma sheet with a thickness of approximately 500 μm was ignited on the dielectric surface. Since the distance of the glass sample to the dielectric was 300 μm , the plasma was in direct contact with the investigated glass surface. Experiments were performed in a discharge power range from 300 to 525 W, applying ambient air, pure N_2 and pure O_2 as process gases. For all three gases, the contact angle was reduced by a factor of approximately 3.5 after a plasma treatment duration of five seconds. Successful cleaning was further confirmed by secondary ion mass spectroscopy (SIMS) and XPS, where a considerable decrease (max. 13-times) in characteristic peak intensities of relevant organic fragments was observed [buc08].

To summarise it can be stated that atmospheric pressure plasma methods are suitable for removing organic contaminations from glass surfaces. Depending on the applied plasma parameters, either hydrophilic or hydrophobic surfaces can be realised since plasma cleaning usually involves a change in contact angle and surface energy, respectively, as presented in more detail in the following sub-section. Plasma surface cleaning and an accompanying hydrophilisation have thus gained importance in the production of flat display-panels or coating processes of facade windowpanes. Atmospheric pressure plasma can moreover be applied in order to remove lacquer coats such as graffiti and acrylic resin from glass surfaces as for example in restoration [mai07] or urban renewal.

Atmospheric pressure plasma activation of glasses

In contrast to plasma-induced cleaning, the aim of plasma activation is a chemical modification of the treated surface. Besides chemical reduction and oxidation, attaching functional groups and/or molecular chains onto the surface by plasma polymerisation is a common application. As an example, oxygen plasmas are used for generating surface-adherent polymerised hydroxyl groups (-OH) or carboxyl groups (-COOH) in order to graft pharmaceuticals as reported by *Cheruthazhekatt* et al. in 2010 [che10]. Another widespread application of plasma activation is the modification in wettability [cer09]. As already discussed above, the contact angle of both a sample surface and test liquids is one of the most commonly-used indication value for successful cleaning. Since the contact angle is directly related to the surface energy and its polar and disperse fractions, respectively, it is also suitable for describing activation effects such as a change in surface polarity [hom13].



In 2004, *Yamamoto* et al. reported on atmospheric pressure plasma-induced hydrophilisation and hydrophobisation of sodium silicate glass where the intended application was to substitute windscreen wipers. As plasma source, a DBD reactor was used, driven at a voltage of 20 kV and a frequency of 60 Hz. Three process gasses, dry air, pure N₂, and He, were applied at different flow rates. The distance from the high-voltage electrode to the glass sample surface was kept constant at 3 mm. It was shown that using this setup, the contact angle was decreased from 45° to 10° after a plasma treatment duration of 10 seconds, reaching its saturation value of 4° after 60 seconds. Further, dry air was identified to represent the most appropriate process gas whereas the flow rate did not influence the resulting contact angle. However, the obtained decrease in contact angle showed a poor durability. After mechanical attrition tests for 5 days, the hydrophilic effect was completely lost. The same behaviour was observed for hydrophobised samples [yam04].

A long-term stable increase in hydrophobicity of glass surfaces using a coplanar DBD setup was presented by *Fang* et al. in 2006. Here, the dielectric separation of both electrodes was realised by the glass sample itself where the discharge gap was 1.5 mm. In addition to the process gas, ambient air, a polydimethyl siloxane fluid was applied to the glass surfaces. In this way, a hydrophobic layer was generated by plasma activation and the interaction of the involved molecules of both the glass surface and the adherent fluid. Experiments were performed at a voltage of 10 kV, resulting in an increase in contact angle from 53° to maximum 122° after a treatment duration of 11 minutes. By applying *Fourier* transform infrared (FTIR) spectroscopy it was ascertained that a new material, consisting of -CH₃-containing groups, was chemically bonded to the glass surface, resulting in long-term stable hydrophobic properties [fan06b].



2.2 Interactions of laser irradiation with glasses

Generally, material evaporation due to pulsed laser irradiation at adequate fluence is referred to as laser ablation. Due to the rapid laser-induced heating of the material surface, a plasma plume is formed during laser ablation, whereas no plasma occurs during laser desorption. The ablation behaviour of any medium and glasses in particular is strongly dependent on both the wavelength λ and the pulse duration τ of the incoming laser irradiation.

Glasses typically feature a high transmission T in the visible (VIS) and near infrared (NIR) wavelength range ($T > 80\%$ from approx. 170 to approx. 2000 nm in the case of fused silica). An appropriate approach for pure laser ablation at low fluence is thus to employ far ultraviolet (FUV) or mid infrared (MIR) laser irradiation. Against this background, fluorine (F₂) excimer lasers (FUV, $\lambda = 157$ nm) are suitable for micro structuring of fused silica as reported by *Ihlemann* et al. in 2003 and 2007 [ihl03, ihl07]. Here the ablation threshold amounts to approximately 1 J/cm². Material removal of fused silica using carbon dioxide (CO₂) lasers (MIR, $\lambda = 10.6$ μ m) is a photo-thermal ablation process, based on fracturing of the glass surface by laser-induced thermal stress, melting and evaporation [bue90]. However, the formation of stress-produced micro cracks can be avoided by heating the glass work piece to be machined as presented by *Yen* et al. in 2006 [yen06]. In addition to material removal for micro structuring, controlled localised CO₂ laser-induced melting and material flow can be used for smoothing and repairing damages on glass surfaces as shown by *Mendez* et al. in 2006 [men06]. Regarding the ablation of fused silica, the authors reported an ablation threshold intensity of 100 kW/cm² at a pulse duration of 300 μ s.

Besides the choice of highly-absorbed laser wavelengths, the use of laser pulses of ultra-short duration is an appropriate way for improving laser ablation of dielectric, transparent media. Here, nanosecond pulses provoke heating of a thin near-surface layer within the pulse duration, resulting in sudden evaporation and the formation of an ionised ablation plasma plume. As a consequence of such heating, disturbing effects such as the formation of re-deposited debris, micro cracks (see above) and burrs can develop. Further, the incoming laser irradiation is usually attenuated by the laser-induced plasma plume due to absorption and scattering at debris particles as well as plasma shielding in the case of high electron densities, consequently resulting in a decrease in ablation rate. The disturbing effects arising during nanosecond ablation can be overcome by applying laser pulses in the picosecond [ger08] and femtosecond [ute11] range. Here, material removal occurs much faster than heating of deeper regions within the bulk material due to the short pulse duration. Relating to ultra short pulse laser ablation, the interaction of both the solid and the incoming laser irradiation can be described by a two-temperature model: First, the energy of the photons is absorbed by electrons. Second, the absorbed energy is transferred to the network, initiating material removal [lad02]. Such material removal is due to ionisation processes within the network and subsequent *Coulomb* explosion². As a result, the network temperature remains constant during absorption of the incoming ultra short laser pulse [gib96]. The improved coupling of energy during ultra short pulse ablation is visualised by the pulse duration-dependent damage threshold fluence of fused silica as reported by *Perry* et al. in 1999 [per99] in figure 2.2.

² *Coulomb* explosion describes the desorption of electron-depleted atoms due to repulsion forces.

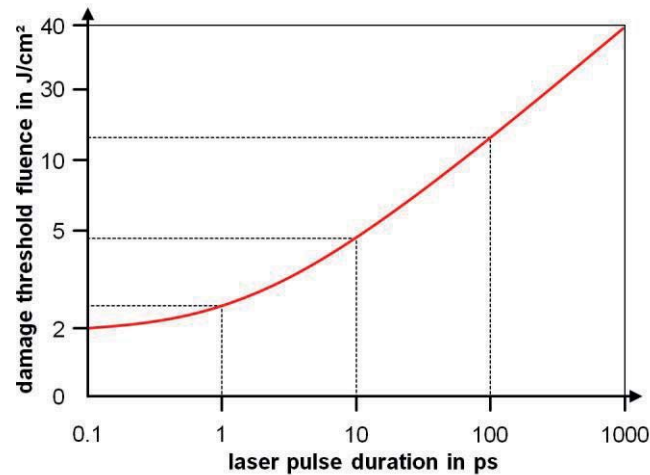


Fig. 2.2: Damage threshold fluence vs. laser pulse duration at a wavelength of 1053 nm, data taken from [per99]

However, in comparison to picosecond and femtosecond laser sources, nanosecond lasers stand out due to a high efficiency as well as low acquisition and maintenance costs. Owing to these advantages, several hybrid ablation methods based on such laser sources were developed in the last decades in order to improve nanosecond laser ablation of transparent media as presented hereafter.

Laser-induced plasma-assisted ablation (LIPAA)

Laser-induced plasma-assisted ablation (LIPAA) is achieved by several plasma interactions at the rear side of the glass sample to be ablated. For this purpose, a laser beam is focussed onto a metallic target surface in order to ignite a plasma-induced ablation plume. As shown in figure 2.3, the glass sample is placed below the metallic target.

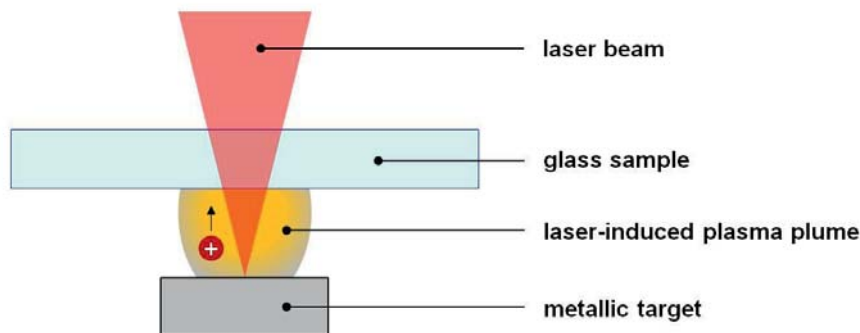


Fig. 2.3: Functional principle of laser-induced plasma-assisted ablation (LIPAA)

LIPAA was first reported by *Zhang et al.* in 1998. Here, a 4th-harmonic Nd:YAG laser at a wavelength of 266 nm and a pulse duration of 6 ns was applied. Experiments were performed in a vacuum chamber (10^{-1} - 10^{-2} Pa) on 0.6 mm-thick fused silica samples; the metallic target was made of stainless steel. The authors observed a strong dependency of the ablation threshold fluence and the etch rate on the distance between both the metallic target and the sample's rear side. At the lowest investigated distance of 20 μm , the ablation threshold fluence was 0.5 J/cm² whereas the etch rate was determined to amount to approximately 35 nm/pulse. In further work it was moreover shown that



LIPPA is suitable for scribing micro gratings in fused silica [zha98a,sug01]. Such enhanced ablation of fused silica at low fluence was explained by three possible interacting mechanisms:

- direct plasma interactions, i.e. a charge exchange amongst ions and electrons of the plasma plume and the sample surface as well as a transfer of kinetic/potential energy, provided by radicals and ions, to the sample surface,
- a plasma heating of the sample surface, and
- the successive deposition of a metallic thin layer on the sample surface and an accompanying increase in absorption at this interface during the process.

Anyhow, the authors suggested the direct plasma interaction to be the dominant mechanism for LIPPA [zha98b]. This was also confirmed by the work of *Hanada* et al., who verified fluence-dependent transient absorption effects within glass substrates due to electron excitation during LIPAA. Here, the absorption decreased linearly when increasing the working distance [han06].

In addition to the distance between the target and the sample surface, the particularly applied laser wavelength has a strong influence on LIPPA characteristics. In this regard, *Zhang* et al. presented a comparative study in 1999 [zha99a]. Here, LIPPA was performed at three different Nd:YAG laser wavelengths, 266 nm, 532 nm and 1064 nm, on fused silica and Pyrex glass at a distance of 1.5-2 mm. An increase in ablation threshold fluence was observed when increasing the laser wavelength, which is generally described by an exponential interrelationship. Simultaneously, the etch rate showed an inverse behaviour. This fact is easily explained by the wavelength-dependent penetration depth of an incoming laser beam into a transparent medium.

Laser-induced backside wet etching (LIBWE)

Another hybrid technique for improving the coupling of laser irradiation into glassy materials is the so-called laser-induced backside wet etching (LIBWE). Here, the rear side of the particular glass sample is brought in contact with an absorbing liquid. As shown in figure 2.4, etching is thus achieved due to the increase in absorption A and the accompanying deposition of laser energy within the liquid close to the sample's rear side, giving rise to photothermal ablation.

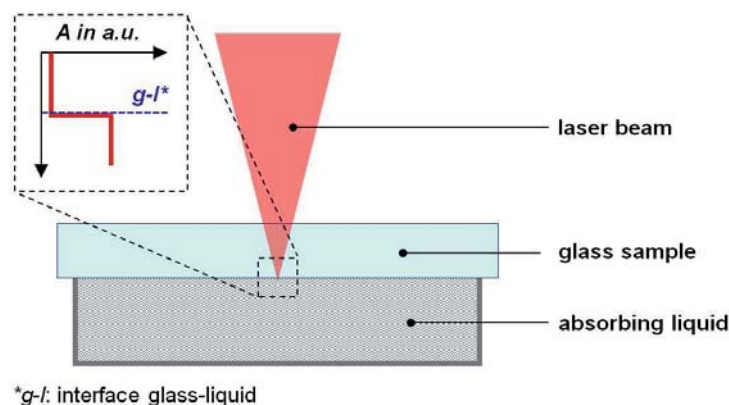


Fig. 2.4: Functional principle of laser-induced backside wet etching (LIBWE)



This technique was introduced by *Wang et al.* in 1999 where a solution of acetone ($(\text{CH}_3)_2\text{CO}$) and pyrene ($\text{C}_{16}\text{H}_{10}$, 0.4 mole/dm³) was applied as absorbing liquid [wan99]. Ablation was performed on 0.5 mm-thick fused silica samples (Suprasil 2 from Heraeus GmbH & Co. KG) using a krypton fluoride (KrF) excimer laser at a wavelength of 248 nm and a pulse duration of 30 ns. By this configuration, ablation was achieved at 0.24 J/cm² whereas the ablation threshold fluence was approximately 10 J/cm² in the case of pure laser ablation in air. Exemplary, etch rates of 5 nm/pulse at 0.4 J/cm² and 25 nm/pulse at 1.3 J/cm² were achieved.

Ding et al. presented LIBWE of fused silica samples using an aqueous solution of naphthalene-1,3,6-trisulfonic acid trisodium salt ($\text{Np}(\text{SO}_3\text{Na})_3$) as absorbing liquid in 2002. Experiments were performed for different molar concentrations $c(\text{Np}(\text{SO}_3\text{Na})_3)$ in the range from 0.4 to 1.0 mole/l, applying a KrF excimer laser with a pulse duration of 30 ns as light source. Ablation was achieved at a threshold fluence of 0.5 J/cm² ($c(\text{Np}(\text{SO}_3\text{Na})_3) = 1.0$ mole/l). For this concentration, etch rates up to approximately 3 nm/pulse at a fluence of 1.6 J/cm² were observed [din02].

In 2003, *Zimmer et al.* reported on LIBWE of five different glasses - Pyrex and 7059 from Corning, Inc., D263 and AF45 from Schott AG and fused silica - using a xenon fluoride (XeF) excimer laser with a wavelength of 351 nm and a pulse duration of 30 ns. Further, the authors investigated the influence of various absorbing solutions consisting of a pyrene admixture with different concentrations in acetone, tetrachloroethylene (C_2Cl_4) and toluene (C_7H_8). It was shown that both the ablation threshold fluence and the etch rate are mainly dependent on the used liquid whereas the glass type, and thus the particular absorption, has a marginal impact on these ablation parameters. Generally, ablation started at 0.45 J/cm² and the etch rate was 6-10 nm/pulse at 1 J/cm² [zim03].

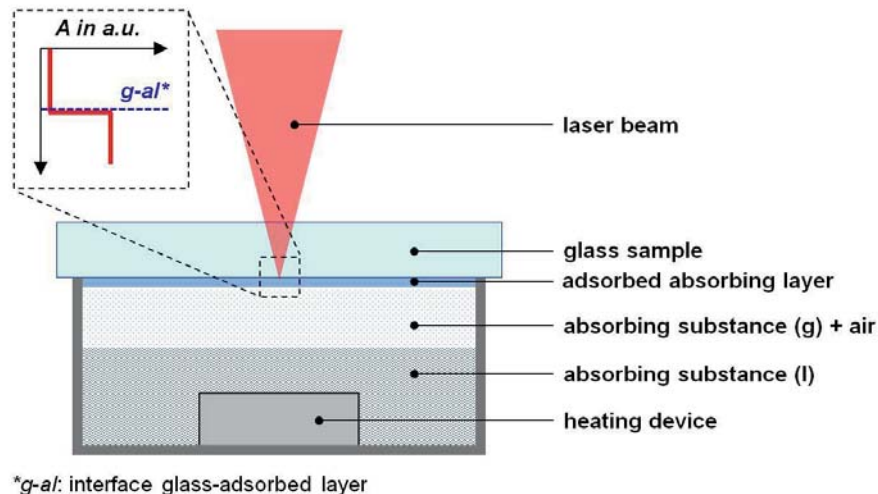
The influence of the absorbance of the used liquid was further demonstrated by *Zimmer et al.* in 2006. By introducing liquid gallium (Ga) to a LIBWE process, where the laser source was a KrF excimer laser with a wavelength of 248 nm and a pulse duration of 25 ns, a relatively high ablation threshold fluence of 1.3 J/cm² was required as a result of the high reflectivity of gallium. However, etch rates up to approximately 1 μm /pulse were achieved for fused silica due to enhanced heating processes on the sample's rear side [zim06a].

Laser-induced backside wet etching was successfully applied for the manufacture of high-precise micro structures on quartz glasses. As an example, *Huang et al.* presented LIBWE scribing of microfluidic channels including bifurcated junctions in quartz glass surfaces in 2007 [hua07]. Such scribing was performed using a 3rd-harmonic Nd:YAG laser ($\lambda = 355$ nm) in combination with a galvanometer laser scanner at a scan speed of 100 mm/s. As absorbing liquid, both pure toluene and pyrenated toluene were applied. In 2010, *Sato et al.* reported on LIBWE micro structuring of complex slanted microstructures in high-purity fused silica from Tosoh Corp., principally based on the primal LIBWE setup according to *Wang et al.* (see above). Such 3D-like scribing was realised by a dynamic positioning of the glass sample along three axes, resulting in inclinations of maximum 30 degrees [sat10].



Laser etching at a surface adsorbed layer (LESAL)

Essentially, laser etching at a surface adsorbed layer (LESAL) is connatural to LIBWE. Here, a near-surface increase in absorption A at the glass sample rear side is achieved by the adsorption of absorbing substances. Such substances are initially available as liquid phase and vaporised by a heating device inside an open topped vessel as shown in figure 2.5. The glass sample to be ablated is placed above the resulting gaseous phase, thus acting as adsorptive surface. The incoming laser irradiation is then absorbed at the interface of both the glass and the adsorbed absorbing layer.



* $g-al$: interface glass-adsorbed layer

Fig. 2.5: Functional principle of laser etching at a surface adsorbed layer (LESAL)

LESAL was first presented by *Böhme* and *Zimmer* as well as *Zimmer* et al. in 2004. In these works, LESAL was performed at fused silica samples using a krypton fluoride (KrF) excimer laser at a wavelength of 248 nm and a pulse duration of 30 ns. The absorbing substance, pure toluene, was evaporated at a temperature of 75°C, which is considerably below its temperature of ebullition (i.e. 110°C). Etching was achieved at an ablation threshold fluence of 0.7 J/cm², representing a reduction of required laser energy for ablation by one order of magnitude. At this fluence, the etch rate was 1 nm/pulse [böh04, zim04]. In further work, an even lower ablation threshold fluence of 0.5 J/cm² was reported [zim06b]. As underlying mechanism for LESAL, the authors suggested a number of interacting effects such as

- a fast heating of the adsorbed layer and the near-surface region of the glass sample due to the local absorption of the incoming laser beam and the resulting structural change of the glass,
- the initialisation of shock waves at the glass-layer interface, and
- the desorption/decomposition of the toluene layer.



Laser-induced backside dry etching (LIBDE)

For laser-induced backside dry etching (LIBDE), enhanced absorption at the glass sample's rear side is achieved by the deposition of metallic coatings. Ablation is thus initiated by the coupling of incoming laser irradiation at the glass-coating interface due to the formation of an absorbing laser-induced plasma [zim09]. This method was introduced by *Hopp* et al. in 2006, where a silver layer with a thickness of 100 nm was vacuum evaporated on fused silica. Subsequent backside ablation was performed applying a KrF excimer laser ($\lambda = 248$ nm, $\tau = 30$ ns). Due to the high absorption of silver at this laser wavelength, a low ablation threshold fluence of 0.19 J/cm² was obtained. In comparison to LIBWE, the LIBDE etch rate was 5 to 6 times higher [hop06].

Investigations regarding the dependency of the LIBDE process parameters on the particularly applied laser wavelength were also performed by *Hopp* et al. in 2008. For tin-coated fused silica with a coating thickness of 125 nm, nanosecond-LIBDE was carried out at three different excimer laser wavelengths, 193 nm, 248 nm and 308 nm, respectively. Table 2.1 shows the reported ablation threshold fluences for LIBDE $F_{th(LIBDE)}$ and, as a comparison, pure laser ablation $F_{th(pure)}$ on polished fused silica rear sides as well as the ratio of both.

Table 2.1: Wavelength λ - and pulse duration τ -dependent ablation threshold fluences F_{th} for LIBDE and pure laser ablation including ratio of both

λ in nm	τ in ns	$F_{th(LIBDE)}$ in J/cm ² [hop08]	$F_{th(pure)}$ in J/cm ² [ihl92a]	$F_{th(pure)}/F_{th(LIBDE)}$
193	20	0.23	3	13
248	18	0.26	11	40
308	22	0.42	7	17

Generally, lower ablation thresholds and higher etch rates were observed when decreasing the particular laser wavelength due to the absorption characteristics of the applied thin film [hop08]. However, LIBDE can also be realised in the visible wavelength range as shown by *Hopp* et al. in 2007. Here, a dye laser ($\lambda = 500$ nm, $\tau = 11$ ns) was used for etching of fused silica where the absorbing medium was an aluminium coating with a thickness of 100 nm. At this configuration, ablation started at a threshold fluence of 0.76 J/cm², resulting in an etch rate of 10 nm/pulse. At a fluence F of 3 J/cm², an etch rate of 160 nm/pulse was observed [hop07].

The efficiency of LIBDE is strongly dependent on the applied coating and its particular absorption characteristics. Recently, the use of silicon oxides as absorbing solid coating was investigated. *Ihlemann* presented ArF excimer laser ablation of fused silica induced by absorption of a 28 nm-thick silicon monoxide (SiO) layer in 2008. The threshold fluence for substrate ablation was 1.1 J/cm². For the maximum fluence applied, the etch rate was approximately 200 nm/pulse for front side ablation and approximately 800 nm/pulse for rear side ablation, respectively [ihl08]. In 2006, *Klein-Wiele* et al. reported on laser micro structuring of silicon suboxide (SiO_x, where $1 < x < 2$) films for scribing phase grating patterns onto SiO_x-coated fused silica. Using an ArF excimer laser with a pulse duration of 20 ns, single-pulse rear side ablation of the 28 nm-thick coating was achieved at a fluence of 540 mJ/cm² [kle06]. Finally, the SiO_x micro structures on the fused silica substrates were oxidised to SiO₂ by a tempering process in or-



der to create a monolithic device with almost homogenous optical properties. A further study on front side and rear side ablation of SiO_x was performed by *Jahn et al.* in 2010, where the influence of different coating thicknesses (20 to 600 nm) and excimer laser wavelengths (ArF and KrF) were investigated. The main results are summarised in table 2.2.

Table 2.2: Wavelength λ -dependent threshold fluences F_{th} and etch rates R_{etch} for front side and rear side ablation of silicon suboxide layers as presented by [jah10]

λ in nm	front side ablation		rear side ablation	
	193	248	193	248
F_{th} in mJ/cm ² (approx.)	260	500	175	290
R_{etch} in nm/pulse @ 1.3 J/cm ² (approx.)	100-110	70	230	-

To centralise, nanosecond LIBDE using silicon dioxide as absorbing solid is not only strongly dependent on the used laser wavelength and the fluence but also on the thickness and the stoichiometry factor $x = O/Si$ of the applied SiO_x coating. In any case it represents a suitable medium for laser-induced front side and rear side dry etching. Against this background, direct atmospheric pressure plasma-induced generation of silicon suboxide layers on fused silica by a modification of the bulk material and related effects and mechanisms are presented in this work.



Experimental Setup, Materials and Methods

In this chapter, the basic experimental setups and procedures used in the present work, i.e. both sequential and simultaneous plasma assisted laser ablation, are introduced. Further, a comparison of the investigated glasses in terms of optical properties and chemical composition is given. The measurement methods applied for evaluation of the experimental results are specified.

3.1 Experimental setup for sequential plasma-assisted laser ablation

For sequential plasma-assisted laser ablation, the investigated glass samples were pre-treated by remote plasmas at atmospheric pressure. The goal was to initiate a modification of the glass composition and optical properties, respectively, in order to enhance the coupling of incoming irradiation during subsequent laser ablation. For this purpose, forming gas 90/10, i.e. 90% nitrogen (N_2) and 10% hydrogen (H_2) was applied as process gas, resulting in the formation of excited molecules and atomic nitrogen (N) and hydrogen (H) by collision and dissociation within the plasma discharge. The plasma pre-treatment was performed using different atmospheric pressure plasma sources: plasma jets based on dielectric barrier discharge (DBD), a radio frequency-excited plasma jet and a DBD-based surface discharge plasma source. After such plasma pre-treatment, the modified glass samples were laser ablated. This sequential procedure is schematically shown in figure 3.1.

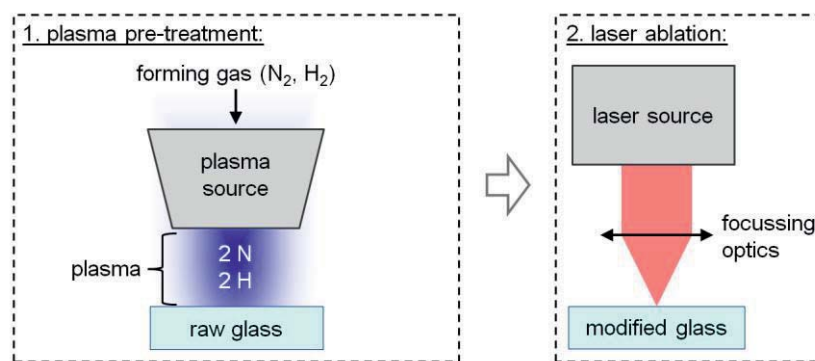


Fig. 3.1: Schematic of the sequential plasma-assisted laser ablation procedure

For ablation, two UV-lasers were employed, an argon fluoride (ArF) excimer laser ($\lambda = 193$ nm) and a 3rd-harmonic Nd:YAG solid state laser ($\lambda = 355$ nm). These laser wavelengths are close to the absorption edge of the particularly ablated glass (compare figure 3.3 in section 3.3) and thus preferentially affected by plasma-induced modifications of optical properties. The particularly used plasma and laser sources as well as the optical setups for focussing are specified and described in more detail in the embedded articles in section 4.1 and chapter 5.

3.2 Experimental setup for simultaneous plasma-assisted laser ablation

In contrast to sequential plasma-assisted alation, no modification of optical properties of the glass samples to be ablated was intended for simultaneous plasma-assisted ablation. The aim was rather to enhance the laser ablation process by benefiting from plasma-physical phenomena such as the formation of a plasma sheath³ or the de-excitation of plasma-generated metastables and the accompanying energy transfer during the laser ablation process. Simultaneous plasma-assisted laser ablation was carried out employing a DBD-based plasma source with an inner concentric aperture, providing a cylindrical plasma beam with a diameter of approx. 200 μm . The used process gas was argon (Ar). The focussed laser beam was guided coaxially to the formed plasma beam as shown schematically in figure 3.2.

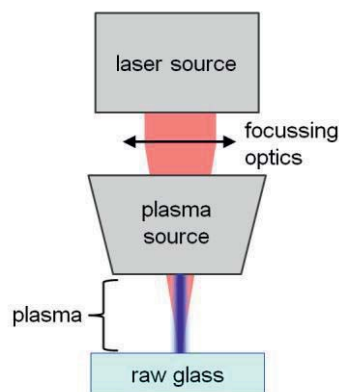


Fig. 3.2: Schematic of the simultaneous plasma-assisted laser ablation procedure

Since in this setup, the ground electrode was placed on the back of the glass sample, a direct plasma discharge was deployed in contrast to the sequential process described in section 3.1, where the plasma pre-treatment was performed by indirect remote plasmas. In addition to the simultaneous ablation process, the impact of the direct plasma treatment on optical glasses and media was investigated without applying any laser irradiation. The results as well as the used plasma and laser source are presented and described more closely in the embedded articles in section 4.2 and chapter 6.

³ The plasma sheath, a.k.a. *Debye* sheath, is defined as the edge layer between a bulk plasma and its limiting walls. Here, the condition of quasi-neutrality is not given, resulting in an acceleration of ions towards the walls.



3.3 Investigated glasses

In this work, plasma-assisted laser ablation of three different glasses was investigated: fused silica (Suprasil 2B and Spectrosil[®] 2000, both from Heraeus Quarzglas GmbH & Co), heavy flint glass (SF5 from Schott AG) and barite crown glass (N-BaK4 from Schott AG). These glasses represent standard materials in optical manufacturing and were chosen due to the significant differences in the particular optical properties. The most common and important parameters for describing the optical properties of any optical glass are the non-dimensional values index of refraction, dispersion and absorption. Physically, the wavelength-dependent index of refraction n represents a proportionality factor, relating the light's phase velocity v_p within an optical medium to v_p in vacuum.

The dispersion characteristics of optical glasses are commonly described by the *Abbe* number v_x , i.e. the relationship of the index of refraction n_x and the main dispersion, $n_y - n_z$, according to

$$v_x = \frac{n_x - 1}{n_y - n_z}. \quad (3.1)$$

Here, the subscripts x , y and z represent element-specific *Fraunhofer* lines and thus discrete wavelengths. In practice, the *Abbe* number is specified for two different *Fraunhofer* lines, e and d , as listed in table 3.1.

Table 3.1: *Fraunhofer* lines and corresponding wavelength/element for the calculation of the *Abbe* number v_e and v_d , respectively. The letter given in brackets represents the particular subscript as introduced in Eq. 3.1

<i>Abbe</i> number	<i>Fraunhofer</i> line	wavelength in nm	element
v_e	e (x)	546.1	mercury (Hg)
	F' (y)	479.9	cadmium (Cd)
	C' (z)	643.9	cadmium (Cd)
v_d	d (x)	587.6	helium (He)
	F (y)	486.1	hydrogen (H)
	C (z)	656.3	hydrogen (H)

By definition, optical glasses with an *Abbe* number < 50 are referred to as flint glasses whereas crown glasses feature an *Abbe* number > 50 .

Disregarding surface and bulk scattering effects, the wavelength-dependent absorption A is given by $1 - (T_i + R)$, where T_i is the pure internal transmission and R the reflexion. One has to consider that A depends on the thickness of an optical medium. Its local dependency at any depth within an optical medium is usually described by the propagation direction-dependent *Bouguer-Lambert* law, a.k.a. *Beer-Lambert* law, according to

$$I_t = I_0 \cdot e^{-k \cdot z}, \quad (3.2)$$

where I_t is the transmitted and I_0 the initial intensity, k is the material-specific absorption coefficient and z represents the position within the optical medium in direction of propagation [bou29].



The differing optical properties of the investigated glasses are due to the chemical composition and the manufacturing process as described hereafter. To give an overview, n_e , v_e , and A of the particular glasses are listed in table 3.2 and shown in figure 3.3.

Table 3.2: Comparison of the index of refraction n_e and the Abbe number v_e of the investigated optical glasses, data taken from [her11, sch14]

	n_e	v_e
fused silica	1.46013	67.56
heavy flint glass (type SF5)	1.67764	31.97
barite crown glass (type N-BaK4)	1.57125	55.7

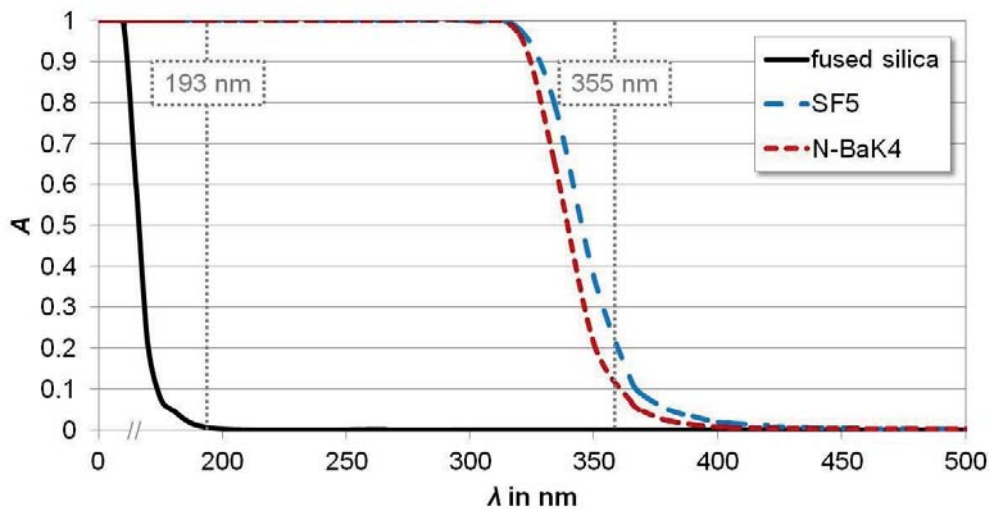


Fig. 3.3: Absorption A of fused silica, heavy flint glass SF5 and barite crown glass N-BaK4 with a thickness of 10 mm vs. wavelength λ , data taken from [her11, sch14]. The laser wavelengths used in the present work are indicated additionally.

Owing to its very low dispersion and high UV-transmission, fused silica is one of the most important materials used in modern optical system technology. As an idealised description, fused silica purely consists of silicon dioxide (SiO_2). Apart from boron trioxide (B_2O_3) and phosphorus pentoxide (P_2O_5), SiO_2 is one of the most important network formers that are used in glass chemistry. Synthetic fused silica of highest purity is produced by a flame hydrolysis process where gaseous silicon tetrachloride (SiCl_4) is pyrolysed. From the gasified silicon, pure solid silicon dioxide is obtained by oxidation and subsequent smelting and cooling. The fused silica network consists of SiO_4 tetrahedrons where each oxygen atom appertains to two silicon atoms. By definition, glasses and amorphous media in general have no long-range order. However, the SiO_4 tetrahedrons represent a short-range order with a mean bond angle θ_{av} of 145° and a theoretical averaged interatomic distance $r_{(\text{Si}-\text{O})}$ of 0.163 nm [sch88]. Due to the mixed bond condition consisting of covalent, ionogenic and double bonds within fused silica, $r_{\text{Si}-\text{O}}$ can vary in the range from 0.157 to 0.172 nm [pau80]. In addition to SiO_4 tetrahedrons, further tetrahedrons of different chemical composition (Si_xO_y , where $0 \leq y \leq 4$), and thus differing bond angles and interatomic distances, can occur in silicon dioxide networks. Systems of that kind are referred to as silicon suboxide (SiO_x).



Heavy flint glasses stand out due to a high index of refraction (e.g. $n_e = 1.93322$ in the case of N-SF66 from Schott AG) which is crucial for a number of applications in optical technology. In contrast to fused silica, heavy flint glass represents a multi-component glass, produced by classical glass making. Here, the involved compounds are mixed to a batch in powder form which is subsequently molten in a furnace, followed by planing and cooling. In addition to the network former SiO_2 , heavy flint glass contains a relatively high amount of lead(II) oxide (PbO) and a certain portion of potassium oxide (K_2O) and sodium oxide (Na_2O), acting as network modifiers and fluxing agents, respectively, for obtaining a high index of refraction. Further, aluminium oxide (Al_2O_3) is added as stabilisation agent. As a result, heavy flint glasses feature a very dense network in comparison to fused silica. The typical composition of this glass family is listed in table 3.3.

Table 3.3: Typical composition of heavy flint (SF) glass incl. the content of the involved oxides in mass-% as reported by [vog65, pfo93]

<i>compound</i>	<i>chemical formula</i>	<i>content in mass-%</i>
silicon dioxide	SiO_2	25-50
lead(II) oxide	PbO	50-70
potassium oxide	K_2O	< 5
sodium oxide	Na_2O	< 5
aluminium oxide	Al_2O_3	< 5

Barite crown glasses feature moderate indices of refraction and dispersion characteristics and are used for a number of standard optical components. In the same manner as heavy flint glass, barite crown glass is made by classical glass making. As listed in table 3.4, its network is formed by SiO_2 and B_2O_3 , replenished with the network modifiers and fluxing agents barium oxide (BaO), zinc oxide (ZnO), K_2O and Na_2O .

Table 3.4: Typical composition of barite crown (BaK) glass incl. the content of the involved oxides in mass-% as reported by [vog65, pfo93]

<i>compound</i>	<i>chemical formula</i>	<i>content in mass-%</i>
silicon dioxide	SiO_2	40-60
barium oxide	BaO	15-30
zinc oxide	ZnO	5-15
potassium oxide	K_2O	5-10
sodium oxide	Na_2O	5-10
boron trioxide	B_2O_3	< 5

In addition to these three optical glasses, the impact of the plasma treatment as described in section 3.2 was investigated for other optical media of interest: boron crown glass, glass ceramic and sapphire.



3.4 Measurement methods

For the evaluation of plasma treated and laser ablated optical glasses, several microscopic, imaging and spectroscopic measurement methods and apparatuses were applied as described in the following subsections.

3.4.1 Microscopic and imaging measurement methods

For the visual inspection of laser ablated areas and spots, the measurement of ablation depths and spot diameters, the determination of form errors (as defined in more detail in [ger13a] in chapter 5) as well as the measurement of surface roughness parameters, several microscopic methods were used.

The evaluation of the ablation spot geometry was mainly performed by a scanning electron microscope (SEM) [ard38] “PSEM eXpress” from Aspex Corp. Here, the measuring electron beam is generated by a tungsten wire as electron source. This beam is then accelerated by an electric field, where the acceleration voltage can be adjusted from 5 to 20 keV, and focussed onto the sample surface. The sample is placed within a vacuum chamber at a pressure of approx. 7×10^{-5} Pa. The SEM image is obtained from the detected primary electrons which are backscattered by the sample. According to the manufacturer’s data sheet, the lateral imaging resolution of the used SEM amounts to 30 nm. This instrument was also applied for the detection of surface-adherent debris after laser ablation. Further, the ablation depths and spot diameters and surface roughnesses were partially measured by a confocal scanning microscope (CSM) “PL μ 2300” from Sensofar Corp. with a lateral imaging resolution of 5 nm and a depth resolution of 1 nm. This comparatively high depth resolution is achieved by the measurement principle as follows: The incident light is focussed onto the sample surface. The reflected signal then forms a confocal intermediate image, where a pinhole is placed at the intermediate image plane. Thus, out-of-focus planes are not considered by further imaging onto the detector via an object lens [ham82]. The lateral scanning is performed by an assembly of pivot-mounted mirrors. Beyond SEM and CSM, a classical light microscope “Axioskop 2 MAT” from Zeiss was used for depths measurements.

The determination of roughness parameters was carried out with an atomic force microscope (AFM) “easyScan 2” from Nanosurf GmbH. This AFM features a maximum lateral scan range of $150 \times 150 \mu\text{m}^2$ and a depth resolution of 0.34 nm. In principle, an AFM setup is comparable to a tactile profilometer since the sample surface is scanned by a flat spring with a cone-shaped measuring tip, a.k.a. cantilever. The back side of this cantilver acts as reflecting surface for a measuring laser beam. The surface profile is then calculated from the deflection of this laser beam during the scanning procedure, caused by atomic forces between both the surface and the measuring tip [bin86].

In addition to the above-mentioned geometric parameters, the impact of the applied plasma treatments on the surface energy was determined. For this purpose, a “Contact Angle Measurement System G10” from Krüss GmbH was used, where the contact angle of different test liquids on the sample surfaces is detected by a camera and an objective lens with appropriate magnification. From the measured contact angles and the known surface tensions of the used test liquids, the surface energy can be calculated according to *Young’s* equation [owe69].



3.4.2 Spectroscopic measurement methods

The impact of the particularly applied plasma treatment on optical characteristics and the chemical composition of the investigated glasses was evaluated by spectroscopic methods.

The transmission (T) and reflexion (R) characteristics in the ultraviolet and visible wavelength range of the investigated glasses before and after plasma treatment were detected by two spectrometers, “Lambda 19” and “Lambda 650”, both from Perkin Elmer Inc. These grating-based spectrometers are operated with a tungsten-halogen visible lamp and a deuterium ultraviolet lamp as light sources and have a spectral resolution of 1 nm. This resolution is achieved by tilting the diffraction gratings and scanning T and R , respectively, for single diffracted wavelengths.

In order to obtain depth-resolved information on the plasma-induced change in stoichiometry as a result of the pre-treatment as introduced in section 3.1, two measurement methods were combined: First, the near-surface stoichiometry was determined using a secondary ion mass spectrometer (SIMS) “Quadrupol 4550” from Cameca SAS. Generally, SIMS analysis is performed by sputtering the sample surface by a primary ion beam. The emitted secondary ions are then identified by a mass spectrometer on the basis of the particular mass/charge ratios (m/q -ratios) of the investigated elements. For the present work, SIMS analysis was performed in cooperation with the Fraunhofer Institute for Surface Engineering and Thin Films IST. Second, the depth of the crater sputtered by the ion beam was measured in cooperation with the Laser Laboratorium Göttingen e.V. Here, a Dektak Stylus Surface Profiler from Bruker Corp. with a depth resolution of 0.1 nm was used. For such profile measurements, the sample surface is scanned by a diamond stylus in contact mode, where the deflection values of the stylus is detected by a fluxgate. From these values, the surface topography is calculated. The combination of both techniques thus allows the depth-resolved determination of the plasma-induced change in stoichiometry of the elements of interest, i.e. silicon (Si), oxygen (O), nitrogen (N) and hydrogen (H). For this purpose, the SIMS apparatus was calibrated at IST using standards with well-defined concentrations of the involved elements of interest, see table 4.1 in [ger12a], section 4.1. The applied acceleration voltages U_{ac} of the primary ion beam (here: a caesium [Cs] ion beam) were 1 kV and 5 kV, respectively.

Further, the built-in energy dispersive X-ray spectroscopy (EDX) device of the above-described SEM instrument was applied for material analysis. The EDX resolution of this device amounts to 133 eV. As a result of the excitation by the incident electron beam, characteristic X-ray signals are emitted by the involved elements, where the signal energy is directly related to the particular element. However, one has to consider that due to the comparatively high penetration depth of the incoming electron beam into the investigated glass samples, a high information depth of approx. 1 μm is resulting. EDX thus allows rather semi-quantitative and qualitative material analysis than a quantitative determination of the chemical composition.





Plasma Treatment of Optical Glasses

In this chapter, the impact of the plasma treatments which were applied for both sequential and simultaneous plasma-assisted laser ablation on optical media is presented. It is shown that in the first case, i.e. the plasma pre-treatment using chemically reactive process gas, a decrease in transmission due to a modification of the glass composition as well as a roughening of the surface is resulting. In contrast, the plasma treatment applied during simultaneous ablation mainly effects a surface smoothing.

4.1 Plasma pre-treatment for sequential ablation

The plasma pre-treatment as introduced in section 3.1 has a considerable impact on optical and chemical properties of the investigated glasses as discussed in more detail hereafter [ger12a, ger13b]. Regarding optical properties, two main effects were observed by UV/VIS spectroscopy: a decrease in transmission T and an (unsteady) increase in reflexion R in the ultraviolet wavelength range. The transmission T is directly related to the absorption A and the extinction coefficient κ , respectively. Further, neglecting scattering due to surface roughness phenomena, R is attributed to the index of refraction n . It can thus be stated that the plasma pre-treatment causes a change in the complex index of refraction N , given by

$$N = n + i\kappa. \quad (4.1)$$

This declaration was also confirmed by supplementary, non-published ellipsometric measurements. As a secondary effect, the dispersion characteristics, represented by the *Abbe* number, are modified. These changes of relevant optical parameters can be explained by a plasma-induced modification of chemical properties as determined by SIMS. First, substoichiometric silicon oxide (SiO_x) was generated within the glass surface layer. Generally, SiO_x features a high UV-absorption. Second, hydrogen was implanted into deeper regions of the glass bulk material by the plasma pre-treatment. Such implantation of hydrogen was further confirmed by supplementary *Fourier* transform infrared spectroscopic investigations. It was also shown that the hydrogen from the used forming gas is of essential importance for the above-described modifications. When applying pure nitrogen as process gas, the resulting increase in absorption was much lower. As the main reason for the above-described modifications of optical properties, hydrogen-based fracturing of cross-linking oxygen,



and the resulting formation of terminal non-bridging oxygen (NBO),



within the network forming SiO_2 tetrahedral can thus be assumed. Consequently, the index of refraction and extinction coefficient are increased. In glass chemistry, this fracturing effect, and the accompanying modification of the index of refraction and dispersion characteristics, is usually accomplished by adding selected cations, so-called network modifiers such as monovalent sodium (Na^+) or divalent calcium (Ca^{2+}), to the glass melt [frü05]. The hydrogen-induced formation of fractures within the SiO_2 network is a further common effect in glass melting where water vapour is provided by the ambient atmosphere inside the melting furnace. It is known as hydrolytic scission which is due to hydrogen ions (H^+) and gaseous or liquid water (H_2O) [ped87]. In this case, bridging oxygen is attacked by hydrogen ions, resulting in an intermediate,



and a subsequent hydrolysis of this intermediate according to



As a result, both hydrogen and hydroxyl groups are implanted into the glass bulk material as shown by *Boksay* and *Bouquet* [bok80] and *Charles* [cha58a,cha58b]. Such implantation of hydrogen strongly affects the optical properties and in particular the transmission characteristics [atk92,nog85].

Apart from an increase in N , the observed unsteady behaviour of R indicates surface roughening, giving rise to both constructive and destructive interference effects of the reflected light. Such roughening was confirmed by AFM measurements. As a result, incoming light is reflected diffusely and scattered, leading to an increased coupling into the surface by multiple reflexions as shown schematically in figure 4.1.

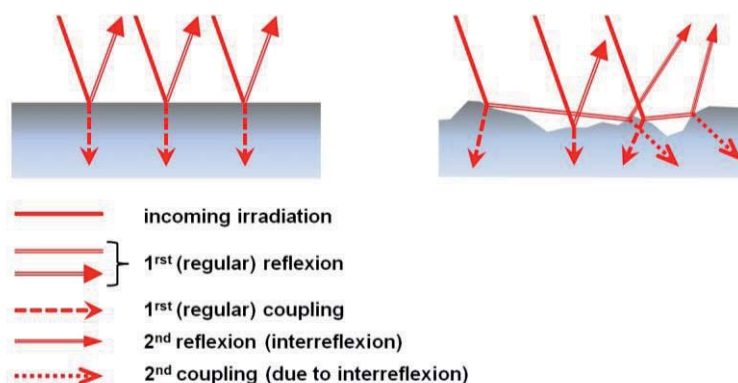


Fig. 4.1: Reflexion and coupling of incoming light at directionally reflective (left) and diffusively reflective (right) surfaces

The surface roughening can be explained by different plasma-induced reduction efficiencies for surface-adherent contaminations such as aluminium and carbon on the one hand and the clean glass surface areas on the other hand. This is also indicated by the



fact that both the contamination clusters and the roughness peaks, observed by SEM and AFM, respectively, have comparable lateral sizes (some microns to tens of microns) as shown in figure 4.2.

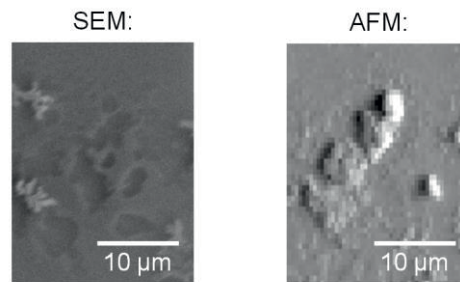


Fig. 4.2: Comparison of contamination cluster sizes, detected by SEM (left) and roughness peaks as measured by AFM (right)

These findings are of essential importance for understanding the underlying mechanisms for improved sequential plasma-assisted laser ablation as presented in chapter 5. To summarise, the plasma pre-treatment allows an enhanced coupling of incoming laser irradiation by

- the formation of an UV-absorbing near-surface SiO_x layer,
- the implantation of hydrogen into deeper regions of the glass bulk material, and
- the appearance of multiple reflexions due to surface roughening.

The above-presented and -discussed results were published in the following articles.





Near-surface modification of optical properties of fused silica by low-temperature hydrogenous atmospheric pressure plasma

by C. Gerhard, D. Tasche, S. Brückner, S. Wieneke, and W. Viöl,
published in *Optics Letters* **37** (2012) 4, 566-568⁴

In this Letter, we report on the near-surface modification of fused silica by applying a hydrogenous atmospheric pressure plasma jet at ambient temperature. A significant decrease in UV-transmission due to this plasma treatment was observed. By the use of secondary ion mass spectroscopy, the composition of the plasma-modified glass surface was investigated. It was found that the plasma treatment led to a reduction of a 100 nm thick SiO₂ layer to SiO_x of gradual depth-dependent composition. For this plasma-induced layer, depth-resolved characteristic optical parameters, such as index of refraction and dispersion, were determined. Further, a significant plasma-induced increase of the concentration of hydrogen in the bulk material was measured. The decrease in transmission is explained by the plasma-induced near-surface formation of SiO_x on the one hand and the diffusion of hydrogen into the bulk material on the other hand.

The application of absorbing layers on glass surfaces allows significant enhancements of laser machining results due to an improved laser energy deposition. In this context, a number of different techniques have been developed. For example, UV-absorbing films of toluene [zim04] or carbon [boh06a] are used for laser induced etching. Indirect laser processing is also performed by a combination of vacuum deposition and structuring of a silicon suboxide (SiO_x, where 1 < x < 2) layer and its terminal oxidation to silicon dioxide (SiO₂) [sch05b]. Further, the use of hydrogenous gases at high temperatures allows a direct reduction of SiO₂-surfaces to SiO_x or silicon monoxide (SiO) [tso82]. SiO_x can also be produced by evaporating powdered SiO in a vacuum [sha83, nak84] or by various physical vapor deposition (PVD) methods, such as plasma ion sputtering, by inserting silicon (Si) into an argon-oxygen gas mixture [sch82]. Such SiO_x features a multiplicity of different realizable optical and electrical properties [sch82, joh66, phi71, hüb80] and is for this account of great interest for the production of optical and optoelectrical micro devices.

In this Letter, we present the generation of near-surface SiO_x on fused silica surfaces using an atmospheric pressure plasma jet (APPJ) at ambient temperature. The plasma provides reactive atomic hydrogen H^{*} and smaller amounts of reactive nitrogen species such as N^{*}, which reduce the SiO₂ boundary layer, resulting in the formation of a UV-absorbing suboxidial layer.

For the plasma treatment of fused silica samples, a coaxial dielectric barrier discharge (DBD)-based low-potential APPJ was used [för05]. This plasma source consists of a grounded cylindrical inner electrode and an outer high-voltage ring electrode. The dielectric separation of both electrodes is performed by a glass tube.

The plasma jet features a ring-shaped profile with an outer diameter \varnothing_o of 7 mm and an inner diameter \varnothing_i of 5 mm. Thus, the samples were placed on a motor-driven xy-linear stage in order to realize a uniform plasma treatment. The area of homogeneous treat-

⁴ Reproduced with kind permission from the Optical Society of America.

ment was 165 mm^2 ; the overall treatment duration was 12 minutes. Plasma treatment was performed at 5 mm thick fused silica samples made of Spectrosil 2000 from Heraeus. The distance d from the plasma jet outlet to the glass surface was 1 mm.

In order to initialize a chemical reduction and modification of the near-surface glass layer, forming gas 90/10, consisting of 90% nitrogen (N_2) and 10% hydrogen (H_2), was used as working gas for operating the APPJ. The APPJ was driven using a pulsed power supply at a peak-to-peak voltage U_{p-p} of 22 kV with a voltage pulse duration t_{pulse} of 0.8 ms and a pulse repetition rate f_{pulse} of 400 Hz. The plasma power was determined to be 720 mW by applying the *Lissajous*⁵ figure method [man43, hel09]. The gas temperature T_{gas} was identified to amount to 300 K, i.e. approximate ambient temperature.

In order to verify the effect of the above-described plasma treatment, the UV-transmission (including reflection losses) of both pure and plasma-treated fused silica samples was measured using a UV/VIS-spectrometer Lambda 650 from Perkin Elmer. As shown in Fig. 4.3, the plasma treatment led to a significant decrease in transmission in the UV spectral range, reaching a maximum value of approximately 4.3% at a wavelength of 200 nm.

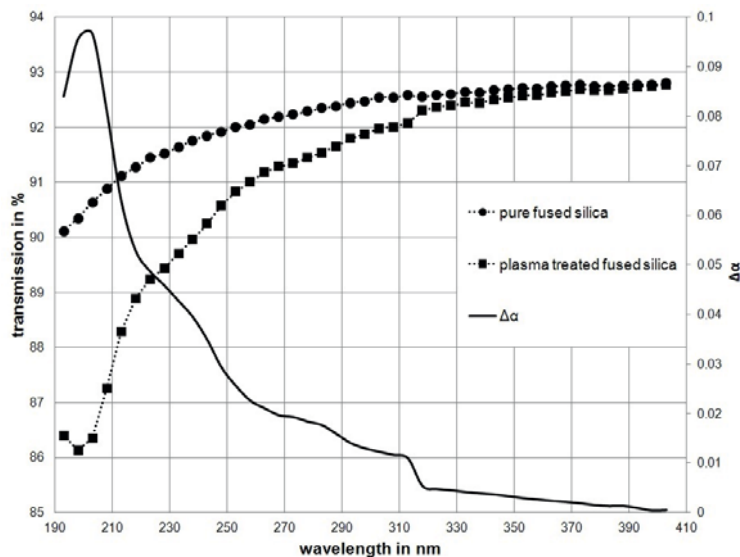


Fig. 4.3: Transmission of both pure and plasma-treated fused silica and resulting change of the absorption coefficient $\Delta\alpha$

Here, the continuous line represents the change of the absorption coefficient $\Delta\alpha$ of the plasma-treated sample with respect to the untreated one, calculated by applying the *Beer-Lambert* law. For lower wavelengths than 200 nm, interference effects get relevant additionally.

The increase of absorption can partially be explained by a plasma-induced near-surface reduction of SiO_2 to UV-absorbant SiO_x . For characterizing this reduction regarding its stoichiometry and depth of penetration, the samples were investigated using a secondary ion mass spectrometer (SIMS) [ben73, ben94] Quadrupol 4550 from Cameca. The relative sensitivity factor (RSF) was calibrated by applying three standards - silicon dioxide

⁵ The *Lissajous* algorithm for calculating the plasma power via its voltage and capacitance is based on the determination of the area of a voltage/charge *Lissajous* figure resulting from plotting the applied voltage and the integrated discharge current.



(SiO₂), hydrogenous amorphous silicon (a-Si:H), and hydrogenous nitrogen doped silicon carbide (SiNC:H) - with well-defined concentrations C as listed in table 4.1.

Table 4.1: Concentrations in % of the used standards for calibrating the SIMS-measurements

standard	$C_{silicon}$	C_{oxygen}	$C_{hydrogen}$	C_{carbon}	$C_{nitrogen}$
SiO ₂	33	66	-	-	-
a-Si:H	-	-	14	-	-
SiNC:H	26.6	-	-	64	8.3

The acceleration voltage of primary ions was 1 kV. The area A of the sputtered crater was 1 mm² with a depth d of 58 nm, measured by the use of a Dektak Stylus Surface Profiler from Bruker. On the basis of the concentrations that were measured in this vein, the stoichiometric ratio of both oxygen (O) and silicon (Si) O/Si of a plasma-treated fused silica surface was calculated with respect to a pure fused silica sample. Figure 4.4 shows the dependency of this O/Si-ratio on the depth of penetration.

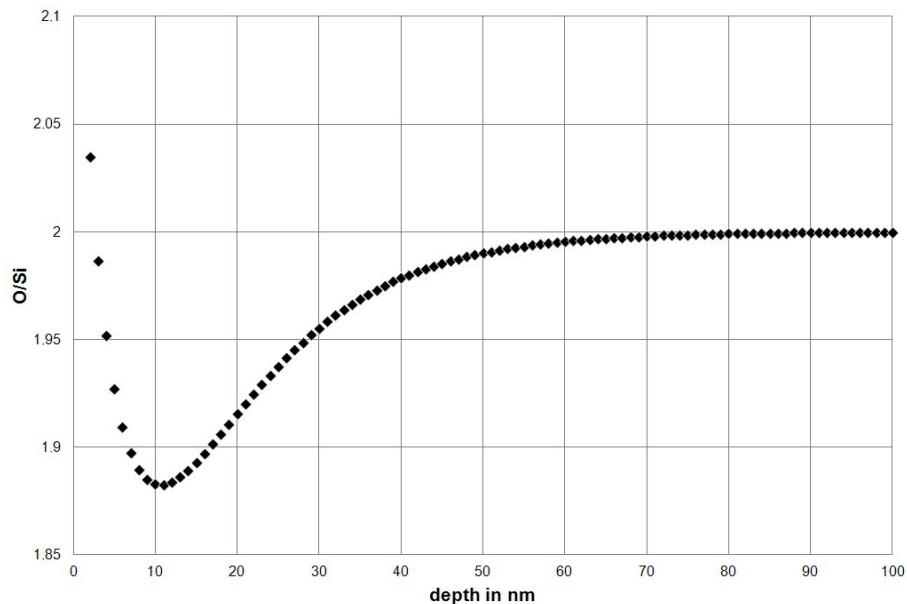


Fig. 4.4: Depth-dependent O/Si-ratio of plasma-treated fused silica with respect to untreated fused silica

The behavior of the 10 nm thick surface layer is due to a transient effect after starting the measurement during the formation of a sputter equilibrium between all components of the sample. At a depth of approximately 10 nm, the secondary ion yield of each species is proportional to its concentration in the sample with respect to its particular bonding conditions.

The action depth of the plasma treatment is approximately 100 nm, where O/Si amounts to 2. By applying the corresponding O/Si-ratio x_t of the plasma-treated reduced layer, its depth-resolved permittivity ε_{SiO_x} in the range of $1.8 < x < 2$ can then be estimated according to the *Philipp's* interpolation formula

$$\varepsilon_{SiO_x} \approx \left(1 - \frac{x_t}{2}\right)^2 \cdot \varepsilon_{Si} + \left(\frac{x_t}{2}\right) \cdot \varepsilon_{SiO_2}, \quad (4.6)$$



where ε_{Si} and ε_{SiO_2} are the particular permittivities of amorphous silicon and pure silicon dioxide [phi71]. By including the approximation for the interrelationship of both the permittivity ε and the index of refraction n in transparent media, $n \approx \sqrt{\varepsilon}$, the depth-resolved, wavelength-dependent index of refraction $n(\lambda)_{SiO_x}$ can be written as

$$n(\lambda)_{SiO_x} \approx \sqrt{\left(1 - \frac{x_t}{2}\right)^2 \cdot n(\lambda)_{Si} + \left(\frac{x_t}{2}\right) \cdot n(\lambda)_{SiO_2}}. \quad (4.7)$$

Figure 4.5 shows a comparison of the spectral index of refraction $n(\lambda)_{SiO_x}$ at different depths according to Eq. (4.7). For this calculation, the theoretical values for pure amorphous silicon [pal85] and Spectrosil 2000 from Heraeus [her10] were used.

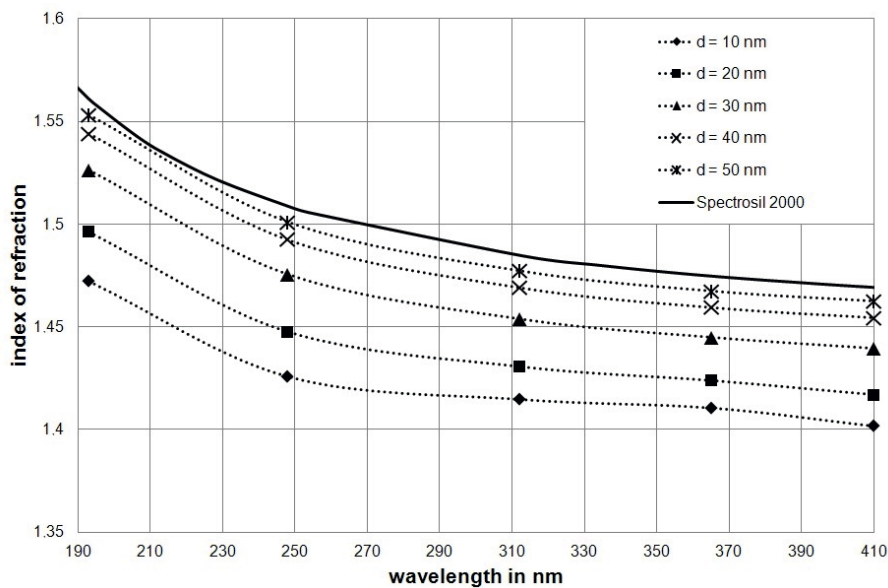


Fig. 4.5: Calculated indices of refraction of the SiO_x -layer in the UV-range at different depths of penetration

Applying Eq. (4.7) further allows determining the depth-resolved dispersion of the SiO_x -layer that can be calculated using the particular *Abbe*-numbers v_d according to

$$v_d = \frac{n_d - 1}{n_F - n_C}. \quad (4.8)$$

Here, n_d , n_F , and n_C are the respective indices of refraction at the Fraunhofer-lines d (587.6 nm), F (486.1), and C (656.3 nm), as listed in table 4.2.

Table 4.2: Indices of refraction of silicon and Spectrosil 2000 at the *Fraunhofer*-lines d , F , and C

	Si [pal85]	SiO_2 (Spectrosil 2000) [her10]
n_d	3.97600	1.45846
n_F	4.37944	1.46313
n_C	3.84164	1.45637

Figure 4.6 shows the resulting n_d - v_d -diagram. Here, the italic numbers indicate the particular depth in nanometers inside the reduced layer.

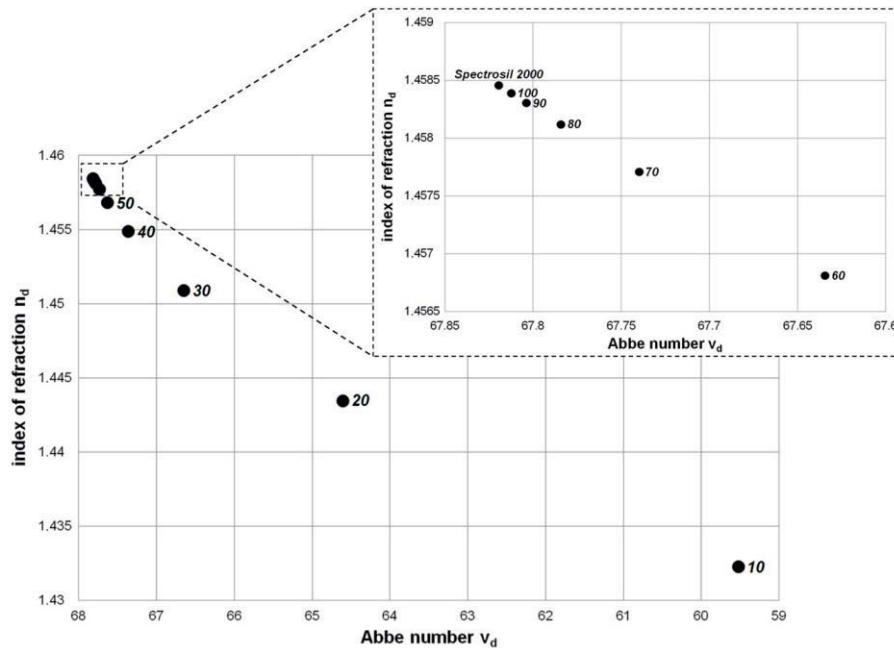


Fig. 4.6: Depth-resolved n_d - v_d -diagram of the plasma-treated near-surface layer of fused silica

The dependency of the depth-dependent *Abbe*-number from the index of refraction (and the depth of penetration, respectively) can be described by a parabolic function.

In addition to the formation of SiO_x , further near-surface effects result from the presented APPJ treatment. It is well known that in principle, hydrogen has a strong influence on the characteristic parameters of glasses [hic60, bol83, kit62]. For example, a marginal change of 10 ppm in the mass concentration of hydroxyl groups causes a change in index of refraction by $1 \cdot 10^{-6}$, and it was shown that such hydrogen-induced effects can also occur at a depth of several millimeters inside the bulk material [lev85].

In order to obtain further information on the penetration of hydrogen into the fused silica bulk material of the plasma-treated samples, its depth-dependent concentration C_H was measured using SIMS at an acceleration voltage of primary ions of 5 kV. The resulting crater size was $A = 0.0625 \text{ mm}^2$ and $d = 660 \text{ nm}$. For the measured depth, C_H was constantly increased by 34% in comparison to pure fused silica. Since hydrogen features a high diffusivity, its penetration depth can be assumed to reach up to several tens of microns. This magnitude is also confirmed when applying a first-order exponential fit to the measured concentrations. The initially presented measured reduction in transmission after plasma treatment can then be explained by the superposition of both the formation of a 100 nm layer of UV-absorbant SiO_x on the one hand and hydrogen diffusion into the bulk material and related effects on the other hand.

The presented plasma treatment using a cost-efficient and reliable APPJ allows a direct near-surface modification of SiO_2 -bulk material at atmospheric pressure and ambient temperature. For example, the resulting decrease in transmission can be applied for improving laser machining processes by the formation of a UV-absorbant SiO_x film in combination with an increased percentage of hydrogen in deeper regions of the bulk material. Such machining experiments were already carried out and will be presented in forthcoming work. Beyond, the near-surface layer features a gradient-like behavior in terms of both index of refraction and dispersion. This effect could, for instance, be applied for generating gradient index (GRIN) micro-optics.





Atmospheric pressure plasma treatment of fused silica, related surface and near-surface effects and applications

by C. Gerhard, T. Weihs, D. Tasche, S. Brückner, S. Wieneke, and W. Viöl,
published in *Plasma Chemistry and Plasma Processing* **33** (2013) 5, 895-905⁶

Abstract

We report on an atmospheric pressure plasma (APP) treatment of fused silica and its related surface and near-surface effects. Such treatment was performed in order to improve laser micro-structuring of fused silica by a plasma-induced modification of the glass boundary layer. In this context, an APP jet applying a hydrogenous process gas was used. By the plasma treatment, the transmission of the investigated glass samples was significantly decreased. Further, a decrease in the superficial index of refraction of approx. 3.66% at a wavelength of 636.7 nm was detected ellipsometrically. By surface energy measurements, a decrease of the surface polarity of 30.23% was identified. These determined modifications confirm a reduction of silicon dioxide to UV-absorbing silicon suboxide as already reported in previous work. Further, a change in reflexion by maximum 0.26% was detected which is explained by the superposition of constructive and destructive interferences due to a surface wrinkling. With the aid of atomic force microscopy, an increase of the surface root mean squared roughness by a factor of approx. 19 was determined. It was found that both the surface energy and the strength of the fused silica surface were reduced by the plasma treatment. Even though such treatment led to a clustering of carbonaceous contaminants, a surface-cleaning effect was confirmed by secondary ion mass spectroscopy and energy-dispersive X-ray spectroscopy. The increase in UV-absorption allows enhanced laser ablation results as shown in previous work.

Keywords

Atmospheric pressure plasma, glass, optical properties, surface modification

Introduction

Atmospheric pressure plasma (APP) has become a versatile and reliable tool for a number of surface treatment applications such as cleaning, etching or activation [bel08, ten06]. For example, applying APP-treatment allows a hydrophilisation due to the removal of carbonaceous contaminants in the case of soda-lime glass and borosilicate glass [sai05]. Such plasma-induced hydrophilisation of glasses facilitates improving the adhesion of coatings as for example polydimethylsiloxane (PDMS) [hon06]. On the other hand, APP can also be used for a hydrophobisation of glasses, for example for realising water-repellent windscreens [yam04]. Another application is the improvement of the efficiency of dye-sensitised solar cells (DSSC) by APP-generated functional groups on fluorine doped tin oxide (FTO) glass surfaces [kim11]. Dielectric barrier discharge (DBD) plasmas at atmospheric pressure and ambient temperature were already used for the modification of tin-doped indium oxide (ITO) on liquid crystal display (LCD)-glasses. In this context, an atmospheric pressure glow discharge was further used

⁶ Reproduced with kind permission from Springer Science+Business Media.

in order to remove organic contaminants from the ITO-coating [kim05]. High-frequency-APP can be applied for both sterilisation and decontamination of glasses that are used for medical engineering [sel01]. Further, the suitability of reactive APP for polishing silicon [wan06, zha08a] and glass [fan06a] surfaces was already shown.

Another widespread range of use of APP is the reduction of near-surface oxides to suboxides. In this context, silicon suboxide (SiO_x , where $1 < x < 2$) is of great interest for a number of applications due to its wide range of different possible optical and electrical properties [joh66, phi71, sch82]. Recently, the use of APP for generating UV-absorbing SiO_x -layers on fused silica (SiO_2) bulk material by chemical reduction was reported [ger12a]. The chemical reduction was achieved by applying a hydrogenous APP jet (APPJ) at ambient temperature. In the present paper, related surface and near-surface effects that are involved in such a plasma treatment are presented.

Experimental setup and experimentation

In this work, 5-mm thick fused silica samples made of Spectrosil 2000 from Heraeus were investigated. For the plasma treatment of the samples, a coaxial DBD-based low-potential APPJ was used [för05]. As shown in Fig. 4.7, this APPJ consists of a grounded cylindrical inner electrode and an outer high-voltage ring electrode.

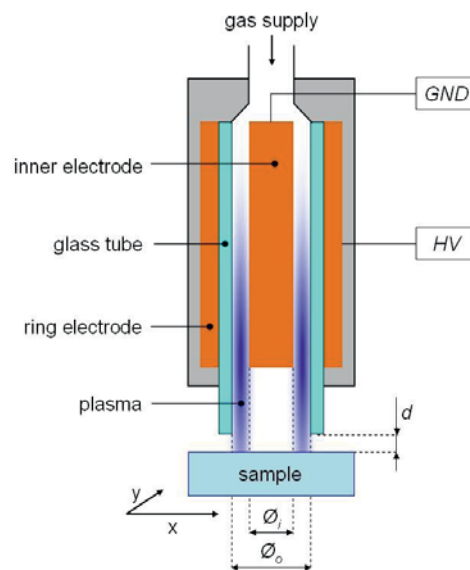


Fig. 4.7 Scheme of the used APPJ and plasma treatment

The dielectric separation of both electrodes is performed by a glass tube. Due to this setup, the source provides a ring-shaped plasma jet with an outer diameter \varnothing_o of 7 mm and an inner diameter \varnothing_i of 5 mm. In order to realise a uniform plasma treatment, the glass samples were placed on a motor-driven xy-linear stage. The resulting area of homogeneous treatment was 165 mm^2 with an overall treatment duration of 12 and 24 min, respectively. The distance d from the plasma jet outlet to the glass surface was 1 mm. For initialising the above-mentioned chemical reduction of the near-surface fused silica layer, forming gas 90/10 (90% nitrogen, 10% hydrogen) with a purity of 99.8% was used as process gas. During the experiments, the APPJ source was driven at a peak-to-peak voltage U_{p-p} of 22 kV with a voltage pulse duration t_{pulse} of 0.8 ms and a pulse repetition rate f_{pulse} of 400 Hz. By applying the *Lissajous* figure method [man43,



hel09], the plasma power can thus be determined to amount to 720 mW. Taking the effective ring-shaped plasma area into account the plasma intensity amounts to 3.8 W/cm^2 .

Results and discussion

Transmission, reflexion and index of refraction

Both the transmission and the reflexion of the investigated fused silica samples were measured before and after plasma treatment using an UV/VIS-spectrometer Lambda 650 from Perkin Elmer. As shown in Fig. 4.8, the plasma treatment led to a significant absolute change of transmission ΔT in the wavelength range of 190-410 nm.

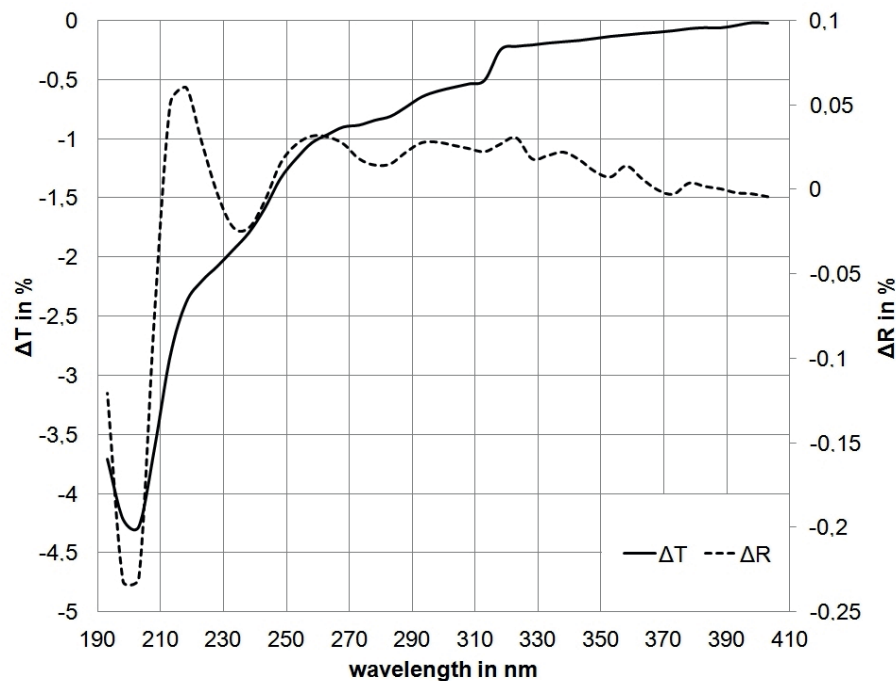


Fig. 4.8 Absolute change in transmission ΔT and reflexion ΔR after 12 min of plasma treatment

This decrease in transmission indicates a generation of UV-absorbing SiO_x due to the plasma treatment which was also confirmed in previous work by secondary ion mass spectroscopy (SIMS) measurements [ger12a]. The maximum change of -4.28% is found at approx. 200 nm. At this wavelength, the absolute change of reflexion ΔR amounts to -0.23% . In contrast to ΔT , the change of reflexion shows no continuous progression. Its most significant changes are found at approx. 200 and 220 nm respectively. In the measured wavelength range, the reflexion changes periodically with a maximum peak-to-peak value of 0.26% . Thus, the main fraction of decrease in transmission which is shown in Fig. 4.8 is not due to reflexion losses.

In previous work, the plasma-induced near-surface change in index of refraction Δn of fused silica was estimated by determining the depth-dependent stoichiometric ratio $x = C_{\text{O}}/C_{\text{Si}}$ of the concentrations C of both oxygen (O) and silicon (Si) and applying the resulting ratio x to the *Philipp's* interpolation formula [phi71]. With the aid of $n^2 \approx \epsilon$, this formula can be written as



$$n_{SiO_x} \approx \sqrt{\left(1 - \frac{x}{2}\right)^2 \cdot n_{Si} + \left(\frac{x}{2}\right) \cdot n_{SiO_2}}, \quad (4.9)$$

where n_{Si} is the index of refraction of pure amorphous silicon and n_{SiO_2} is the index of refraction of fused silica. For a 20-nm thick surface layer, which is within the range of penetration depth of the evanescent field of an incoming measuring light beam, the averaged change in index of refraction Δn_{av} at a wavelength $\lambda = 636.7$ nm amounts to -0.0549 according to Eq. (4.9). In order to verify this value, the plasma-induced change in index of refraction Δn was determined by measuring the Brewster angle at $\lambda = 636.7$ nm using an ellipsometer nanofilm_ep3se from Accurion. Here, a Δn of -0.0547 was detected. The marginal difference of both Δn_{av} and Δn of approx. 3.6% can be explained by measurement uncertainties of the used measurement equipment and slight variations in homogeneity of the different fused silica samples. However, this comparison exemplifies the reproducibility of the presented plasma treatment method for reducing the near-surface glass layer.

As reported in previous work, such APP treatment allows a considerable reduction of a near-surface layer within the fused silica bulk material. It was shown that after a plasma treatment duration of 12 min, the stoichiometric ratio x at a depth of 10 nm was decreased from 2 to 1.875 [hof12]. Such modification was also signified by X-ray photoelectron spectroscopy (XPS). Here, a continuous decrease in binding energy of the Si(2p) peak was observed when increasing the plasma treatment duration.

Besides the near-surface reduction of SiO_2 to SiO_x , the plasma treatment effects the implantation of atomic hydrogen into the glass bulk material as confirmed by SIMS measurements using a spectrometer Quadrupol 4550 from Cameca. Here, the acceleration voltage of primary ions U_{ac} was 5 kV; the sputtered crater area was 0.0625 mm² with a sputter depth of 660 nm. As shown by the concentration ratio of hydrogen of both treated and untreated fused silica H_t/H_{ref} in Fig. 4.9, the amount of hydrogen was constantly increased by the plasma treatment.

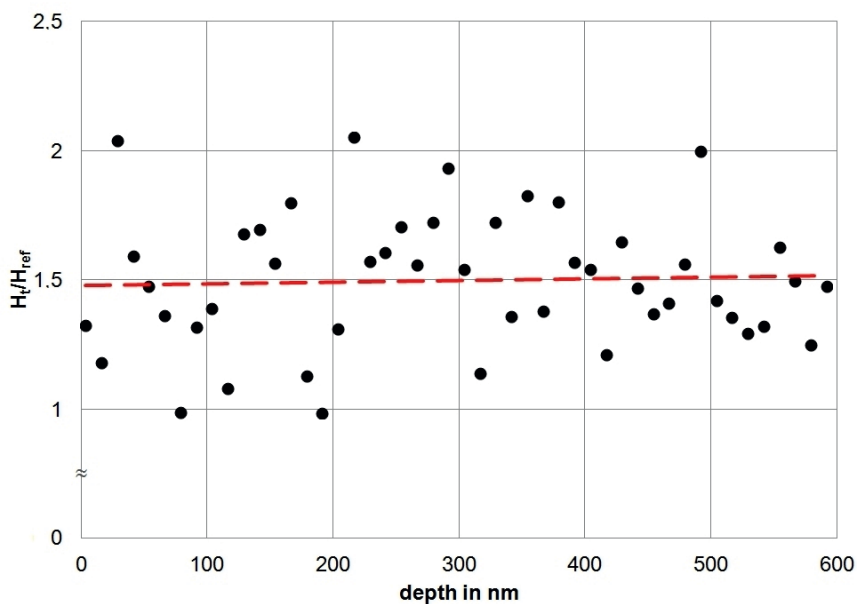


Fig. 4.9 Ratio of concentrations of hydrogen of treated and untreated fused silica including linear fit (dashed line)



In comparison to untreated fused silica, this increase amounts to approx. 34%. Such increase contributes relevantly to the above-mentioned decrease in transmission since implanted atomic hydrogen has a strong influence on the optical density of glasses [lev85]. Comparative investigations were also performed using pure nitrogen as process gas in order to consider the influence of the hydrogen involved in the used forming gas. For this purpose, a comparable APPJ source, but with adjustable cone-shaped electrodes, was applied in order to fulfil identical discharge conditions for the used gases according to *Paschen's* law. In the case of nitrogen, a significantly lower decrease in transmission was observed (i.e. approx. 3.5-times lower at a wavelength of 193 nm after a plasma treatment duration of 60 min), verifying the key function of hydrogen for the presented modification process. In addition, the time-dependency of the described process was investigated for both gases as shown in Fig. 4.10. Using forming gas as process gas, a continuous increase in UV-absorption A was determined, gaining a maximum saturation value A_{max} (193 nm) of approx. 45% after a plasma treatment duration of 98 min.

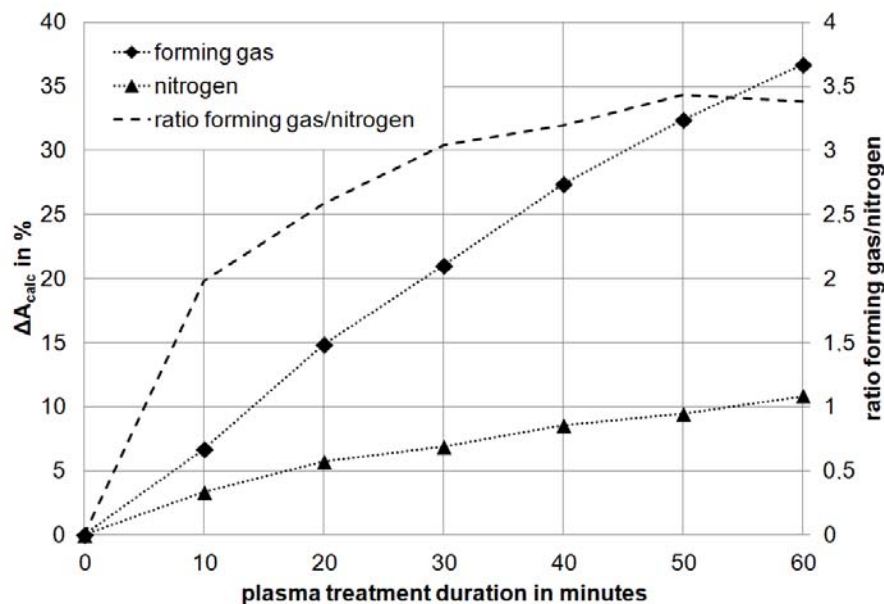


Fig. 4.10 Calculated change in absorption ΔA_{calc} versus plasma treatment duration for different process gases: forming gas 90/10 and nitrogen incl. ratio of both

It was shown that such plasma-induced decrease in transmission allows enhancing laser machining results of fused silica. Due to the improved laser energy deposition into the glass surface, which is explained by the plasma-induced increase in near-surface absorption, a high contour accuracy was achieved during ArF excimer laser ablation experiments using a mask projection. Further, the peak-to-valley height R_z of the ablated area was decreased by a factor of 2.3 whereas the ablation threshold was reduced by a factor of 4.6 in comparison to pure laser ablation when applying a plasma pre-treatment. It was shown that by a tempering process, the initial transmission characteristics of the plasma-treated samples could nearly be reconstituted [brü12].



Surface roughness

The above-mentioned non-continuous reflexion behaviour indicates a non-uniform surface wrinkling caused by the plasma treatment. In this context, the roughness of both the untreated and treated fused silica surfaces was measured using an atomic force microscope (AFM) easyScan 2 AFM from Nanosurf, applying a polynomial fit. For a measured area of $110 \times 110 \mu\text{m}$, the root mean squared roughness Rq of a treated surface amounts to 32-33 nm, whereas untreated surfaces feature a Rq of 1.7 nm. This reference value corresponds to the typical surface roughness of an optically polished glass surfaces. As shown by the comparison in Fig. 4.11, the AFM-measurements confirm a non-uniform surface wrinkling due to the plasma treatment.

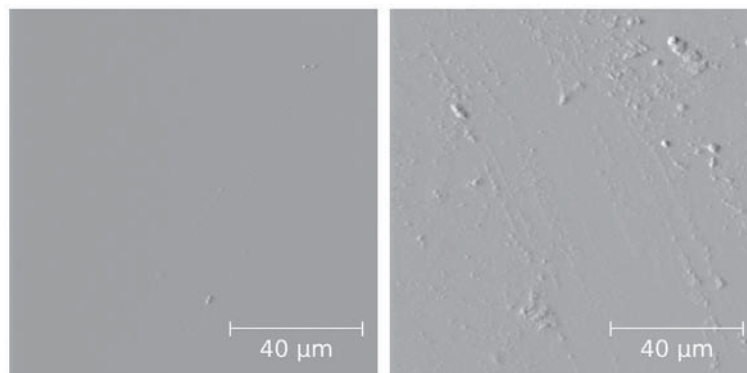


Fig. 4.11 AFM-topography maps of an untreated (left) and a plasma treated (right) fused silica surface

By sectioning the measured area and applying measuring zones of $10 \times 10 \mu\text{m}$, randomly distributed local roughnesses in the range from minimum 3.2 nm to maximum 112 nm were measured after plasma treatment. Thus, the measured non-continuous behaviour of reflexion after plasma treatment can be explained by the superposition of both constructive and destructive interferences caused by plasma-generated surface structures in the range of half and quarter the particular measuring wavelength. In some areas, the surface topography of the treated fused silica surfaces features a preferred orientation which can be explained by residues from the cleaning procedure. However, the plasma-induced structures are statistically distributed. Due to the negligible electron and ion densities of APPJs, this surface wrinkling is most likely not caused by ion bombardment. For the presented setup, the gas temperature corresponds to ambient temperature of approx. 27°C . Since the softening point of Spectrosil 2000 amounts to approx. $1,600^\circ\text{C}$ [her11], thermal effects can be excluded as well. Thus, the above-described chemical reduction leads to an inhomogeneous modification of the surface topography. Such surface wrinkling was already reported for the case of plasma oxidation processes [sch09]. In the present case, the observed wrinkling appears to be an effect arising from different reduction efficiencies for (a) the silicon dioxide sample material and (b) surface-adherent contaminations as discussed in ‘‘Surface Cleaning’’ section.

Surface energy and strength

In order to verify the chemical reduction and the related increase in UV-absorption by the plasma treatment, the polarity P of the glass surfaces before and after plasma treatment was determined from the surface energy γ_s and its polar fraction γ_s^P according to



$$P = \frac{\gamma_s^P}{\gamma_s}. \quad (4.10)$$

These values were measured by applying the Owens-Wendt-Rabel-Kaelble method [kae69, owe69]. Here, a contact angle measurement system G10 from Krüss was used. As shown by the measured values in table 4.3, the polarity is decreased by approx. 30% by the plasma treatment. This change verifies a chemical reduction as also observed by SIMS in previous work [ger12a] since a decreased polarity is directly related to a lower degree of oxidation.

Based on the surface energy measurements, the strength σ of the fused silica samples before and after plasma treatment was calculated by applying the *Griffith's* equation according to

$$\sigma = \sqrt{\frac{2 \cdot E \cdot \gamma_s}{d}}. \quad (4.11)$$

Here, E is the modulus of elasticity of Spectrosil 2000 ($= 7 \times 10^4 \text{ N/mm}^2$ [her11]) and d the depth of cracks on the glass surface [pau91]. For the optically polished sample surface, a typical crack depth of 30 nm was assumed. The calculated values are shown in table 4.3. In addition to a reduction of both the surface energy and the polarity, the strength of the glass sample is reduced by approx. 5%.

Table 4.3: Surface energy, polarity and strength of fused silica before and after plasma treatment

	γ_s (mJ/m ²)	P	σ (N/m ²)
Untreated	67.34	0.56	534.49
Plasma-treated	60.87	0.43	508.17

Surface cleaning

Besides the above-described phenomena, the plasma treatment also has a surface-cleaning effect. By SIMS-measurements ($U_{ac} = 1 \text{ kV}$), a significant plasma-induced decrease of the concentration of carbon in the near-surface region was detected as shown in Fig. 4.12.

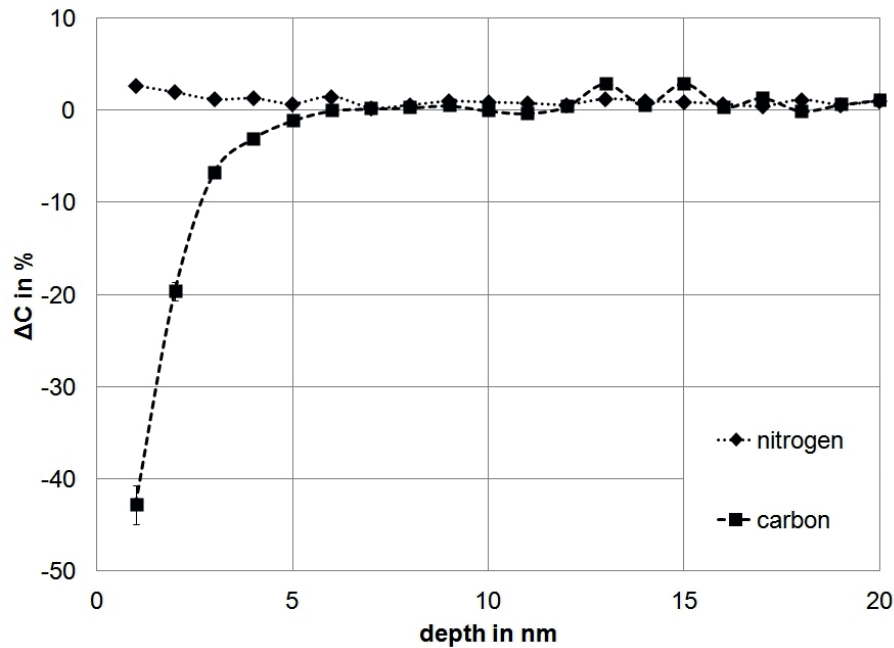


Fig. 4.12 Change of concentration ΔC of both nitrogen and carbon due to the plasma treatment, measured by SIMS

The slight increase of the near-surface concentration of nitrogen can be explained by accretion from the used forming gas. However, by energy-dispersive X-ray spectroscopy (EDX) using a scanning electron microscope (SEM) PSEM eXpress from Aspek, a number of carbonaceous clusters of several microns in diameter were detected close to the sample edge after plasma treatment as shown in Fig. 4.13.

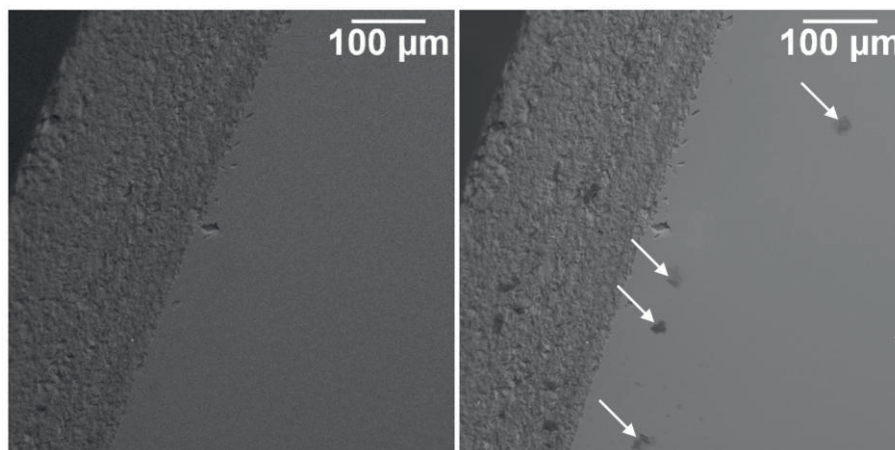


Fig. 4.13 SEM-image of the border area of a fused silica surface before (left) and after (right) plasma treatment including carbonaceous clusters

Such clusters contribute to the above-mentioned increase in surface roughness. The diminution of carbon on the glass surface seems thus to be due to a clustering of surface-adherent carbon. In other regions of the sample's border area, crystal-like aluminium-containing and agglomerated carbonaceous contaminants were detected before plasma treatment. After plasma treatment, these contaminants were removed as shown by the comparison of the SEM-images in Fig. 4.14.

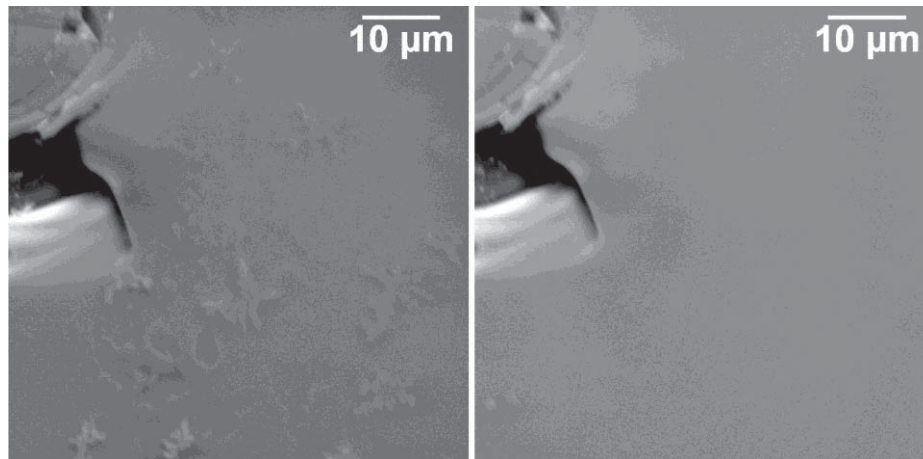


Fig. 4.14 SEM-image of the border area of a contaminated fused silica surface before (left) and after (right) plasma treatment

Apparently, the plasma treatment effected a removal of residues of aluminium oxide (Al_2O_3), a well-established polishing agent for finishing optical glass surfaces [bli08], which was remaining after the final polishing process of the fused silica surfaces. This diminution could be explained by a reduction of Al_2O_3 to aluminium according to



and/or



where electron-excited hydrogen molecules H_2^* and excited atomic hydrogen H^* are provided by the forming gas plasma and a subsequent removal of molecular aluminium by the process gas flow. The possibility of such plasma-based reduction of Al_2O_3 was already investigated in order to improve material characteristics [lyu00, rai70]. Anyhow, the efficiency of plasma-chemical reduction can be estimated to be significantly lower in case of Al_2O_3 with respect to SiO_2 due to the considerable differences in bond strength of both oxides. In terms of standard enthalpy of formation ΔH_f^0 , this difference amounts to a factor of 1.8 ($\Delta H_f^0(\text{SiO}_2) = -899.91$ kJ/mole; $\Delta H_f^0(\text{Al}_2\text{O}_3) = -1,632.85$ kJ/mole [lid91]). The oxide-dependant degree of chemical reduction could contribute to the observed increase in surface roughness since the randomly distributed aluminium-containing residues show irregularly-shaped structures with some microns in diameter (compare Fig. 4.14, left). As a result, the efficiency of reduction on the sample surface is comparatively randomly distributed which is also confirmed by the random distribution of local roughnesses as presented in ‘‘Surface Roughness’’ section. Generally, due to the high depth of penetration of the measuring electron beam that is used for EDX, very thin films cannot be detected. On the basis of the extreme chemical reactivity of aluminium it can thus be assumed that a thin layer of aluminium oxide is remaining on the glass surface.



Conclusions

The measured decrease in transmission and the resulting increase in UV-absorption allow a higher coupling of laser irradiation into the fused silica surface. In addition, the required energy for breaking the linkage of the fused silica surface is decreased due to the plasma-induced surface activation as shown by the decrease of both the surface energy and the strength. In this context, the resulting surface wrinkling could be an advantageous effect in order to obtain a higher coupling of laser energy into the glass surface by multiple reflexions. In addition, the surface cleaning effect of the applied plasma could be used for removing residues of polishing and cleaning agents from sensitive UV-optics surfaces. Against this background, further experiments such as XPS and UPS analysis will be performed in order to investigate this cleaning effect, and particularly the presence of a thin aluminium oxide layer, as well as the surface modification in more detail.



4.2 Plasma treatment during simultaneous ablation

The effect of the plasma treatment which was applied during simultaneous plasma-assisted laser ablation, introduced in chapter 3.2, was investigated for different optical glasses and media. In contrast to the plasma pre-treatment as discussed in the previous section, the treatment led to a considerable smoothing of rough surfaces [ger13c]. Qualitatively, such smoothing was independent from the sample material and could also be confirmed for ceramics in further work [ger13d]. It can thus be stated that a certain selective material removal, i.e. the abrasion of roughness peaks, was obtained by the used comparatively low-energetic argon plasma beam. Here, high electric field strengths at these roughness peaks can be offered to be the underlying mechanism as also supported by simulation results. The plasma-induced material removal is even increased during simultaneous ablation as discussed later in chapter 6, most likely due to further arising plasma-physical processes.

The observed plasma-induced smoothing presented in this section has considerable relevance for the topic of the present work. Particularly with regard to an integrated ablation process of optical glasses for the realisation of high quality (UV-) optical components as suggested in chapter 8, surface smoothing is of great interest in order to minimise scatter. By a further running of the plasma source for a short time (some minutes) after the actual simultaneous ablation process, the ablated area could be finished applying the effect described in the following article.





Polishing of optical media by dielectric barrier discharge inert gas plasma at atmospheric pressure

by C. Gerhard, T. Weihs, A. Luca, S. Wieneke, and W. Viöl,

published in *Journal of the European Optical Society: Rapid Publications* **8** (2013) 13081 (5pp)⁷

Abstract

In this paper, surface smoothing of optical glasses, glass ceramic and sapphire using a low-power dielectric barrier discharge inert gas plasma at atmospheric pressure is presented. For this low temperature treatment method, no vacuum devices or chemicals are required. It is shown that by such plasma treatment the micro roughness and waviness of the investigated polished surfaces were significantly decreased, resulting in a decrease in surface scattering. Further, plasma polishing of lapped fused silica is introduced. Based on simulation results, a plasma physical process is suggested to be the underlying mechanism for initialising the observed smoothing effect.

Keywords

Atmospheric pressure plasma, polishing, optical glasses, glass ceramic, sapphire, scattering

Introduction

For a number of high-end systems and devices such as laser sources, UV lithography optics and high performance mirrors, precisely-shaped and -polished optics surfaces are required. Against this background, precision polishing of relevant optical media is of great interest in order to realise surface roughnesses in the nanometre or even angstrom range. Such precision smoothing can be achieved by classical polishing using pitch tools and a polishing agent, i.e. a suspension of water and fine abrasives [coo90]. However, this technique is usually limited to spherical and plane surfaces. Polishing of glass surfaces is also achieved by laser-induced heating above the glass transition temperature. As a result of the accompanying decrease in viscosity, material flow due to surface tension mechanisms occurs [bue90]. Here, carbon dioxide (CO₂) lasers are usually employed due to the improved energy coupling at glass surfaces at this particular laser wavelength of 10.6 μm. Beyond laser processing, atmospheric pressure plasmas (APP) are suitable for thermally-induced polishing of rough glass surfaces. Paetzelt et al. reported such polishing of fine ground fused silica by a microwave-powered APP jet source where a mixture of argon and helium was used as process gas. Applying this technique at a microwave power of 135 W, the surface arithmetic mean roughness *Ra* was significantly decreased from 550 nm to 0.64 nm due to a surface heating to 1900 K [pae13]. Polishing of glasses and silicon (Si) -based media in general at low temperature can be performed by APP techniques using fluorine (F)-containing process gasses. Here, material removal is achieved by chemical reactions according to

⁷ Reproduced with kind permission from the European Optical Society.



and



respectively. Applying this technique, *Zhang et al.* accomplished smoothing of silicon surfaces where a reduction from 2.39 to 1 nm (root mean squared roughness Rq) and 1.76 to 0.63 nm (Ra) was achieved [zha08a]. A reduction in surface roughness was also reported in the case of plasma jet machining of silicon carbide (SiC) surfaces [arn10]. *Yao et al.* and *Jin et al.* presented plasma machining of Zerodur[®] using a RF-excited plasma jet at atmospheric pressure. It was shown that the surface roughness was strongly dependent on the process parameters and in particular on the mixing ratio of the working gas, SF₆ and O₂ [yao10, jin10]. However, such plasma figuring methods can provoke surface roughening due to inhomogeneous etching, an effect which was also observed in the case of reactive ion etching (RIE) of pyrex glass [li01]. Such roughening can be overcome by the choice of the applied gas mixture in order to mitigate the sputter effect of heavy ions from the inert gases [li03a].

Against this background, atmospheric pressure plasma polishing of different technically relevant optical media is presented in this contribution. Here, the goal was not to perform any surface figuring but to provide a novel technique for surface smoothing based on a chemically neutral APP. In contrast to existing APP techniques, surface smoothing was achieved at low temperature below 100°C and low power without applying any reactive process gas mixtures.

Experimental setup and procedure

Plasma polishing experiments were performed on optically polished plane samples made of fused silica Suprasil 3, boron crown glass BK7, glass ceramic Zerodur[®] and sapphire. These materials are well-established and commonly used for the realisation of high precision optical devices as for example, in case of fused silica and sapphire, UV optics. In this context, precision polishing and finishing in the (sub)nanometer scale is of great interest in order to reduce scattering and interreflection effects. For plasma polishing of these optical media, a dielectric barrier discharge (DBD) at atmospheric pressure was applied using a rotational-symmetric cone-shaped plasma source [brü11, viö11]. As shown in Figure 4.15, this plasma source consists of an internal high-voltage (HV) electrode and an external ground (GND) electrode. The dielectric separation of both electrodes was realised by the particular sample itself, where the effective discharge gap d_{eff} was 21 mm.

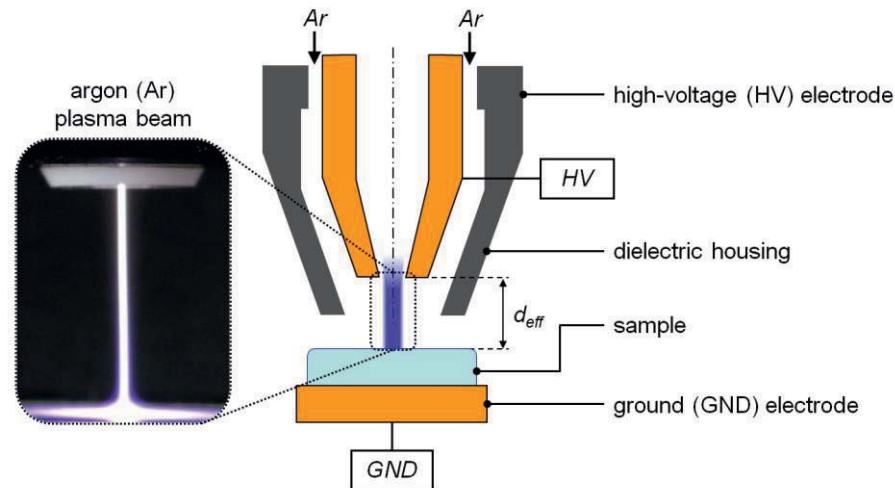


Fig. 4.15 Experimental setup for APP polishing of optical media

By the process gas flow, i.e. argon (Ar) 4.6 from Linde at a flow rate of 4 standard litres per minute (slm), a stable compressed plasma beam with an $1/e^2$ diameter of approx. $200\ \mu\text{m}$ was formed within the discharge gap (compare inset in Figure 4.15). However, the resulting plasma tracing point on the sample surface showed a surface discharge-like behaviour due to an accumulation of charge carriers. This tracing point was several millimetres in diameter, featuring a Gaussian rotation symmetric intensity distribution as confirmed by high-speed camera measurements. During the experiments, neither the plasma source nor the sample was moved. The plasma source was driven at a pulse repetition rate f_{rep} of 7 kHz with an averaged plasma power P_{av} of 1.19 W. Taking the applied plasma energy of 0.17 mJ for each HV-pulse train with a duration of approx. $80\ \mu\text{s}$ into account, the fluence per pulse within the plasma beam can be calculated to amount to $540\ \text{mJ}/\text{cm}^2$. As ascertained by spectroscopic measurements, the electron temperature was approx. 1 eV. Plasma treatment was performed in steps of 30 seconds up to a total treatment time of 90 seconds (boron crown glass, glass ceramic) and 150 seconds (fused silica, sapphire), respectively. For each step, both the arithmetic mean roughness Ra and the root mean squared roughness Rq were measured by the use of an atomic force microscope (AFM) easyScan 2 AFM from Nanosurf where the measured area was $50 \times 49.5\ \text{m}^2$.

For comparison, plasma polishing using argon as process gas (flow rate = 0.9 slm) was also performed on lapped fused silica surfaces. Here, the plasma beam diameter was approx. $500\ \mu\text{m}$ whereas the effective discharge gap amounted to 14.5 mm. The fluence per pulse was $15\ \text{mJ}/\text{cm}^2$. Plasma treatment was carried out in steps of 10 minutes up to a total treatment time of 60 minutes. In addition to the roughness parameters Ra and Rq , the transmission T was measured after each step using an UV/VIS-spectrometer Lambda 650 from Perkin Elmer.

Results

By the plasma treatment as described above, significant topographic surface modifications of the investigated optical media were achieved. As shown in Figure 4.16 and listed in table 4.4, Ra was continuously decreased with increasing plasma treatment duration. The same effect was observed for Rq .

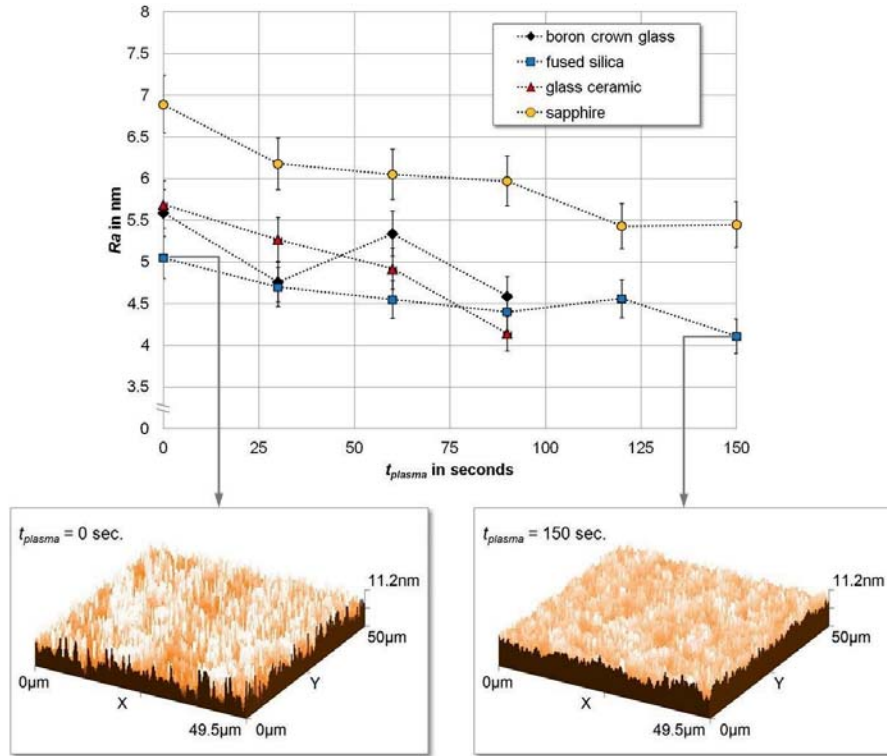


Fig. 4.16 Arithmetic mean roughness Ra of different optical media vs. plasma treatment duration t_{plasma} including 3D AFM views of polished fused silica at $t_{\text{plasma}} = 0$ (left) and 150 (right) seconds

Table 4.4: Absolute change Δ in arithmetic mean roughness Ra and maximum depth of waviness w_d after particular overall plasma treatment duration

	ΔRa (%)	Δw_d (%)
boron crown glass	-17.9	-31.6
fused silica	-18.6	-81.3
glass ceramic	-27.2	-69.8
sapphire	-20.9	-38.8

Such surface smoothing of optical glasses was already observed in previous work where the same plasma source and treatment procedure was applied to barite crown glass N-BaK4 and heavy flint glass SF5. After a plasma treatment duration of 60 seconds, Ra was reduced by 7.8% (N-BaK4) and 59.7% (SF5), respectively [ger12b]. Generally, a reduction in surface roughness comes along with a decrease of the surface contact angle, corresponding to an increase in total surface energy γ_s [law99]. Against this background, γ_s was measured using a Contact Angle Measurement System G10 from Krüss. For instance, γ_s of fused silica was increased from 68.66 mJ/m² to 72.69 mJ/m² (i.e. +5.9%) after a plasma treatment duration of 60 seconds, verifying the observed surface smoothing at this instant of time ($\Delta Ra = -9.9\%$ and $\Delta Rq = -7.5\%$). Moreover, no mentionable change in the polar fraction of the total surface energy was detected. Since this



parameter is directly related to the molecular structure and orientation of near-surface bonds within the sample bulk material it can thus be stated that no modification in chemical and, as a consequence, optical properties occurred due to the plasma treatment.

In addition to the roughness parameters, the waviness w as well as the maximum depth of waviness w_d was extracted from the AFM profiles using the evaluation software Gwyddion from the Department of Nanometrology of the Czech Metrology Institute. Here, the measuring length l_{meas} was $70\ \mu\text{m}$, i.e. the diagonal of the overall measured area. As also observed in the case of roughness parameters, the depth of waviness of the investigated optical media was reduced continuously by the plasma treatment as shown in Figure 4.17.

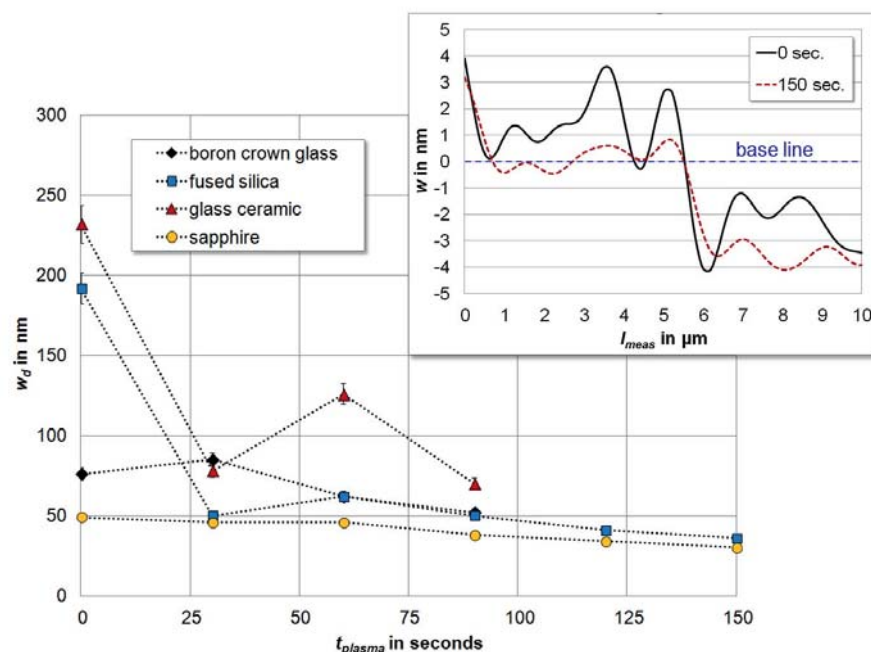


Fig. 4.17: Maximum depth of waviness w_d of different optical media vs. plasma treatment duration t_{plasma} , inset: example for waviness w of polished fused silica at $t_{plasma} = 0$ and 150 seconds vs. measuring length l_{meas}

According to DIN 4760, the surface roughness is a 3rd and 4th order irregularity of form whereas the waviness represents a 2nd order form deviation. It can thus be stated that as a result of the plasma treatment not only high order but also low order irregularities were decreased as listed in table 4.4.

For comparison, plasma polishing was also carried out on lapped fused silica surfaces with a comparatively high initial surface roughness. As shown in Figure 4.18, a considerable decrease in surface roughness was achieved by such plasma treatment. Consequently, the transmission T was progressively increased.

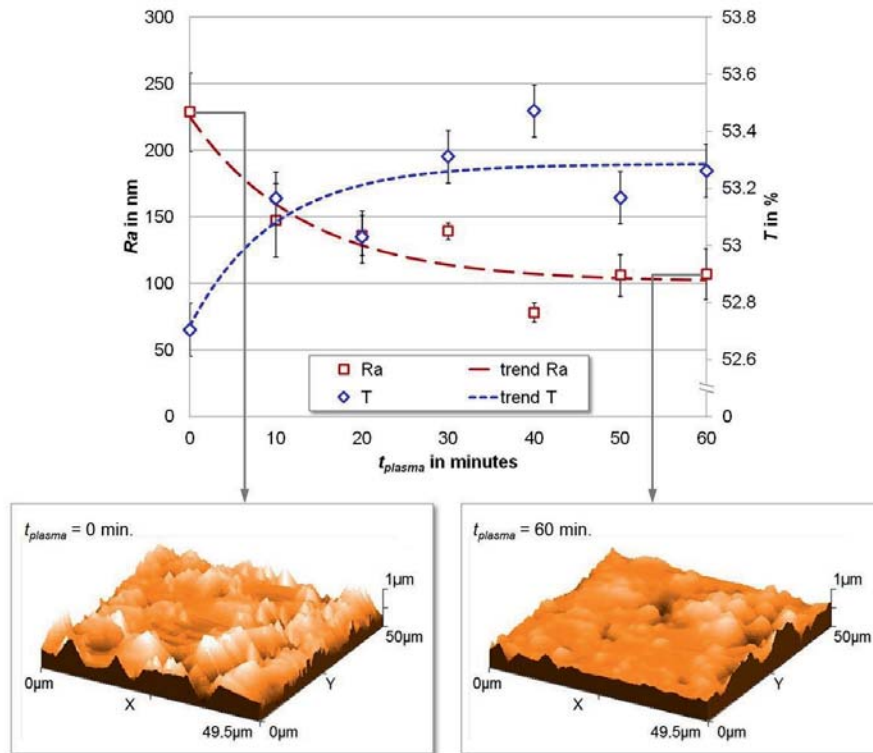


Fig. 4.18: Comparison of the arithmetic mean roughness Ra and the transmission T ($\lambda = 193$ nm) of a lapped fused silica sample vs. plasma treatment duration t_{plasma} including 3D AFM views of lapped fused silica at $t_{\text{plasma}} = 0$ (left) and 60 (right) minutes

The increase in transmission as a result of the reduction of diffuse reflection on the rough fused silica surface is further supported by the measured decrease in waviness by a factor of 4.8 after a plasma treatment duration of 60 minutes. The observed decrease in both surface roughness and waviness of polished and lapped surfaces clearly indicates a selective material removal of roughness peaks and contour maxima by the plasma treatment.

Discussion

In previous work, the heating of a glass sample surface exposed to the used plasma beam was measured using an infrared camera VarioCAM[®] from InfraTec/Jenoptik. Here, a surface temperature of 88°C was determined [gre13]. Since this temperature is significantly below the softening temperature of the investigated media, thermal smoothing due to surface melting (which is the underlying mechanism in the case of laser-induced surface smoothing) can be excluded in the present case. The presented method thus differs significantly from thermal APP jet polishing as reported by Paetzelt et al. [pae13] (compare introduction section). The observed decrease in surface roughness and waviness is rather explained by plasma physical effects. In principle, the concentration of argon plays an important role for plasma etch mechanisms. Li et al. showed that during etching of fused silica by the use of fluorine-based plasmas, an increase in argon concentration allows increasing the etch rate [li03b]. For pure silicon, Coburn and Winters observed certain etching by pure argon ion bombardment [cob79]. Against this background, the presented surface smoothing using argon as inert process gas can be explained by different mechanisms: First, a slight argon ion bombardment by reason of the formation of plasma sheath at the sample surface, resulting in an accelera-



tion of ions towards the surface [lan23], can contribute to material removal. Second, material removal can be due to the de-excitation of excited argon and metastable argon species and an accompanying energy transfer to the sample surface. Here, the possible underlying effects are electron quenching, two- and three-body collisions with argon atoms and *Penning* ionisation at the sample surface [ger12b]. The existence of such species in the near-surface area can most likely be assumed due the direct plasma ignition on the substrate based on electron excitation and ion-impact excitation in the plasma sheath close to the sample surface [bag05] and/or resonant neutralisation. In the last case, argon metastables are provided as a result of the recombination of argon ions with the negative surface charge on the dielectric sample [nie12]. However, both effects, ion bombardment and de-excitation of argon species, should result in an almost uniform material removal. Due to the selective removal of surface texture maxima it can thus be assumed that the plasma discharge causes high electric field strengths at roughness peaks, initialising the observed erosion effect. This assumption was confirmed by a simulation of the distribution of the electric field strength on a rough dielectric surface within a parallel-plate capacitor, which is an appropriate model for the plasma discharge used in the present work. Such simulation was performed using the COMSOL Multiphysics software. The simulated dielectric was fused silica with different micro volume elements (i.e. hemispheres with radii r in the range from 1 to 100 nm and a pyramidal peak with a height h of 150 nm and a point angle α of 30°), representing the roughness and waviness profile. As shown in Figure 4.19, the highest electric field strengths are found on the top of the particular volume elements whereas low electric field strengths occur within the valleys in between roughness peaks and surface texture maxima, respectively.

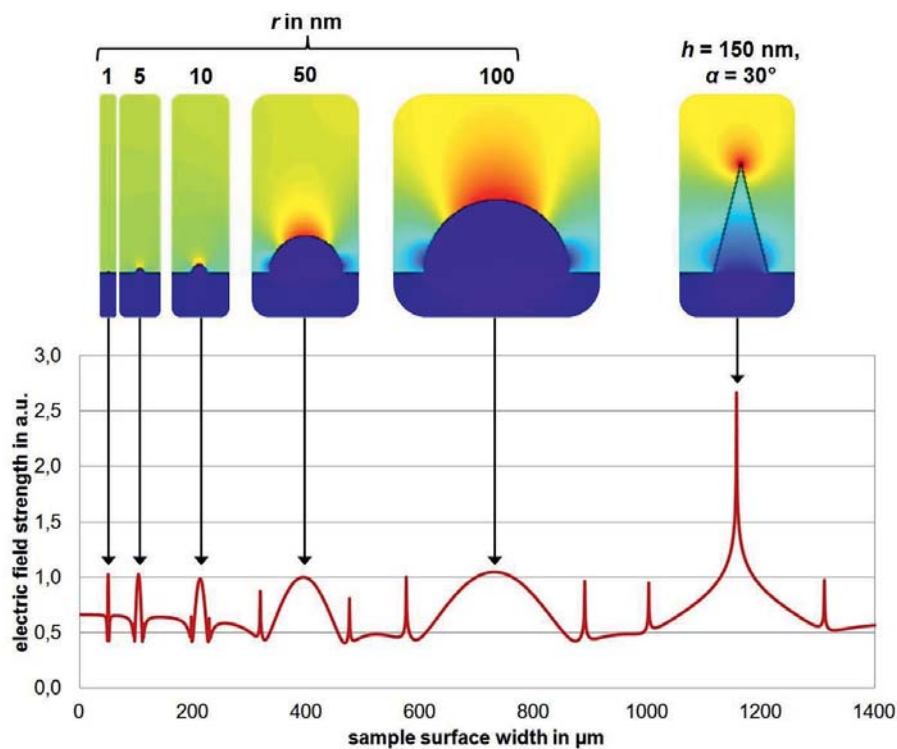


Fig. 4.19 Qualitative distribution of the electric field strength on a dielectric surface (bottom) with micro volume elements (top)



This simulated behaviour confirms a selective material removal of maxima at rough and wavy surfaces. An increase in electric field strength due to an increased electrode surface roughness, initialising an additional potential, was also already reported by *Zhao et al.* on the example of a parallel-plate capacitor [zha99b]. The above-presented surface smoothing of polished optical media has a considerable impact on surface scatter characteristics. Basically, the amount of light scattered at a technical surface can be calculated from its root mean squared roughness Rq by applying the total integrated scatter (*TIS*) which is given by

$$TIS = 1 - e^{-\left(\frac{4\pi \cdot Rq \cdot \cos AOI}{\lambda}\right)^2} \quad (4.15)$$

Here, *AOI* is the angle of incidence of the incoming light and λ its wavelength [ben61]. As an example, at perpendicular incidence ($AOI = 0$) and a wavelength of 546 nm, *TIS* was reduced by a factor of 1.08 (boron crown glass), 1.17 (fused silica), 1.62 (glass ceramic) and 1.38 (sapphire), respectively, after a plasma treatment duration of 60 seconds. Regarding the quality of imaging optics, such decrease in surface scattering generally improves the contrast ratio. The observed decrease in waviness further contributes to a reduction of blurring. As a result of these plasma-induced surface effects, the modulation transfer function (MTF) of an optical system could be improved by the presented method. Moreover, image distortions could be mitigated in consequence of the diminution of form deviations.

Conclusions

The presented low-power plasma polishing technique allows a considerable surface smoothing of different optical media of high technical relevance. In the case of polished surfaces, a reduction in surface roughness by approx. 18-28% was achieved. In contrast to other precision polishing techniques using lasers or hot plasmas, surface smoothing is not induced by heating. Thermally-induced disturbing effects such as stress birefringence are thus avoided. The presented method could be applied for post-processing and finishing of high-end optics after precision figuring, for example by RIE or ion beam etching (IBE) methods in order to reduce surface scattering. However, relatively high final roughness values were achieved in comparison to other techniques which are based on thermally-induced mechanisms. Further, the observed removal of roughness peaks approaches a certain saturation which can be explained by the smoothing process and the accompanying increasing uniformity of the electric field strength distribution. In ongoing work, the variation of crucial plasma parameters will thus be investigated in order to improve the process efficiency and to evaluate the limits of this method. Here, a continuous and regulated increase in voltage during the plasma polishing process is of essential interest to maintain the required high electric field strengths on the top of the continuously shrinking roughness peaks and waviness maxima. Owing to the advantage of a negligible substrate heating due to the used dielectric barrier discharge, which is commonly referred to as a cold plasma, the treatment of temperature-sensitive optical media and materials such as coatings is made possible by the presented method. The smoothing of such surfaces will be investigated in the near future.







Sequential Plasma-Assisted Laser Ablation

In this chapter, the impact of plasma pre-treatment as introduced in section 4.1 on subsequent laser ablation of glasses is presented. The main advantages of such sequential plasma-assisted laser ablation, i.e. a reduction in ablation threshold, form error, surface roughness and the mitigation of debris are shown and discussed.

The plasma-induced changes in optical properties, and especially the increase in absorption as presented in section 4.1, have a strong impact on subsequent laser ablation of plasma pre-treated glasses. Such sequential plasma-assisted ablation, hereinafter called seqPAA, was performed on fused silica and heavy flint glass. For this purpose, appropriate laser wavelengths were chosen depending on the transmission characteristics of the particular glass.

In the case of ablation of fused silica at a laser wavelength of 193 nm, the ablation threshold fluence was significantly decreased in relation to pure laser ablation. Further, both the contour accuracy and the roughness of the ablated areas were increased [brü12, hof12]. A reduction in the ablation threshold and an increased contour accuracy were also observed in supplementary work where seqPAA of fused silica was performed at a laser wavelength of 266 nm (4th-harmonic Nd:YAG solid state laser) [ger12c].

Another expedient effect of seqPAA is the mitigation of debris which was observed in the case of heavy flint glass at a laser wavelength of 355 nm. Even though the plasma pre-treatment resulted in a slight decrease in transmission in comparison to fused silica, the contour accuracy of the ablation spots was also notably increased. These results were published in the research articles embedded in this chapter.

These observed enhancements can be explained by the above-discussed plasma-induced effects discussed in section 4.1, i.e. the formation of UV-absorbant silicon suboxide, the implantation of hydrogen and a surface roughening, giving rise to an improved coupling of laser irradiation into the glass surface during the first few laser pulses. However, the ablation rate during seqPAA was found to be constant for higher numbers of pulses (up to 35) and approx. 1.5-times higher than in the case of untreated fused silica. This behaviour indicates the importance of implanted hydrogen in deeper regions of the bulk material to the ablation process and can be explained as follows:

In supplementary, previously unreleased work in cooperation with the Laser Laboratorium Göttingen e.V and the Fraunhofer Institute for Surface Engineering and Thin Films IST, SIMS was performed on the bottom of ablated spots on both plasma pre-treated and untreated fused silica. It was found that in the first case, a suboxiadial layer with an averaged O/Si-ratio of 1.44 and a thickness of approx. 80 nm was formed after each laser pulse. In contrast, this effect was marginal for untreated fused silica, where O/Si



was 1.92. It can thus be assumed that the implanted hydrogen acts as reaction partner for oxygen from the network-forming silicon dioxide, where the chemical reaction is provoked by laser-induced heating. As a result, an UV-absorbing suboxidial layer is formed by each single laser pulse, facilitating the coupling of the following laser pulse.

Such successive formation of SiO_x also impacts laser ablation using infrared picosecond laser irradiation as observed in supplementary, un-published work in cooperation with Trumpf GmbH & Co. KG. Here, seqPAA was carried out on fused silica employing an Yb:YAG laser with a pulse duration of 6 ps and a wavelength of 1030 nm. In comparison to pure fused silica, higher ablation rates were obtained by seqPAA. However, no plasma-induced increase in absorption was observed at this wavelength. An enhanced evaporation-based ablation mechanism by a pure increase in absorption and the accompanying improved heating of the sample material (as in the event of nanosecond ablation) can thus be excluded as the main underlying effect. The increase in ablation depth rather turns out to be due to the comparatively short pulse duration. As introduced in section 2.2, ultra-short pulse laser ablation is described by a two-temperature model. For the first step of this model, i.e. the interaction of the incoming laser pulse and the electrons of the substrate material, the band gap of the sample material is of essential importance, where the required laser energy for material removal is reduced for lower band gaps [gat08]. As a result of the chemical composition of silicon suboxide, its band gap is lower than in the case of silicon dioxide. For instance, *Bar-ranco* et al. reported particular band gaps of 3.8 eV for $\text{SiO}_{1.3}$, 4.4 eV for $\text{SiO}_{1.5}$, 5.0 eV for $\text{SiO}_{1.7}$, and 8.7 eV for SiO_2 [bar05]. It can thus be stated that in the case of picosecond ablation, the observed increase in ablation depth is most likely due to the plasma-induced chemical reduction of the near-surface bulk material region and the accompanying lowering of its band gap.



Hybrid laser-plasma micro-structuring of fused silica based on surface reduction by a low-temperature atmospheric pressure plasma

by S. Brückner, J. Hoffmeister, J. Ihlemann, C. Gerhard, S. Wieneke, and W. Viöl, published in *Journal of Laser Micro/Nanoengineering* 7 (2012) 1, 73-76⁸

Abstract

In this contribution, we report on a novel hybrid laser-plasma method for material processing applications. This method is based on the combination of both an ArF excimer laser ($\lambda = 193$ nm) and a low-temperature atmospheric pressure plasma jet source for the chemical reduction of glass surfaces. Here, a hydrogen-containing plasma gas was applied. Due to the layer of silicon suboxide that is generated in this vein, the absorption of the incoming machining laser beam is significantly increased after 15 minutes of plasma-treatment. Several machining experiments in terms of front-side ablation were performed on fused silica. Here, both pure and plasma-treated surfaces were ablated using single laser pulses with a pulse duration of 20 ns. By introducing the presented hybrid technique, the ablation threshold for micro-structuring was reduced significantly by a factor of 4.6 whereas the peak-to-valley height R_z of the machined area was decreased by a factor of 2.3. Further, back-side ablation using the presented method was considered. By a terminal tempering process, the initial transmission characteristics of fused silica can be reconstituted.

Introduction

Due to its specific properties, fused silica is a well-established and suitable optical medium for the production of a variety of optical components such as UV-transparent optics, semiconductor devices and integrated micro-optical elements. Regarding laser based methods for the manufacture of such components, material removal of fused silica and glasses in general can be achieved by several techniques such as laser ablation using UV-, IR- or NIR-laser radiation [ihl92b, ger08, bue90], or laser induced backside wet etching [wan99, sat10]. Further, laser induced etching techniques introducing UV-absorbing films such as toluene [zim04] and carbon [böh06a] or laser induced plasma-assisted ablation [zha98a] can be applied. Beyond, an indirect processing method of fused silica surfaces consists of the vacuum deposition and laser structuring of UV-absorbing silicon suboxide layers (SiO_x) and their subsequent oxidation to SiO_2 [sch05b]. Also, since fused silica consists of pure silicon dioxide (SiO_2), its surface can be directly reduced to silicon suboxide (SiO_x , where $1 < x < 2$) or silicon monoxide (SiO) by applying hydrogenous gases at high temperatures [tso82].

The presented hybrid laser-plasma removal method is based on the surface reduction of fused silica by a low-temperature atmospheric pressure plasma and a subsequent laser ablation. To our best knowledge, this is the first work on surface processing of fused silica using such a plasma source. In contrast to the pulsed laser deposition method (PLD) [lac03] or the deposition of metastable silicon suboxide by vacuum evaporation [sch05b], the introduced plasma generates atomic hydrogen from the used forming gas

⁸ Reproduced with kind permission from the Japan Laser Processing Society.

which directly generates a suboxidal layer onto the fused silica substrate. This effect allows a significant decrease in required energy for laser ablation of fused silica.

Experimental setup and experimentation

For the plasma-treatment of the investigated 2 mm-thick fused silica samples, a low-temperature potential-free atmospheric pressure plasma jet “kinpen 09” from neoplas tools GmbH was applied. The plasma source was directed perpendicular onto the sample’s surface. During the plasma-treatment, the samples were moved by a xy-linear stage. The working distance of the plasma jet nozzle to the fused silica surface was 1 mm. In order to initialise the reduction process, forming gas 90/10 (consisting of 90% nitrogen and 10% hydrogen) was used as working gas. The treatment time at each point of the sample surface was varied in the range from 0 to 15 minutes with a gas flow rate of 25 slm. After 5 and 15 minutes, transmission spectra (including reflexion losses) were taken in order to verify the reduction progress with respect to a pure fused silica sample.

The subsequent laser ablation was performed after a maximum plasma-treatment duration of 15 minutes using an ArF excimer laser “LPX 315” from Lambda Physik ($\lambda = 193$ nm). By an optical setup, consisting of two convex lenses ($f_1 = 750$ mm, $f_2 = 100$ mm), a mask imaging was realised in order to image a diaphragm on the fused silica sample’s surface as shown in figure 5.1.

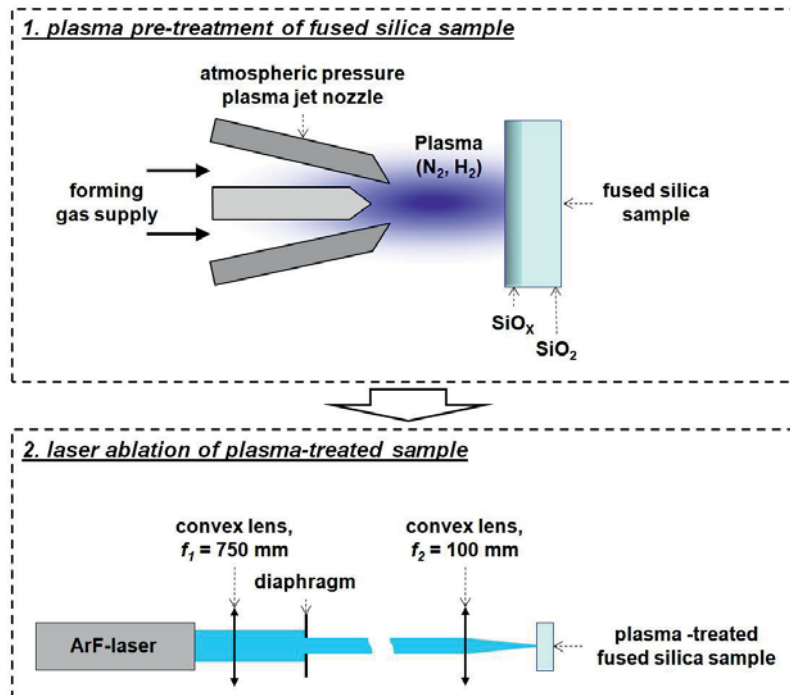


Fig. 5.1: Schematic and functional principle of the setup for plasma pre-treatment and subsequent front-side ablation of fused silica

The aperture of this diaphragm was 3 mm. The demagnification was about 15-times, leading to an irradiated spot of about 200 μm in diameter on the front-side of the sample. In addition to this standard front-side configuration, some experiments in the back-side configuration (where the beam passes through the sample and the image plane is on the back-side [ihl92b]) have been carried out.



In order to investigate the influence of the plasma-treatment on the machining properties of the fused silica surface, the fluence threshold Φ_{min} for substrate ablation of both treated and untreated reference surfaces was determined by applying a series of single laser pulses with increasing energy. The pulse duration t was 20 ns. Following, ablation experiments were performed just above the particular ablation threshold.

Results and discussion

By applying the plasma-treatment, the transmission of the investigated fused silica samples was reduced significantly as shown in figure 5.2.

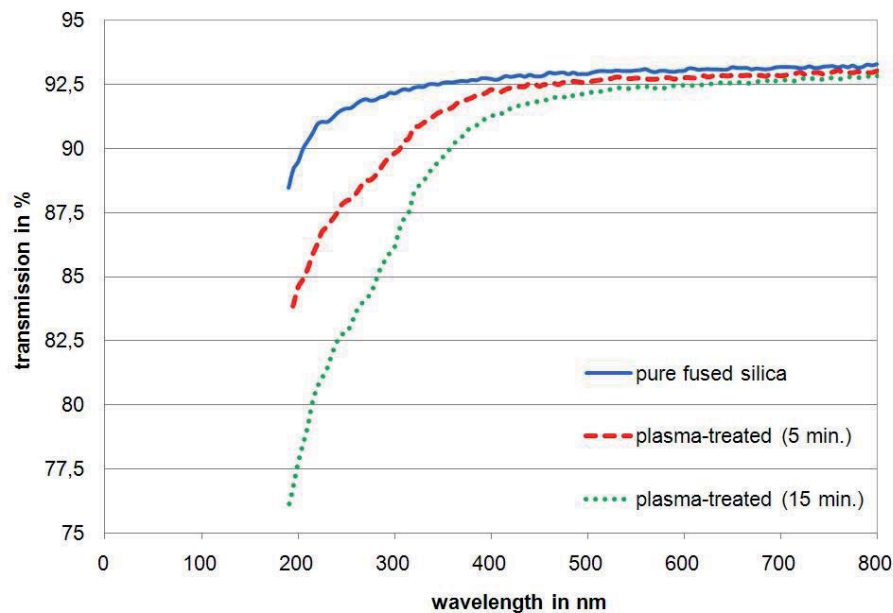


Fig. 5.2: Transmission spectra of a pure fused silica sample (solid line) and after plasma-treatment for 5 min (dashed line) and 15 min (dotted line)

In comparison to a pure fused silica sample, the transmission at the wavelength of the used laser of 193 nm was reduced by a total percental value of 5.8% after 5 minutes and 14.1% after 15 minutes plasma-treatment.

For front-side ablation of pure fused silica using a single laser pulse with a pulse duration of $t = 20$ ns, an ablation threshold of 6 J/cm^2 was determined. In comparison, the plasma-treated surfaces show a significant decrease in required fluence for ablation due to the increased absorbance by means of the reducing-acting forming gas. Here, front-side ablation was already achieved at a fluence of 1.3 J/cm^2 . Hence, the ablation threshold was reduced by a factor of 4.6 by applying the plasma-treatment. Furthermore, disturbing effects such as micro-cracks and melt are avoided in this vein. The resulting geometry was measured using a confocal scanning microscope “PL μ 2300” from Sensofar as shown in figure 5.3.

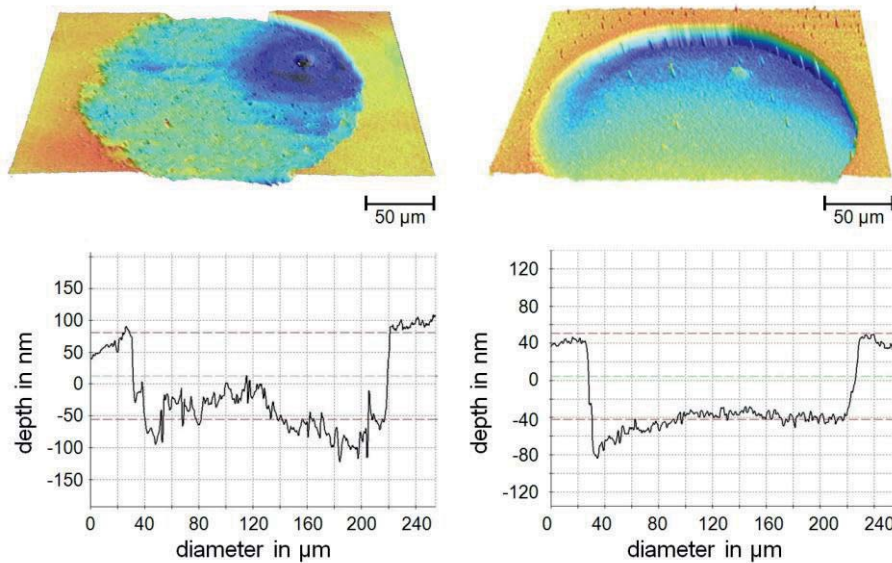


Fig. 5.3: Isometric projection (above) and cross-section (below) of pure (left) and plasma-treated (right) fused silica surfaces after single pulse front-side ablation near the particular ablation threshold (6 J/cm^2 left, 1.8 J/cm^2 right)

In addition to the above-mentioned reduction of ablation threshold, the peak-to-valley height R_z of the plasma-treated machined area ($R_z = 34.7 \text{ nm}$) is reduced by a factor of 2.3 with respect to pure laser ablated fused silica, where $R_z = 79.8 \text{ nm}$. As shown in figure 5.4, in the case of the plasma-treated surface, the complete irradiated spot of about $200 \mu\text{m}$ diameter is ablated with a smooth surface and perfect contour accuracy according to the mask diaphragm. In contrast, for the untreated surface, the ablated area looks quite porous and does not fill the complete irradiated spot.

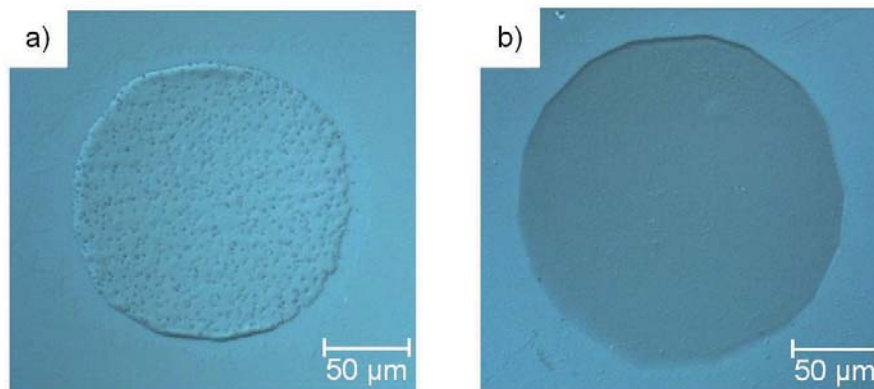


Fig. 5.4: Microscope image of the pure (a) and plasma-treated (b) fused silica sample after front-side ablation with a single pulse near the particular ablation threshold (6 J/cm^2 left, 1.8 J/cm^2 right)

In comparison to pure laser ablation, a lower ablation depth is achieved by the presented laser-plasma hybrid method. However, this enables precise control of the ablation profile by fine adjustment of the fluence.

Furthermore, a comparison of both front-side and back-side ablation of plasma-treated fused silica surfaces was carried out. Whereas single pulse back-side ablation of untreated samples is not possible with this setup, because ablation starts already at the front-side at the required high fluence, for single-pulse back-side ablation of plasma-treated samples at 1.3 J/cm^2 , a higher removal rate was observed. Figure 5.5 shows both



an isometric projection and cross-section of an ablated spot at the back-side of the sample.

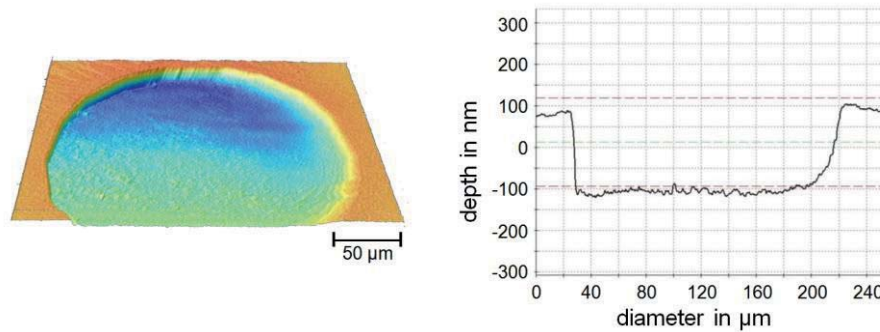


Fig. 5.5: Isometric projection (left) and cross-section (right) of a plasma-treated fused silica surface after single pulse back-side ablation at a fluence of 1.3 J/cm^2 .

Compared to front-side ablation, where the depth of ablation d was 45 nm , the depth of ablation was increased by a factor of 3.9 in the case of single-pulse back-side ablation at a fluence of 1.3 J/cm^2 ($d = 175 \text{ nm}$). Comparable increases were also found for higher fluences as shown by the corresponding ablation depths in figure 5.6.

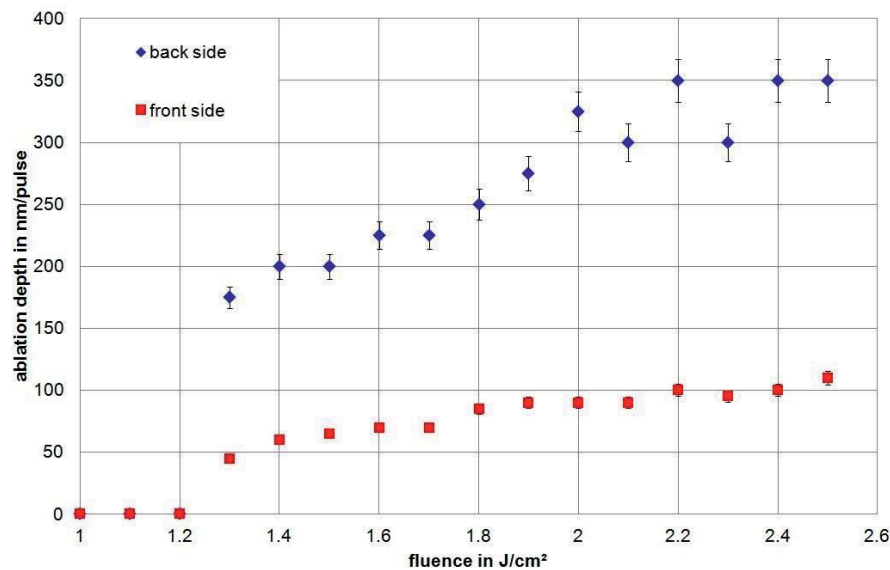


Fig. 5.6: Ablation depth vs. fluence for both front-side and back-side single-pulse ablation of plasma-treated fused silica

In addition, for back-side ablation, the peak-to-valley height R_z of 14.5 nm is 2.4 times lower in comparison to single-pulse front-side ablation at a fluence of 1.3 J/cm^2 . Such significant differences in front- and back-side ablation were already observed in previous work and could be explained by the attenuation of the ablating laser pulse by the plume of the removed material, which is only effective for front side irradiation [ih192b]. In the case of ablation at higher number of pulses, the ablation depth increased linearly. When applying 35 laser pulses at 2.4 J/cm^2 , an ablation depth of approx. $11 \text{ }\mu\text{m}$ was achieved, still featuring good machining quality.

After the micro-structuring, the transmission can be increased by a tempering process. For this purpose, the sample was tempered at 1000°C in air for inducing a reoxidisation

of the plasma-treated layer. As shown in figure 5.7, the transmission at $\lambda = 193$ nm amounts to 83.8% after 24 hours and 86.8% after 48 hours of tempering.

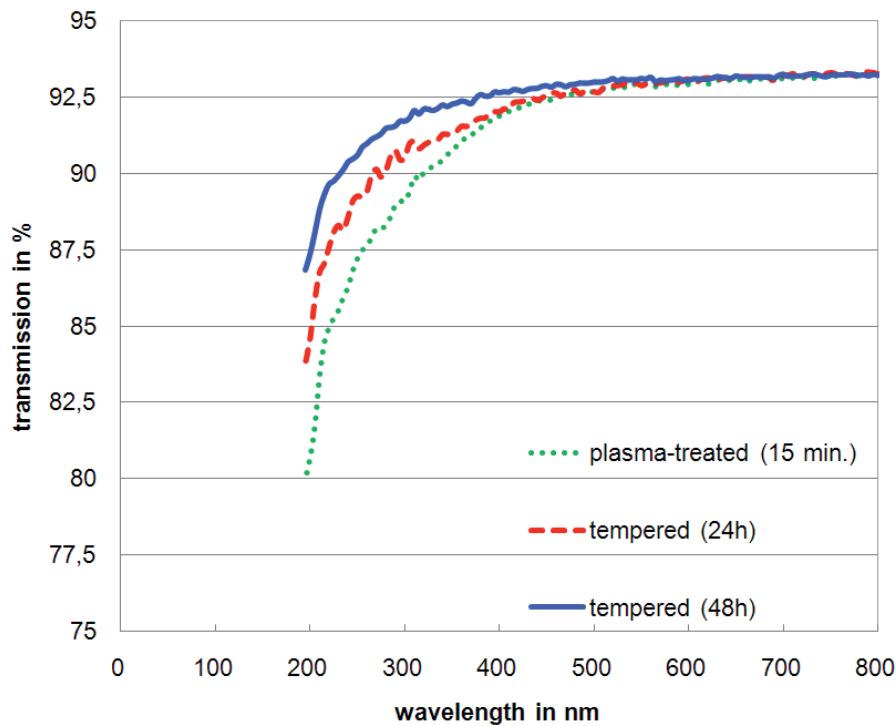


Fig. 5.7: Transmission spectra of a plasma-treated fused silica sample (dotted line) after 24 hours (dashed line) and 48 hours (solid line) of tempering

In comparison, a transmission of 88.4% at $\lambda = 193$ nm was measured for the pure, untreated fused silica sample at the beginning. Thus, almost the initial transmission characteristics can be reconstituted in this vein.

Conclusion

In terms of front-side ablation, the presented hybrid laser-plasma micro-structuring method allows a significant decrease of required fluence for ablation of fused silica by a factor of 4.6. In addition, a significant enhancement of the contour accuracy of the imaged mask was observed. Further, the resulting peak-to-valley height R_z of the machined area is reduced by a factor of 2.3. The depth of ablation is reduced by 20% in the case of laser-plasma single-pulse ablation.

The resulting surface roughness was furthermore reduced by applying back-side ablation. Here, a higher removal rate was obtained additionally.

By a terminal tempering, the plasma-treated samples can be re-oxidised, almost resulting in the initial transmission characteristics. Thus, this technique offers a novel and economic alternative for the manufacture of high-precision micro-structures in fused silica substrates. Further improvement could be achieved by introducing a laser beam homogeniser to the presented optical setup.



Laser micro-structuring of fused silica subsequent to plasma-induced silicon suboxide generation and hydrogen implantation

by J. Hoffmeister, C. Gerhard, S. Brückner, J. Ihlemann, S. Wieneke, and W. Viöl, published in *Physics Procedia* **39** (2012) 613-620⁹

Abstract

A low-temperature atmospheric pressure plasma jet was used for chemical reduction of fused silica. For this purpose, a hydrogen-containing plasma was applied. A silicon suboxide layer was generated and hydrogen was implanted into the bulk material. Changes in stoichiometry, concentration of hydrogen and optical transmission were determined. An ArF excimer laser was used for the ablation of untreated and plasma-treated fused silica. The ablation threshold was significantly decreased by a factor of 4.6 in case of plasma treated substrates. Furthermore, in multi-pulse experiments, the ablation rate remained constant at least up to a depth of 10.5 μm .

Keywords

hybrid laser-plasma technology; atmospheric pressure plasma; fused silica; silicon suboxide; micro-structuring

Motivation

Fused silica is an important material for semiconductors technology, UV-transparent optics and integrated optical components. For laser-based processing of this material, wavelengths from the UV to the IR spectral range are used [ihl92b, ger08, bue90]. However, the high UV-transparency limits the possibilities of laser manufacturing. In addition to direct processing methods that require high energy densities on the substrate surface or UV-absorbing layers, further indirect methods are in hand as for example laser induced backside wet etching [wan99, sat10] and laser-induced plasma-assisted ablation [zha98a]. Direct and indirect laser ablation can be performed on silicon suboxide (SiO_x , where $1 < x < 2$) layers that are deposited by pulsed laser deposition (PLD) [lac03] or by vacuum deposition on fused silica substrates [sch05b]. When the suboxide layer is used for indirect ablation, its strong absorption is utilized for enhanced energy coupling into the substrate. As a result, ablation of UV-transparent fused silica is achieved [ihl08]. In case of direct ablation, only the suboxide layer is ablated. After the ablation process, the suboxidal layer can be re-oxidised at temperatures around 1000°C [sch05b]. The laser plasma hybrid technology described in the present work is based on the formation of a silicon suboxide layer in the near-surface region of fused silica substrates [tso82]. For this purpose, the fused silica is reduced to silicon suboxide by applying a forming gas plasma (10% hydrogen and 90% nitrogen). In contrast to the above-mentioned deposition techniques, the introduced plasma generates atomic hydrogen from the forming gas which directly generates a suboxide layer at the fused silica surface and additionally implants hydrogen into the bulk material. As plasma source, a low-temperature atmospheric pressure plasma jet is used. Beside an increased ablation rate, the required fluence threshold for laser ablation of plasma-treated fused silica is

⁹ Reproduced with kind permission from Elsevier.



reduced significantly in comparison to untreated fused silica [brü12]. The presented method thus allows ablation of fused silica at lower laser energies, resulting in both an advanced ecological efficiency and costs reduction for production. Further advantages are the increase of ablation rates and diminution of chemical operating supply items compared to a number of other hybrid laser-based micro-structuring techniques. In comparison to lithographic processes, the ablation process is faster. In this context, the laser plasma hybrid technology enables a versatile processing since no complex procedures using etch masks etc. are required.

Experimental setup and procedure

Fused silica samples with a thickness of 2 mm were treated by a rf-excited potential-free atmospheric pressure plasma jet (1.1 MHz, 2-6 kV_{pp}, input power 8 W). The plasma jet outlet was placed at a distance of 1 mm to the fused silica surface. For the plasma-treatment, the samples were moved by a xy-linear stage. A schematic of the setup for plasma-treatment is shown in figure 5.8. The fused silica samples were treated with forming gas 90/10, resulting in both a reduction of SiO₂ to SiO_x and the implantation of atomic hydrogen. The total processing rate was 10 mm²/h. The specific processing time at each point of the sample was varied from $t = 0$ to 15 minutes, in steps of one minute. After 5 and 15 minutes, transmission spectra in the wavelength range from 190 nm to 800 nm were measured using a UV/VIS/NIR spectrometer Lambda 19 from Perkin Elmer. Further, secondary ion mass spectroscopy (SIMS) measurements were performed by using a Quadrupol SIMS 4550. For restoring the initial optical properties, the plasma-treated samples were tempered at 1000°C in a tempering oven for 24 h and 48 h, respectively. By such tempering, the samples are re-oxidised to SiO₂.

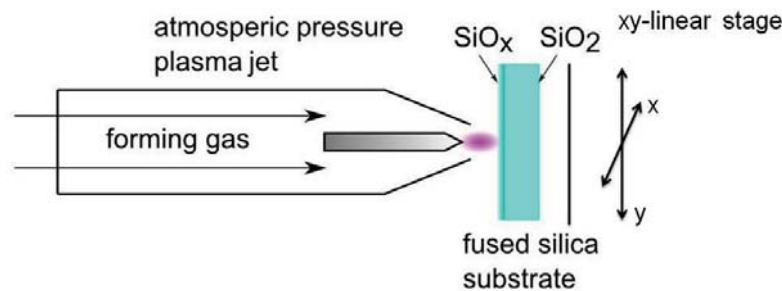


Fig. 5.8: Schematic and functional principle of the setup for plasma-treatment of fused silica samples by using an atmospheric pressure plasma jet

After a plasma-treatment of 15 minutes, the samples were ablated using an ArF-laser LPX 315 from Lambda Physik ($\lambda = 193$ nm) with a pulse duration of $\tau = 20$ ns. The beam path used for this purpose was a mask projection as shown in figure 5.9, consisting of an iris diaphragm, two convex lenses ($f_1 = 750$ mm and $f_2 = 100$ mm) and a beam splitter. Two energy detector heads behind the sample (sample removed) and the beam splitter were used for measuring the laser energy during laser ablation. The iris aperture was set to a diameter D of 3 mm. This configuration results in ablation spots on the surface of 200 μ m. The treated samples were ablated at rear-side and front-side, respectively. As a reference, an untreated substrate was ablated.

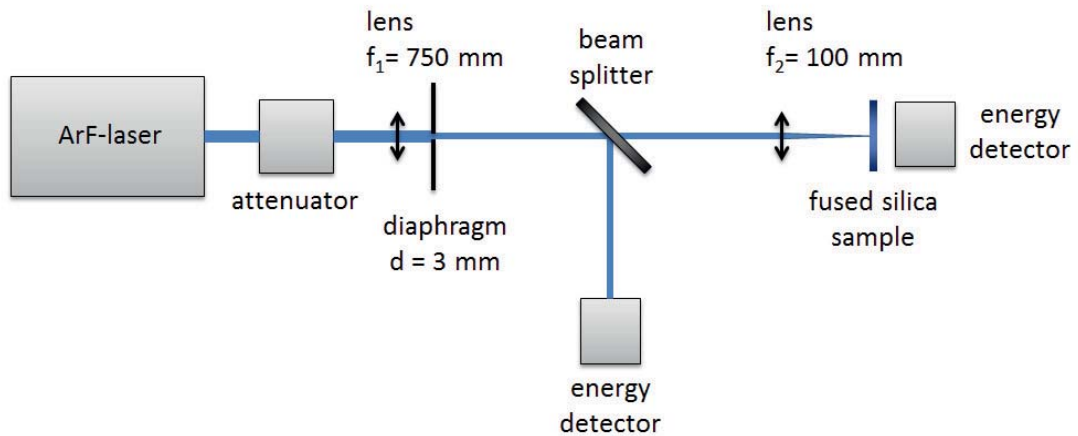


Fig. 5.9: Subsequent front- and rear-side ablation of fused silica at 193 nm

The ablation threshold was determined by applying single pulses with an increasing fluence onto the sample surface. In addition, subsequent series of tests were carried out by increasing the number of pulses at constant fluence.

Results and Discussion

Figure 5.10 shows the transmission T at a wavelength of 193 nm which is significantly reduced after plasma-treatment with forming gas. After a processing time t of 5 minutes, a transmission T of $84.7\% \pm 1.7\%$ was obtained. In comparison to an untreated fused silica sample, which was used as reference, the transmission is reduced by $4.4\% \pm 1.7\%$. For further plasma treatment of 10 minutes in duration, the transmission of the samples was decreased to $78.4\% \pm 3.9\%$ which is $10.7\% \pm 3.9\%$ lower than the transmission of an untreated sample. Such reduction in transmission is due to the formation of a suboxide layer and additional hydrogen implantation into the glass bulk material. Tempering at 1000°C led to a transmission of $87.5\% \pm 2.9\%$ after 24 hours. After 48 hours of tempering, the plasma-treated samples had regained a transmission of $87.9\% \pm 0.9\%$ at a wavelength of 193 nm.

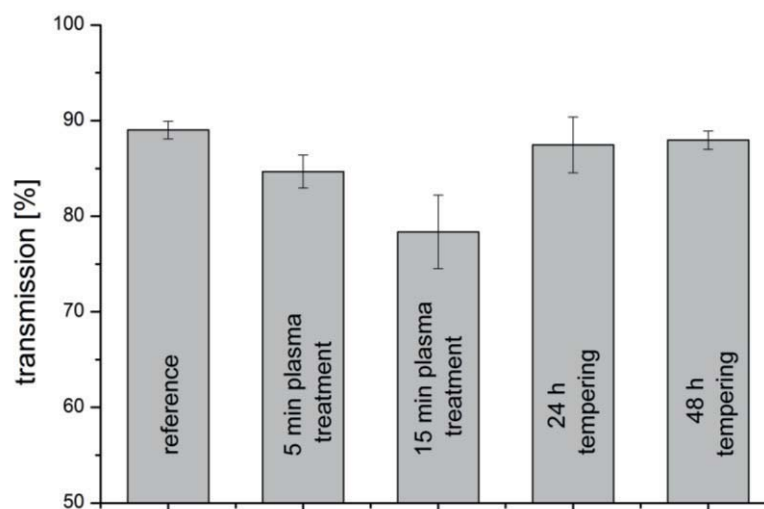


Fig. 5.10: Transmission spectra of untreated, plasma-treated and tempered fused silica samples at 193 nm



Plasma-treated samples were also investigated by SIMS. Here, the acceleration voltage of primary ions was adjusted to 5 kV. The occurring crater had a depth of $d = 660$ nm and an area of $A = 0.0625$ mm². Figure 5.11 shows the measured concentration of hydrogen within the first 700 nm of the bulk material. The linear fit-functions have been added for better clarification. In comparison to untreated substrates, the concentration of hydrogen of plasma-treated substrates was increased by 33% for the measured depth. Hydrogen strongly influences the characteristic parameters of glasses [lev85, hic60, kit62, bol83]. For instance, a hydrogen mass concentration of 0.001% changes the index of refraction by approx. $1 \cdot 10^{-6}$. The hydrogen-induced effect can also be assumed to occur at a depth of several millimetres inside the bulk material because of the high diffusivity of atomic hydrogen [lev85]. Due to the implantation of hydrogen, the absorption coefficient is increased. Thus, the laser ablation threshold for plasma-treated substrates can also be reduced.

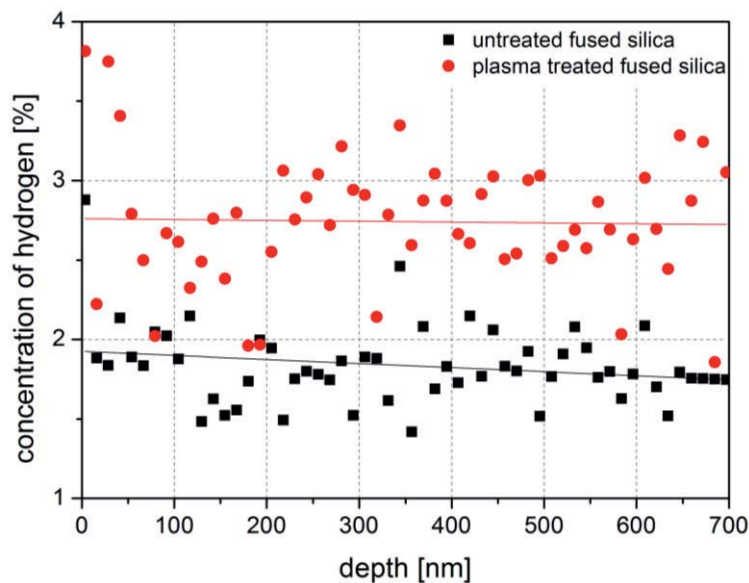


Fig. 5.11: Depth-dependent concentration of hydrogen of untreated and plasma-treated fused silica

Further, a modification of the near surface layer of fused silica is achieved by the plasma treatment. By SIMS measurements, a change in the surface stoichiometry was observed [ger12a]. Figure 5.12 shows the measured stoichiometry ratio of silicon and oxygen determined at an acceleration voltage of primary ions of 1 kV. Here, the accelerating voltage of primary ions was reduced in order to increase the resolution to detect near-surface changes in stoichiometry. The behaviour in stoichiometry of the first 10 nm of the plasma-treated fused silica can be explained by surface contaminants and a certain depth required for obtaining a sputter equilibrium for all involved atomic species. At a depth of 10 nm, the stoichiometry decreases from 2.0 to 1.875. This indicates a silicon suboxide bonding. At increasing depth, the distribution of stoichiometry increases and approaches the stoichiometry of untreated fused silica at a depth of approx. 50 nm.

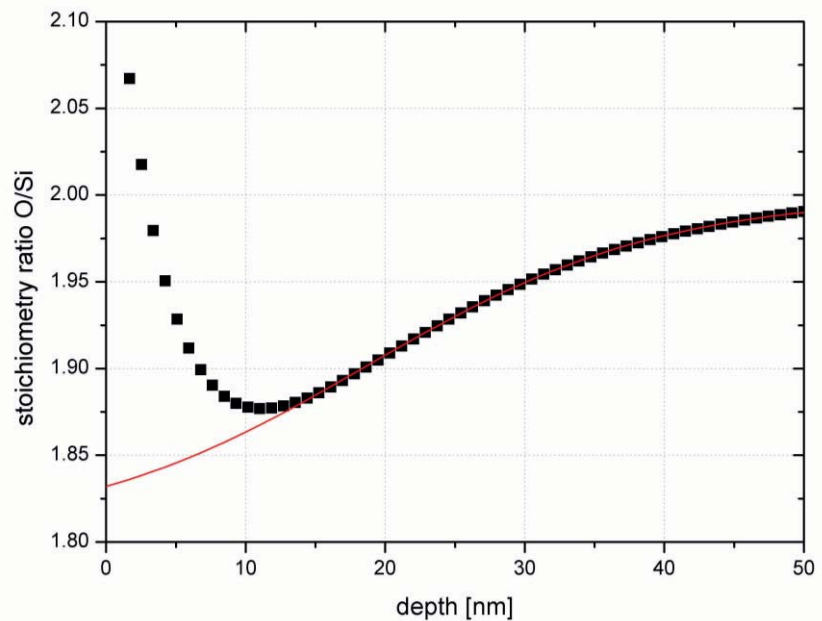


Fig. 5.12: Measured (dots) and fitted (solid line) stoichiometry ratio of silicon and oxygen of plasma-treated fused silica

Both untreated and plasma-treated (15 min) fused silica samples were laser ablated under variations of the fluence. The ablation experiments were carried out at front-side and rear-side using single pulses. Figure 5.13 shows the front-side ablated spot of an untreated sample at a fluence of 6 J/cm^2 . The isometric image and the profile were measured by a confocal scanning microscope “Pl μ 2300” from Sensofar.

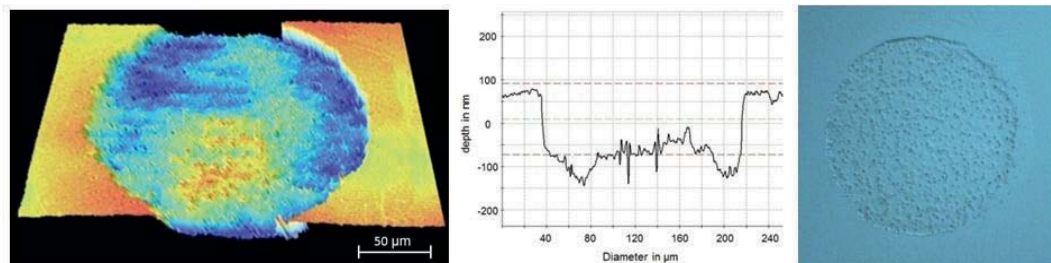


Fig. 5.13: (a) Isometric presentation; (b) cross-section; (c) microscope image of a single pulse ablated spot on untreated fused silica at a fluence of 6 J/cm^2

For laser ablation of plasma-treated substrates, the ablation threshold amounts to 1.3 J/cm^2 in the case of both, front-side and rear-side ablation. The rear-side ablation threshold of untreated fused silica could not be determined using the presented setup since front-side ablation took place simultaneously due to the energy density required for rear-side ablation of an untreated sample.

The ablation threshold was reduced by a factor of 4.6 for plasma-treated substrates. Further, the peak-to-valley height R_z was also reduced significantly. The ablation spot on the front-side of an untreated substrate features a R_z of 79.8 nm and 34.7 nm for the plasma-treated case. For the rear-side ablation spot, R_z was further reduced to 14.5 nm. At plasma-treated substrates, a smooth ablation spot, showing an accurate contour with a diameter D of approx. $200 \mu\text{m}$ was obtained (see figure 5.14). In contrast, the ablation spot size on untreated substrates shows smaller dimensions than the irradiated area. In addition, the surface of this spot features high porosity as shown in figure 5.13.

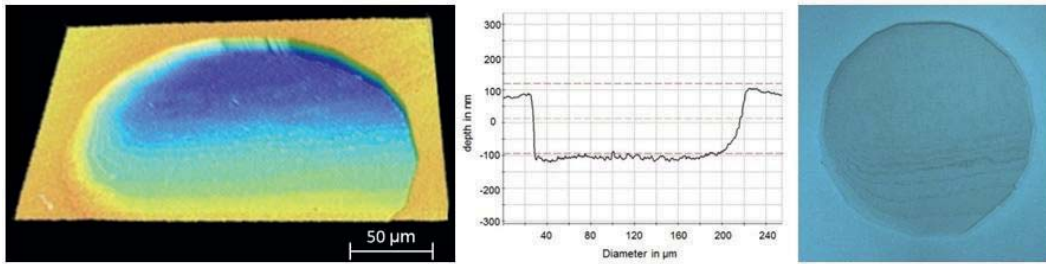


Fig. 5.14: (a) Isometric presentation; (b) cross-section; (c) microscope image of a single pulse rear-side ablated spot on plasma-treated fused silica at a fluence of 1.3 J/cm^2

After the determination of the ablation threshold for single pulse ablation, multi-pulse ablation was investigated. Here, multi-pulse rear-side ablation shows the best results. The ablation depths for rear-side ablation and the front-side ablation of plasma-treated substrates at different fluences are represented in figure 5.15.

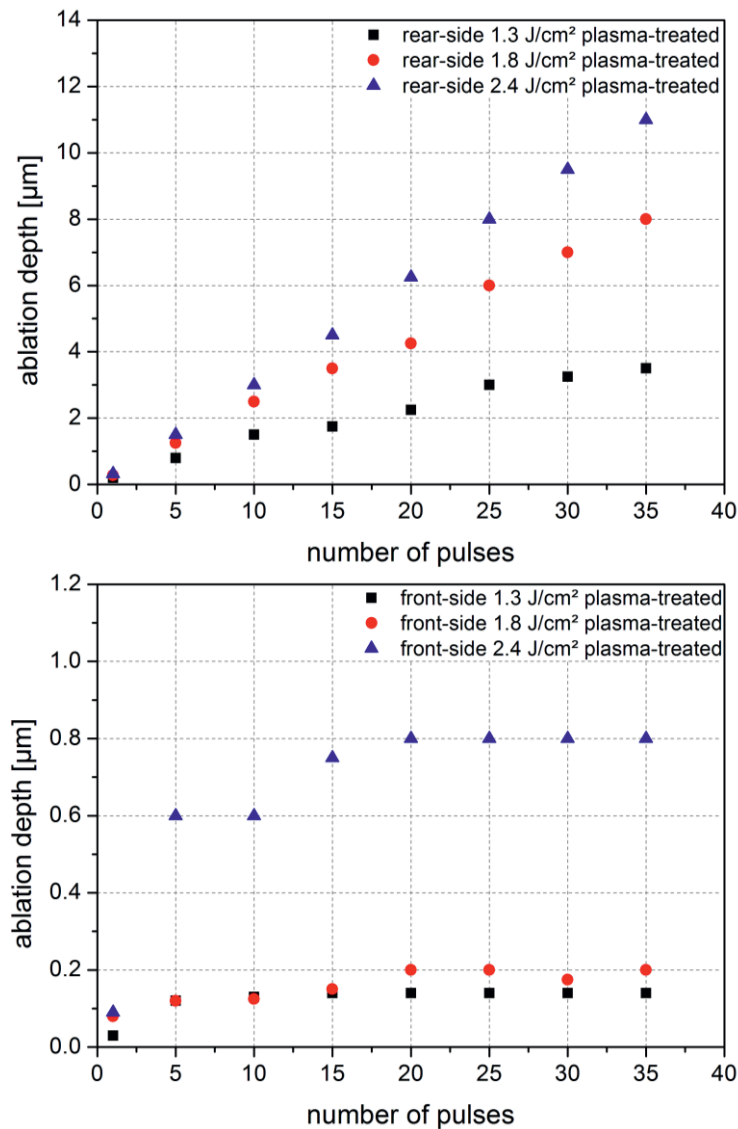


Fig. 5.15: Ablation depth vs. number of pulses for different fluences of (top) rear-side single-pulse ablation and of (bottom) front-side ablation of plasma-treated fused silica

For rear-side ablation, the ablation depth is $10.5 \mu\text{m}$ for 35 pulses at a fluence of 2.4 J/cm^2 . At 1.3 J/cm^2 , an ablation depth of $3.5 \mu\text{m}$ was achieved when applying the



same number of pulses. At a fluence of 1.8 J/cm^2 , the ablation depth is $8 \text{ }\mu\text{m}$. The ablation depth increases linearly with a rate of 300 nm/pulse in the case of rear-side ablation. In comparison to an untreated fused silica substrate the ablation rate measured at the respective threshold fluence increases by a factor of 2. Over this whole depth range, the spot contour accuracy is maintained. In the case of front-side ablation, lower depths were achieved. For 35 pulses and a fluence of 2.4 J/cm^2 , the depth is approx. 13-times lower ($0.8 \text{ }\mu\text{m}$).

The significant difference between both front-side and rear-side ablation can be partly explained by an attenuation of the incoming laser pulse by the inhomogeneous plume of debris. This effect only occurs in case of front-side irradiation. Thus, high ablation depths could be achieved in the case of multi-pulse rear-side ablation as shown in figure 5.16.

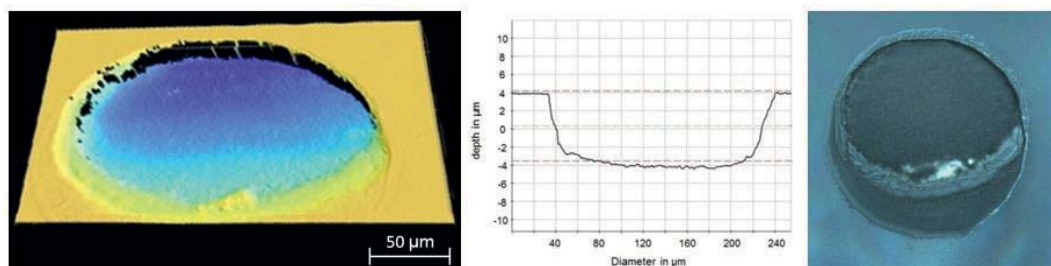


Fig. 5.16: (a) Isometric presentation; (b) cross-section; (c) microscope image of a rear-side ablated spot on plasma-treated fused silica at a fluence of 1.8 J/cm^2 applying 35 pulses

The high ablation depth in the micrometre range and the constant ablation rate over the whole depth range cannot be explained by a pure ablation mechanism caused by a suboxidal layer. However, it can be assumed that the hydrogen implantation increases the absorption of the substrate over a large depth range, allowing the high ablation depth and stable spot quality in the case of multi-pulse ablation.

Conclusion

It was shown that the presented method offers some advantages for the laser microstructuring of fused silica. For laser plasma hybrid ablation, the ablation threshold was reduced by a factor of 4.6. The ablation rate per pulse measured at the respective threshold fluence increases by a factor of 2. The roughness of the ablated spots shows a significantly reduced peak-to-valley height R_z by a factor of 2.3 for front-side ablation. In addition, the plasma treated substrates feature a better spot contour accuracy. In contrast to pure laser ablation, the plasma treatment allows the single pulse rear-side ablation of fused silica at 193 nm for the given setup.

In conclusion, the plasma treatment allows the use of cost-efficient lasers for microstructuring of fused silica. The presented method could be used for shortening the station times and leads to an increase of ecological efficiency due to the energy economisation and abandonment of chemicals compared to other methods such as micro lithography and LIBWE. Thus, by laser plasma hybrid technology, the productivity can be increased, since this time-saving method leads to better processing results as shown by the presented results for both the peak-to-valley height R_z and the spot contour accuracy.





A hybrid laser-plasma ablation method for improved nanosecond laser machining of heavy flint glass

by C. Gerhard, J. Heine, S. Brückner, S. Wieneke, and W. Viöl,
published in *Lasers in Engineering* **24** (2013) 5-6, 391-403¹⁰

Abstract

In this work we present a hybrid laser-plasma ablation method for improving laser machining of heavy flint glass using a third-harmonic Nd:YAG laser operating at a wavelength of 355 nm in the nanosecond pulse duration range. For this purpose, the glass samples were treated by a hydrogenous plasma at atmospheric pressure, resulting in an absolute decrease in transmission of 2.43% for the used laser wavelength after 30 minutes of plasma treatment. Machining experiments were performed on both pure and plasma treated heavy flint glass. It was shown that by the presented method, the roundness form error of the ablated holes could be reduced by a factor of 1.9. Further, no formation of debris was observed when applying the hybrid laser-plasma ablation method.

Keywords

Nd:YAG laser, hybrid laser ablation, heavy flint glass, atmospheric pressure plasma, surface reduction, absorbent layer, roundness form error, debris deposition

Introduction

Laser ablation has become one of the most important techniques in micro-structuring of a number of miniaturised components. In the last decades, lasers were also applied for manufacturing micro-optical components such as diffraction gratings or micro lenses. In this context, achieving high contour accuracies is of great necessity [vei01]. It was shown that F₂-excimer laser processing (wavelength $\lambda = 157$ nm) allows structuring high-quality micro lenses onto the end face of optical fibres [dou08]. Further, scribing diffractive optical elements on polyimide-coated fused-silica substrates by using laser irradiation at $\lambda = 248$ nm was demonstrated [beh97]. A comparable technique was used for realising three-dimensional micro-structures by an additional mask projection. It was shown that in this case, the accuracy of the surface topology is partially dependent on debris deposition [zim06c]. Generally, debris is caused by heating-based ablation in air when applying long laser pulses in the range of some nanoseconds [ger08]. For the reduction and prevention of debris formation, several methods based on different laser sources were developed for different materials [mai08]. In this context, laser-induced backside wet etching (LIBWE) is one of the most important techniques, where debris-free micro-structuring of glasses is achieved for a number of different laser wavelengths and pulse durations [che05, wan99, yas02]. Here, several variations are in hand such as the combination of both LIBWE and a mask projection technique [zim02, böh02] or the use of toluene layers [zim04].

Another possibility for improving the machining quality during micro-structuring of glass is the use of PMMA-coatings [kaw06]. In the case of fused silica surfaces, vac-

¹⁰ Reproduced with kind permission from Old City Publishing.

uum-deposited UV-absorbing silicon suboxide (SiO_x) layers allow enhanced indirect processing. In order to regain the transmission characteristics of pure fused silica, these SiO_x layers are re-oxidized to silicon dioxide (SiO_2) after the laser structuring [sch05b]. SiO_x films can be generated in different ways [hüb80], for example by vacuum-evaporation of powdered silicon monoxide (SiO) [sha83, nak84] or by bringing silicon to a mixture of both argon and oxygen during plasma ion sputtering [sch82]. Moreover, applying hydrogenous gases at high temperatures allows a direct reduction of SiO_2 surfaces to SiO_x or even SiO [tso82].

The goal of this work was to improve the laser machining properties of heavy flint glass when using a cost-efficient and economic flash lamp pumped Nd:YAG laser at $\lambda = 355 \text{ nm}$ and pulse durations in the nanosecond range. For this purpose, the possibility of direct chemical reduction of glass edge layers by the use of an atmospheric pressure surface discharge plasma at ambient temperature was investigated. Since such a reduction leads to a loss in transmission and an increase of absorption respectively, an improved energy coupling of incoming laser irradiation into this edge layer is resulting.

Experimental set-up and procedures

The plasma source and treatment

In order to reduce the glass edge layers chemically, forming gas 90/10 (90% nitrogen, 10% hydrogen) was used as process gas. This gas was supplied into a plasma discharge zone where reactive atomic hydrogen and smaller amounts of reactive nitrogen species were generated. The glass sample's surfaces were directly placed into the discharge zone. For this purpose, a surface discharge plasma source (SDPS) was used as shown in figure 5.17.

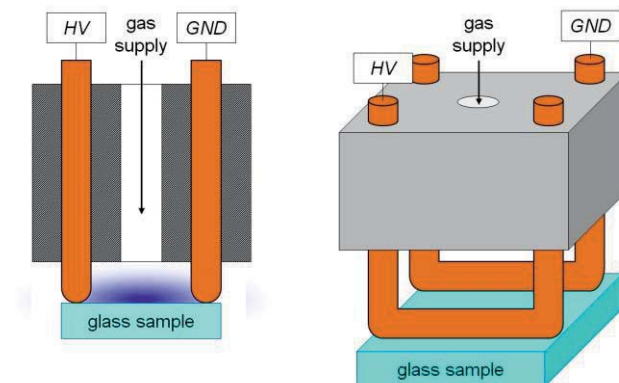


Fig. 5.17: Schematic diagram of the used SDPS

The SDPS was run at a damped sinusoidal oscillation with a peak-to-peak voltage U_{p-p} of 21 kV with a pulse repetition rate f_{rep} of 500 Hz and a voltage pulse train duration Δt of 0.4 ms at 10 kHz. According to the *Lissajous* figure method [man43, hel09], the plasma power P_{plasma} amounts then to 394 mW. Due to the geometry of the used electrodes, the plasma treated area on the glass surfaces amounts to approx. 250 mm². The plasma treatment was carried out for maximum 30 minutes. In order to verify its influence, the transmission of the investigated glass samples before and after plasma treatment was measured using a UV/VIS-spectrometer (Lambda650; PerkinElmer, Inc.).



The laser source and ablation

Subsequently, machining experiments were performed to determine the influence of the plasma treatment in terms of the resulting laser machining properties. For this purpose, a third-harmonic Nd:YAG laser (Powerlite 9010; Continuum, Inc.), operating at a wavelength of 355 nm with a pulse duration Δt of 8 ns and a repetition rate f_{rep} of 10 Hz was used. The applied average pulse energy E_{pulse} was 48 mJ. The raw beam diameter $2w$ of this laser source amounts to 9.5 mm, the full angle of divergence θ is 0.45 mrad. Since the laser beam was focused by a plano-convex lens with a focal length f of 100 mm, the beam waist diameter $2w_0$ is then 106 μm according to a beam path simulation using WinLens3D (Qioptiq Photonics, Inc.) [thö09]. Thus, the fluence Φ in the focal plane amounts to approx. 0.5 J/cm². The resulting ablated holes on the glass surfaces were evaluated using a scanning electron microscope (SEM) (PSEM eXpress; Aspex Corporation).

The investigated glasses

In this work 5 mm thick samples made of heavy flint glass (SF5; Schott, Inc.) were investigated. For the used laser wavelength of 355 nm, this glass features an internal transmission T_i of 72.32%, resulting in an absorption $A = 1 - T_i$ of 27.68% [sch11]. By the plasma treatment and the accompanying reduction of the glass surface, a further temporary increase of absorption is expected, improving the laser energy coupling into the glass surface. For comparison, the plasma treatment was also performed on both fused silica (Spectrosil 2000; Heraeus Quarzglas, GmbH) and barite crown glass (N-BaK4; Schott, Inc.).

Results and discussion

Effect of plasma treatment

Reduction of transmission

By measuring the transmissions T (including reflexion losses) of the glass samples before and after plasma treatment of 30 minutes, the absolute change in transmission ΔT in the UV-range was determined. In the case of heavy flint glass SF5, the plasma treatment led to a considerable change in transmission, as shown in figure 5.18.

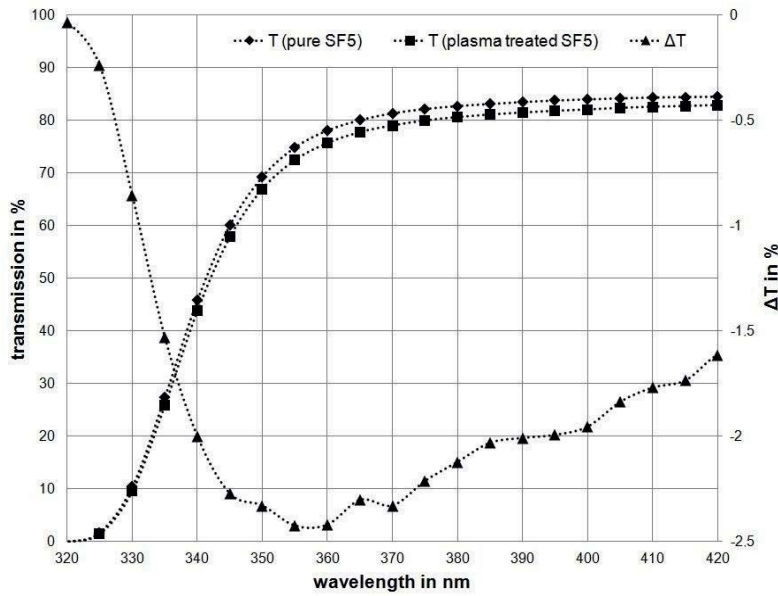


Fig. 5.18: Transmission of the SF5 heavy flint glass *versus* wavelength before and after plasma treatment and the resulting absolute change in transmission

At a wavelength of 355 nm, this treatment led to a decrease in transmission of 2.43%. The amount of ΔT is strongly dependent on the plasma treatment duration, as shown in figure 5.19.

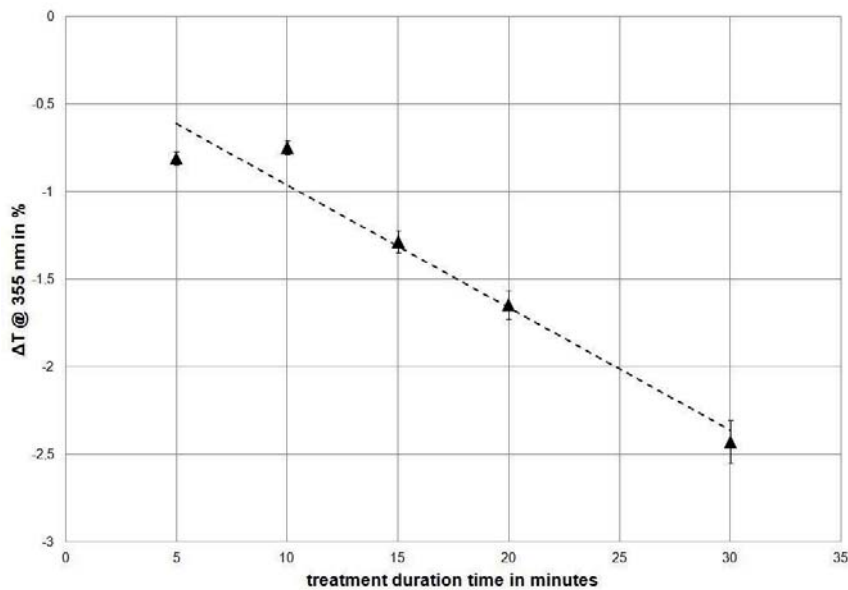


Fig. 5.19: Absolute change in transmission of the SF5 heavy flint glass at $\lambda = 355$ nm *versus* treatment duration time

When applying a linear fit to the measured values, the treatment duration-dependent absolute change in transmission can be determined to amount to -0.07% per minute, confirming a continuous reduction of the heavy flint glass surface. However, for the investigated samples made of fused silica and barite crown glass, no change in transmission was detected.



Bond strength of the investigated glasses

The energy required for breaking a chemical compound is generally described by its standard enthalpy of formation, ΔH_f^0 , where lower values of ΔH_f^0 describe stronger bonds. Besides silicon dioxide (SiO_2), the main compounds of the investigated glasses are in general: barium oxide (BaO) and zinc oxide (ZnO) for barite crown glasses and lead(II) oxide (PbO) for heavy flint glasses. As shown by the comparison of the particular standard enthalpies of formation in table 5.1, lead(II) oxide is the weakest of the involved compounds.

Table 5.1 Standard enthalpies of formation [mas83] and corresponding energy of the main compounds of the investigated glasses

	SiO_2	BaO	ZnO	PbO
ΔH_f^0 (kJ/mole)	-859.4	-553.5	-348.3	-217.9
E (eV)	8.9	5.9	3.6	2.3

Thus, the change in transmission could be explained by a reduction of PbO to metastable lead suboxide which is induced by the hydrogenous plasma whereas the other involved compounds were not affected by the plasma. In general, atmospheric pressure plasmas can be assumed to have an electron temperature T_e of approx. 1 eV. Due to the *Maxwellian* energy distribution, considerable amounts of electrons can reach temperatures up to 10 eV partially. However, the main chemical reactions carried out in the present case are in the low eV-range. Such a loss in transmission was also observed in the case of heat treatment of glasses containing lead oxide in a reducing surrounding atmosphere [kit62].

Re-oxidization after ageing

After the plasma treatment, the heavy flint glass samples were aged at ambient temperature and atmospheric pressure. The transmission was then measured after 24 hours and 14 days. After an ageing time of 24 hours, the difference in transmission at 355 nm was -1.13% with respect to the initial value. Moreover, the initial value was re-obtained after 14 days which can be explained by a re-oxidation of the reduced glass surface. Thus, the presented plasma treatment using a hydrogenous process gas allows reducing the transmission of heavy flint glass SF5 temporarily and re-obtaining the initial transmission characteristics by simple ageing at ambient conditions.

Laser machining results

Comparison of ablated holes

Subsequently to the plasma treatment, laser machining experiments were performed on the heavy flint glass samples. A comparison of the ablated holes for pure laser ablation and hybrid laser-plasma ablation with respect to the applied number of pulses is shown in figure 5.20.

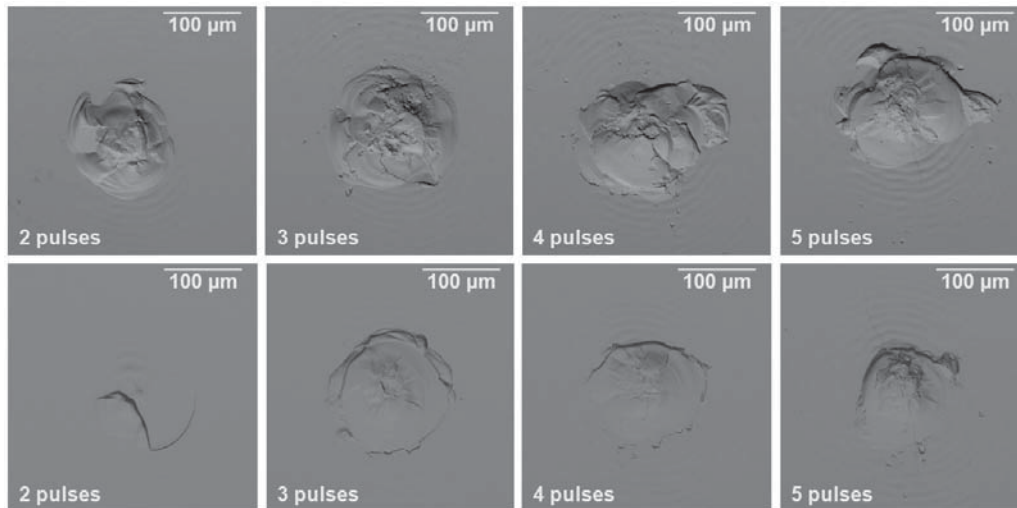


Fig. 5.20: SEM micrographs of laser ablated spots on the SF5 heavy flint glass: (top) pure laser ablation; (bottom) hybrid laser-plasma ablation

For a single laser pulse, no material ablation was observed in both cases. However, for higher number of pulses, the machining results for pure and hybrid ablation differ significantly. In the case of pure laser ablation, the ablated holes feature strong random flaking in the boundary area, resulting in a high roundness form error δ . In contrast, a higher circularity can be observed for the hybrid laser-plasma ablated holes.

Determination of roundness form error

The roundness form error of each ablated hole was determined by applying the minimum zone circle (MZC) method according to DIN ISO 1101. Here, δ is given by the difference of the radii r of concentric circles, an outer enveloping circle (r_o) and an inner minimum circle (r_i) as shown in figure 5.21.

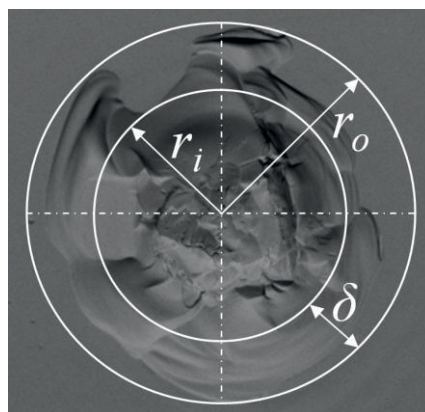


Fig. 5.21: SEM micrograph of a laser ablated spot on the SF5 heavy flint glass with the methodology for determining the roundness form error according to DIN ISO 1101 superimposed

Figure 5.22 shows a comparison of the resulting roundness form errors with respect to the number of applied laser pulses.

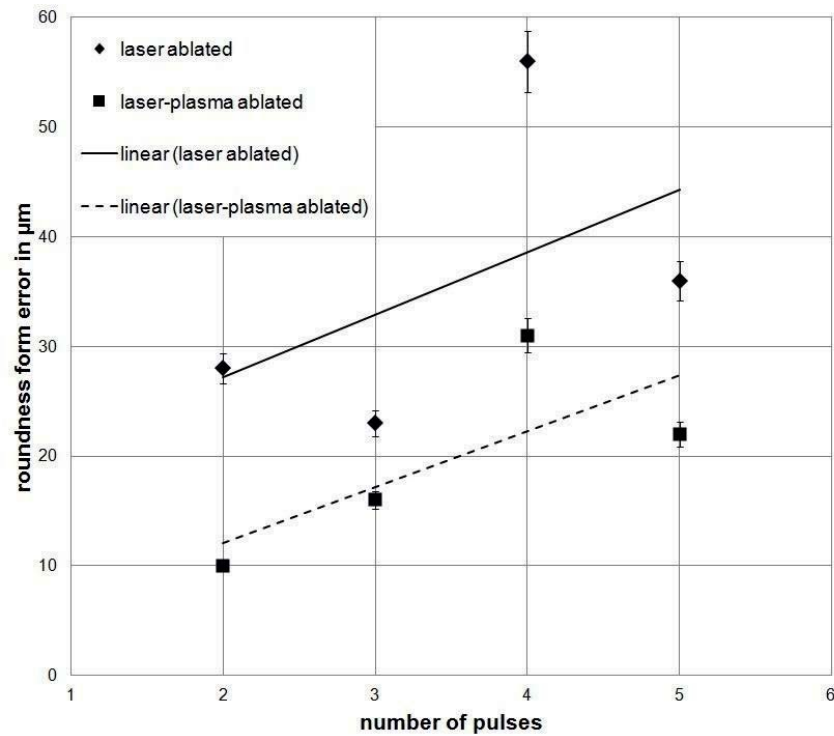


Fig. 5.22: Roundness form error for laser ablated and hybrid laser-plasma ablated holes in the SF5 heavy flint glass *versus* number of applied of pulses

Compared to pure laser ablation, the averaged roundness form error of the ablated holes was reduced by a factor of 1.9 when applying the presented hybrid laser-plasma ablation method.

Comparison of formation of debris

In addition to the roundness form error, the formation of debris on the glass surface was examined. In the case of pure laser ablation, areas with a significant amount of debris were observed whereas in the case of hybrid laser-plasma ablation, no debris could be detected visually. In order to quantify this difference, areas of interest; that is, areas featuring considerable formation of debris, were investigated. For this purpose, the measured SEM images were evaluated photometrically, as shown in Figure 5.23.

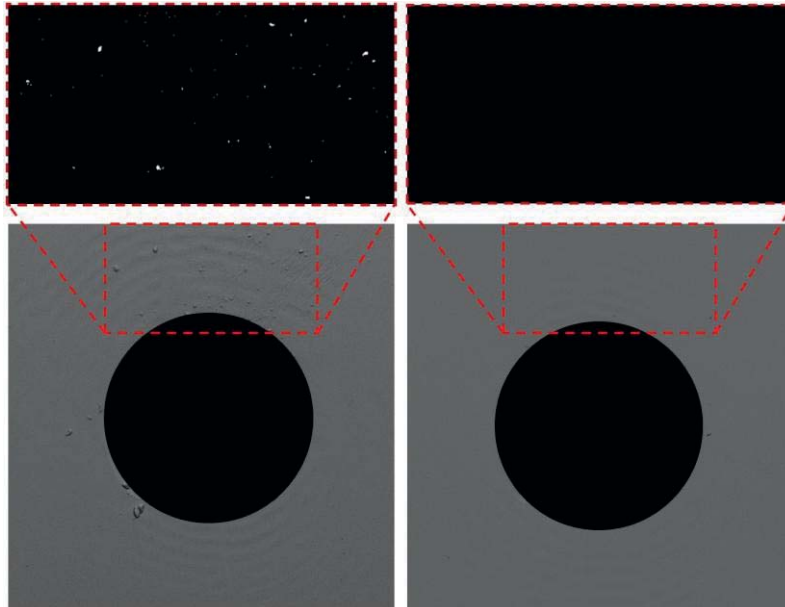


Fig. 5.23: Evaluation of debris within a defined area of interest: (left) ablated by pure laser ablation and (right) hybrid laser-plasma ablation after three laser pulses.

In order to eliminate the influence of the boundary area of the ablated hole which is enclosed by the outer enveloping circle (see figure 5.21), the surface area of this circle was blackened. After converting the SEM-image of the areas of interest into a bicoloured image, its histogram was read out by calculating the percentages of both black and white pixels numerically. Using the example of figure 5.23 for ablation with three laser pulses, a percentage of white pixels, i.e. an amount of debris of 0.7% was measured in the case of pure laser ablation. For hybrid laser-plasma ablation, no debris was detected.

Geometrical ablation values

In addition to both the roundness form error and the formation of debris, the size of the ablated holes was investigated. Due to the irregular shapes (see figure 5.20), no geometrical approach can be applied for calculating the hole volume. However, the ablation depth d allows a comparison of the depth ablation rates, i.e. the ablated depth per pulse. The depth of the ablated holes was measured using a light microscope (Axioskop 2 MAT; Zeiss, GmbH). Further, the radius r , which is given by the arithmetic mean of r_o and r_i (see Section “Determination of roundness form error”) was determined, as shown in figure 5.24.

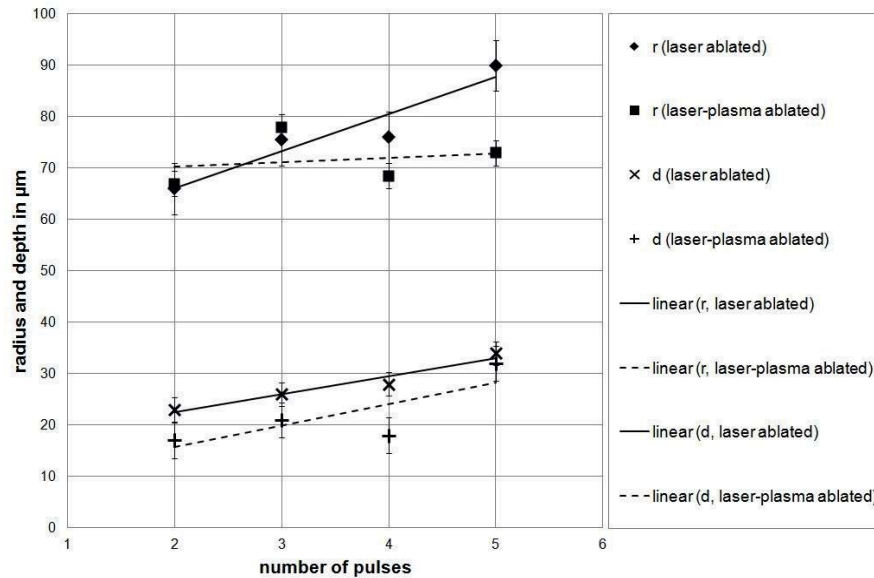


Fig. 5.24: Comparison of the radii and depths of the ablated holes

It can be observed that the hybrid laser-plasma ablation leads to a reduction of both the depths and the radii of the ablated holes. At an average, the depth ablation rate is 1.3-times higher for pure laser ablation. However, the averaged deviation from the laser beam waist diameter $2w_0 = 106 \mu\text{m}$ is reduced by the same factor in the case of hybrid laser-plasma ablation when comparing the radii.

Conclusions

By applying a hydrogenous surface discharge plasma, the transmission of heavy flint glass SF5 was decreased by an absolute value of -2.43%. This decrease can easily be removed by a simple ageing of the treated glass sample at ambient temperature and atmospheric pressure. Even though both the depths and radii of ablation are reduced when applying the presented hybrid laser-plasma method, the contour accuracy is improved significantly. Furthermore, the formation of debris on the glass surface is avoided. These effects are due to the reduction in transmission and the accompanying increase in absorption, resulting in a higher laser energy deposition into the glass surface and an improved evaporation of the molten material.

The presented hybrid ablation method, using a surface discharge plasma for reducing the glass edge layer by a hydrogenous plasma, allows generating a considerable decrease in transmission of the investigated heavy flint glass. Such decrease was not achieved in the case of fused silica and barite crown glass N-BaK4. However, it was shown in forthcoming work that by the aid of a plasma jet, surface reduction of fused silica can be achieved at atmospheric pressure. Similar experiments using the above-mentioned plasma jet source shall thus be performed on N-BaK4, SF5 and other glasses in future work.





Simultaneous Plasma-Assisted Ablation

In this chapter, the impact of simultaneously applied assisting argon plasma on classical laser ablation of optical crown and flint glass is presented. It is shown that such combination allows a considerable increase in ablation rate. Further, plasma-induced modifications of the glass surfaces are introduced.

The simultaneous plasma-assisted ablation (simPAA) method as introduced in section 3.2 was used for ablation of optical heavy flint and crown glass. Here, a significant increase in ablation rate was achieved. In contrast to sequential plasma-assisted ablation, where plasma-chemical mechanisms play the key role for enhancing the ablation process by prior modification of the glass composition, plasma-physical mechanisms were introduced to the ablation process. As already presented and discussed above, a certain material removal of optical media can be achieved by the argon plasma beam which came into operation during simPAA. This effect is even higher during simultaneous laser ablation as presented in the following article. Besides the influence of high electric field strengths on the glass surface (compare section 4.2 and [ger13c]) and a certain ion bombardment of the glass surface as a result of the sheath-effect, direct interactions of both the plasma and the laser beam gain importance during simPAA, e.g.:

- a pre-ionisation of the laser beam path by the coaxially-guided plasma beam,
- the formation of scatter centres within the glass surface due to UV-irradiation provided by the plasma beam and the accompanying enhanced absorption of the incoming laser beam, and
- the de-excitation of argon metastables at debris particles and an accompanying energy transfer close to the glass surface.

The observed increase in ablation rate is most likely mainly due to the last listed effect. The de-excitation of argon metastables delivers a considerable amount of energy, i.e. approx. 11.5 eV [bie13]. As shown by Allison et al., such de-excitation due to collision with molecules leads to a transfer of electronic energy and can cause the dissociation of target molecules [all81]. In the present case, this additional energy transfer gives rise to an increased ablation rate during simPAA as presented in the following article.





Low-temperature atmospheric pressure argon plasma treatment and hybrid laser-plasma ablation of barite crown and heavy flint glass

by C. Gerhard, S. Roux, S. Brückner, S. Wieneke, and W. Viöl,
published in *Applied Optics* **51** (2012) 17, 3847-3852¹¹

Abstract

We report on atmospheric pressure argon plasma-based surface treatment and hybrid laser-plasma ablation of barite crown glass N-BaK4 and heavy flint glass SF5. By pure plasma treatment, a significant surface smoothing, as well as an increase in both the surface energy and the strength of the investigated glass surfaces, was achieved. It was shown that for both glasses, hybrid laser plasma ablation allows an increase in the ablation depth by a factor of 2.1 with respect to pure laser ablation. The ablated volume was increased by an averaged factor of 1.5 for N-BaK4 and 3.7 for SF5.

Introduction

Laser-based methods for micro-machining of transparent media and glasses in particular are of great interest for a number of applications such as wafer structuring or scribing optoelectronic and microelectro-mechanical systems (MEMS). For this purpose, the suitability and characteristics of glass ablation by short laser pulses in the range of some nanoseconds, picoseconds [ger08], or femtoseconds [sha01, ute10] were investigated in the last years. In the case of nanosecond-ablation, drilling of bariumalumo-borosilicate glass [rud99] and fused silica [ihl92a] was demonstrated in the UV-wavelength range. It was further shown that nanosecond-laser-induced plasma-assisted ablation (ns-LIPAA) allows high-quality machining of different glass materials such as fused quartz and Pyrex glass in the UV-, visible (VIS)-, and near infrared (NIR)-wavelength range [zha99a, nik05, zha98a]. However, nanosecond laser ablation typically involves disturbing artifacts due to thermal effects [ger08, rus02]. Against this background, nanosecond-laser-based hybrid techniques allow enhanced machining results. For example, several etching techniques such as laser-induced backside wet etching (LIBWE) [wan99, sat11] or the use of UV-absorbing films [zim04, böh06a] can be applied. By an atmospheric pressure plasma treatment of fused silica using a hydrogenous process gas, optical parameters of the bulk material such as its UV-absorbance can be modified [ger12a]. This effect can be used for improving nanosecond laser micro-structuring properties and reducing the energy required for ablation [brü12].

Further, plasma-based etching presents another established technique for micro-machining of glasses [ten06]. Surface smoothing of ultra low expansion (ULE) glass was already performed by applying a reactive atomic plasma technology (RAPT) at atmospheric pressure. Here, argon (Ar) was used as carrier gas for exciting nitrogen trifluoride (NF₃) [fan06a]. For deep reactive ion etching (DRIE) methods, different work gasses such as sulfur hexafluoride (SF₆) [par05, li01], carbon trifluoride (CHF₃) [lee99], or octafluorocyclobutane (C₄F₈) [aka06, kol08] are used. For the last case, the influence of Ar additives on the etching of fused silica was investigated. Here, an increased Ar concentration led to an increase of the etch rate for particular sets of param-

¹¹ Reproduced with kind permission from the Optical Society of America.

ters [li03b]. Further, it was shown that in principle, etching silicon by pure Ar ion bombardment is possible [cob79]. Against this background, the influence of a pure Ar plasma at atmospheric pressure in combination with UV laser ablation of different glasses was investigated in the presented work.

Experimental setup and experimentation

For the investigation of the influence of a low-temperature atmospheric pressure Ar plasma beam on the laser material removal of optical glasses, a hybrid laser-plasma-beam setup was assembled. Here, the laser source was a Nd:YAG laser Powerlite 9010 from Continuum, operating at the third-harmonic wavelength λ of 355 nm with a pulse duration Δt of 8 ns and a repetition rate f_{rep} of 1 Hz. The applied pulse energy E_{pulse} was 35.7 mJ. The raw beam diameter $2w$ of this laser amounts to 9.5 mm with a full angle of divergence θ of 0.45 mrad. The laser beam was focused by a plano-convex lens with a focal length f of 100 mm. Taking the beam propagation factor M^2 of 1.4 for this TEM₀₀-beam into account, the beam waist diameter $2w_0$ is then 106 μm according to a beam path simulation using WinLens3D from Qioptiq Photonics [thö09]. Thus, the Rayleigh-length z_R amounts to approximately 25 mm.

The used plasma source, featuring a rotation-symmetric plasma nozzle, is based on a dielectric barrier discharge (DBD), realizing a low-temperature plasma in non-thermal equilibrium [brü11]. In this setup, an internal high-voltage (HV) hollow-core copper electrode is embedded in a housing made of polyoxymethylene. A gap between both the electrode and the housing acts as gas channel. For the presented work, Ar 4.6 from Linde at a flow rate of approximately 4 standard liters per minute (slm) was used as working gas. Due to the cone-shaped geometry, a fine and stable gas flow is resulting at the outlet port of the plasma nozzle, confining the formed plasma filaments to a compressed plasma channel. A ground electrode made of aluminium was mounted in front of the outlet port. In between, the investigated glass samples were placed. Thus, the samples act as dielectric in order to realize a DBD. The geometry of the hollow-core electrode allows a coaxial access to the plasma filament. As shown in figure 6.1, both the focused laser beam and the atmospheric pressure argon plasma beam propagate along a common axis of propagation.

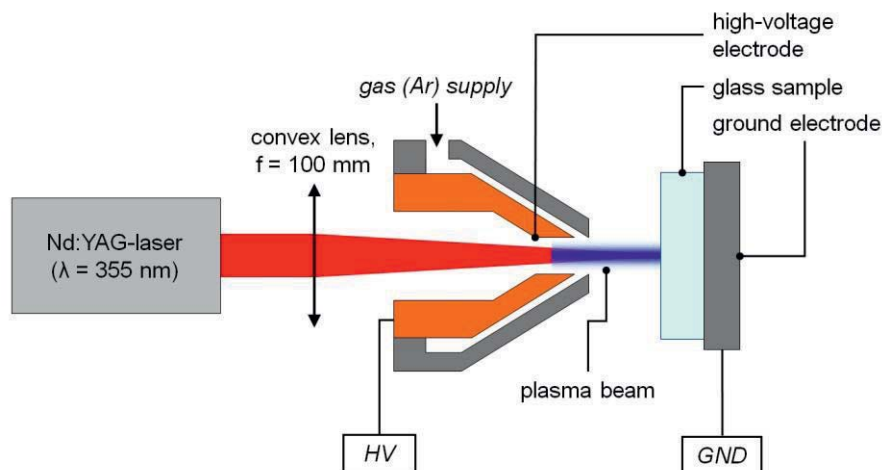


Fig. 6.1: Common-path laser plasma setup for glass processing



The electrode distance can be varied in the range from 10 to 29 mm, maintaining a stable plasma beam with a diameter d_{plasma} of approximately 200 μm . In the present case, the distance of the HV-electrode to the ground electrode was 20 mm. For this coaxial laser-plasma beam setup, investigations on the plasma-induced focus shift of the laser beam were performed by caustic measurements. It was observed that this focus shift amounts to maximum 1.8 mm, which is a marginal value with respect to the Rayleigh-length of 25 mm. The diameter of the plasma discharge area on the glass surface was much broader than the Ar plasma beam within the discharge gap, reaching up to several millimeters in diameter with a radial rotation-symmetric intensity distribution. The plasma energy E_{plasma} of the plasma source was 0.17 mJ for each HV-pulse train with a duration of approximately 80 μs . This energy value was determined using the *Lissajous*-algorithm [man43, hel09]. Due to the applied pulse repetition rate f_{rep} of 7 kHz, the averaged power P_{av} amounts to 1.19 W, i.e., approximately 33 times the applied averaged laser power of 35.7 mW. For the particular laser focus and plasma beam diameters, the fluences Φ amount to $\Phi_{laser} = 404.5 \text{ J/cm}^2$ and $\Phi_{plasma} = 0.54 \text{ J/cm}^2$, resulting in a considerable factor of approximately 748. During the hybrid laser-plasma ablation experiments, both the laser and the plasma source were not synchronized. Over a single pulse train of the plasma power supply, there are multiple ignition events with a temporal distance up to 20 μs . Since both the laser pulse duration and the lifetime of a single plasma filament are in the nanosecond range, it can be assumed that, as a rule, the laser and the plasma do not impact the sample surface at the same time.

In this work, glass samples made of barite crown glass N-BaK4 (thickness $t = 4 \text{ mm}$) and heavy flint glass SF5 ($t = 5 \text{ mm}$), both from Schott, were investigated. In order to determine the influence of the Ar plasma beam on characteristic parameters of the investigated glass surfaces, both N-BaK4 and SF5 samples were plasma-treated for 60 s without applying any laser irradiation. Both the surface energy and the surface roughness were determined before and after such plasma treatment.

Results and discussion

Influence of pure Ar plasma

For an area of $50 \times 50 \mu\text{m}^2$, the surface roughness of the investigated glass samples was measured before and after plasma treatment of 60 s using an atomic force microscope (AFM) easyScan 2 AFM from Nanosurf including a mechanical edge guide for relocating the samples. By the plasma treatment, a considerable decrease of both the arithmetic mean roughness Ra and the root mean squared roughness Rq was observed as shown in table 6.1.

Table 6.1: Comparison of the arithmetic mean roughness Ra , root mean squared roughness Rq , and particular percentage change Δ of N-BaK4 and SF5 surfaces before and after plasma treatment

	N-BaK4			SF5		
	Untreated	Treated	Δ in %	Untreated	Treated	Δ in %
Ra nm	1.4	1.29	-7.8	2.9	1.17	-59.7
Rq nm	2.4	1.95	-18.8	4.3	1.51	-64.9

As shown by the change of the particular surface roughness, the atmospheric pressure Ar plasma treatment causes a considerable surface smoothing. In comparison to N-



BaK4, SF5 features a higher decrease in surface roughness by a factor of $Ra_{SF5}/Ra_{N-BaK4} = 1.56$ and $Rq_{SF5}/Rq_{N-BaK4} = 2.31$. This difference can partially be explained by the different *Knoop* hardnesses $HK_{0.1/20}$ of N-BaK4 and SF5, i.e., $HK_{0.1/20}(N-BaK4) = 550$, and $HK_{0.1/20}(SF5) = 410$ [sch11]. Further, SF5 features a lower chemical bond strength compared to N-BaK4 as discussed in Subsection “Hybrid laser plasma ablation results”.

The surface energy γ before and after plasma treatment was measured according to the Owens-Wendt-Rabel-Kaelble method [kae69, owe69]. Here, a Contact Angle Measurement System G10 from Krüss was used. From the measured surface energies, the strength σ of the glass surfaces before and after plasma treatment can be calculated by the *Griffith's* equation according to

$$\sigma = \sqrt{\frac{2 \cdot E \cdot \gamma}{d}}. \quad (\rightarrow 4.11)$$

Here, E is the modulus of elasticity of the glass (i.e., $E_{N-BaK4} = 77 \times 10^3 \text{ N/mm}^2$, $E_{SF5} = 56 \times 10^3 \text{ N/mm}^2$ [sch11]) and d the depth of cracks on the glass surface [pau91]. For the optically polished glass surfaces, a typical crack depth of approximately 33 nm, corresponding to a mean diameter of the used polishing particles of approximately 10 nm was assumed. The plasma-induced change in strength of both glasses can then be estimated by applying the particularly measured surface energy as shown in table 6.2.

Table 6.2: Comparison of surface energy γ , resulting strength σ , and particular percentage change Δ of N-BaK4 and SF5 surfaces before and after plasma treatment

	N-BaK4			SF5		
	Untreated	Treated	Δ in %	Untreated	Treated	Δ in %
γ in mJ/m^2	48	68	+42	39	51	+31
σ in N/m^2	150	178	+19	115	132	+15

In summary, the above-described plasma treatment of 60 s has a strong influence on the glass surfaces: Besides a considerable surface smoothing, both the surface energy and the strength are increased significantly.

Hybrid laser plasma ablation results

Both pure laser ablation and hybrid laser-plasma ablation experiments were performed applying 10, 20, 30, and 40 laser pulses. The ablated holes were evaluated using a scanning electron microscope (SEM) PSEM eXpress from Aspex as shown in figure 6.2 for N-BaK4 and figure 6.3 for SF5.

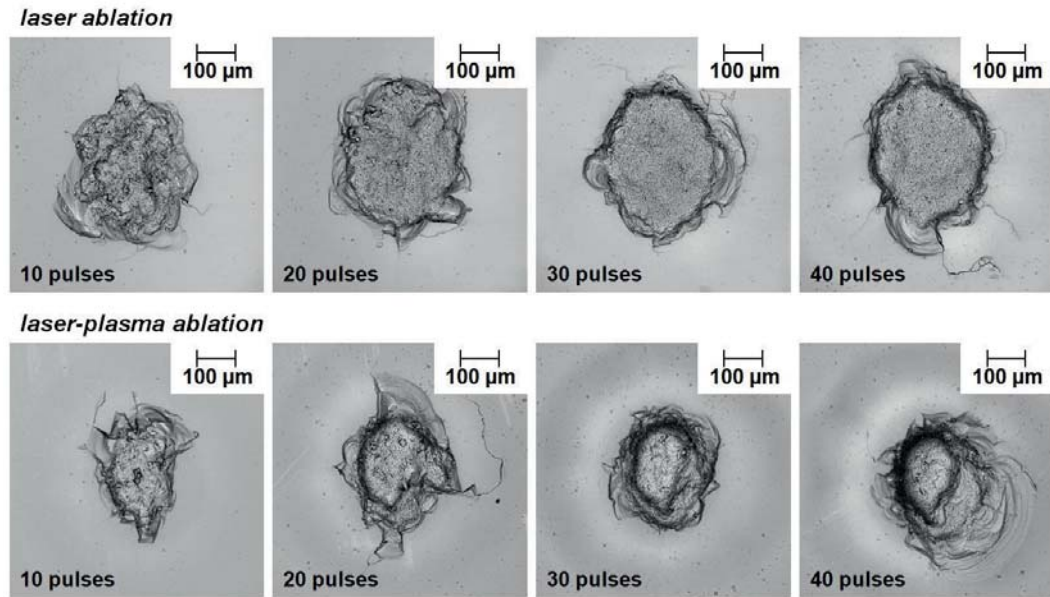


Fig. 6.2: SEM images of laser ablated (top) and laser-plasma ablated (bottom) barite crown glass N-BaK4

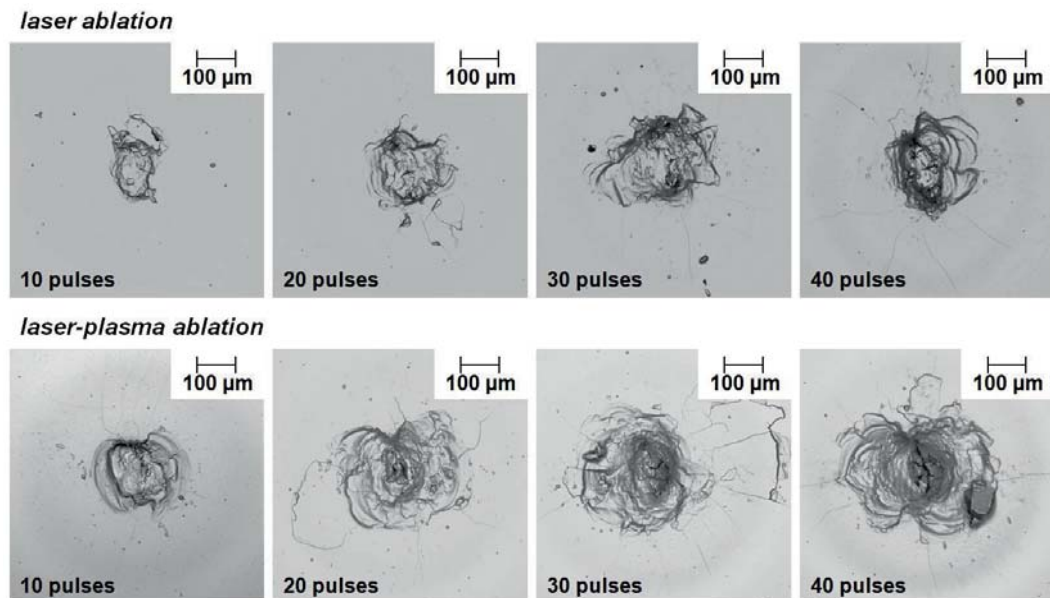


Fig. 6.3: SEM images of laser ablated (top) and laser-plasma ablated (bottom) heavy flint glass SF5

In the case of N-BaK4, a reduction of the hole area can be observed for laser-plasma hybrid ablation in comparison to pure laser ablation. In contrast, SF5 shows an inverse behavior. In both cases, random flaking and cracks in the boundary area of the holes as well as a formation of debris on the glass surface occur. Such disturbing effects are typical for surface processing when applying long laser pulses in the nanosecond range and are due to the heating-based ablation mechanisms [ger08, rus02]. In addition, no appreciable change in the roundness form error δ of the ablated holes, which was determined by applying the minimum zone circle (MZC) method according to DIN ISO 1101, could be observed. At an average, the ratio of the roundness form errors $\delta_{laser-plasma}/\delta_{laser}$ amounts to 0.97 for N-BaK4 and to 1.05 for SF5.

However, a significant difference in ablation depth was measured using a light microscope Axioskop 2 MAT from Zeiss as shown in figure 6.4.

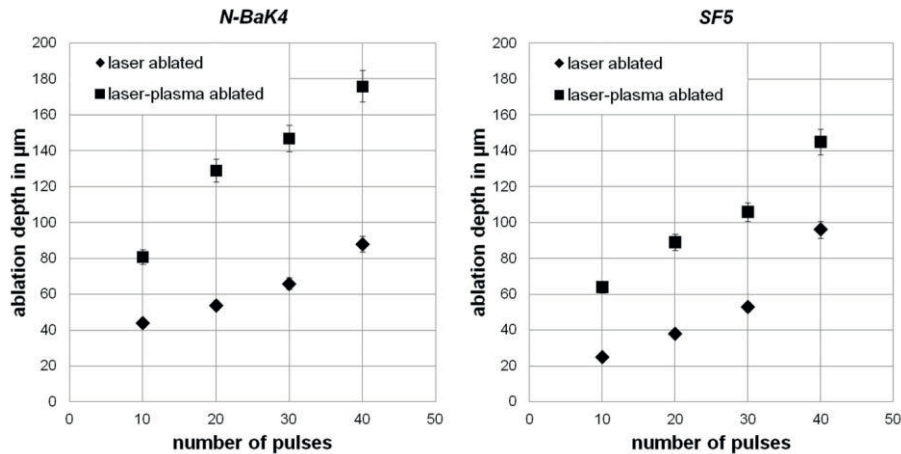


Fig. 6.4: Ablation depth versus number of pulses for N-BaK4 (left) and SF5 (right)

At an average, the ablation depth was increased by a factor of 2.1 for both glasses when applying hybrid laser-plasma ablation. In case of pure laser ablation, the ablation rate (i.e., $4 \mu\text{m}/\text{pulse}$) is comparable to published results for nanosecond ablation of glasses [rud99, ihl92a]. For calculating the ablated volume as shown in figure 6.5, a cylindrical approach was used in the case of N-BaK4, whereas for SF5, a cone-shaped geometry of the ablated holes was assumed. The base areas were calculated from the averaged radius of both circles that are resulting from the MZC-evaluation.

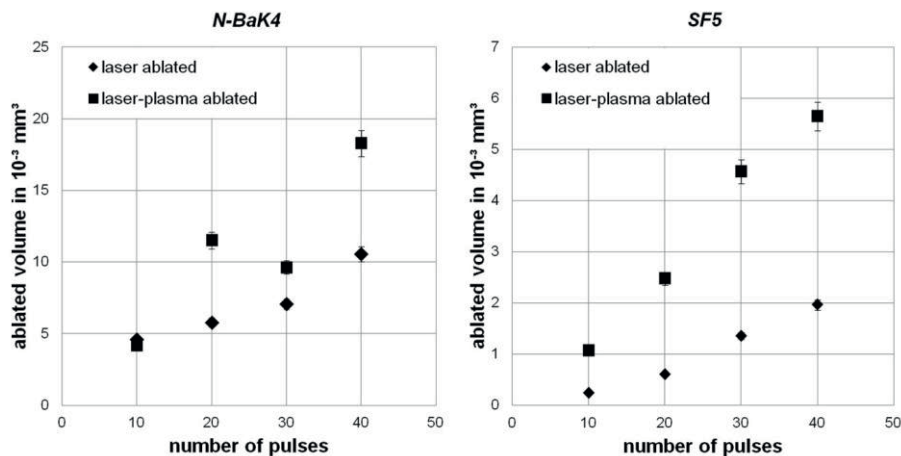


Fig. 6.5: Ablated volume versus number of pulses for N-BaK4 (left) and SF5 (right)

Generally, both the ablation depth and the ablated volume of N-BaK4 is higher in comparison to SF5. The depth-dependent amount of specific energy E , which is applied to a transparent medium, is given by both the reflectivity and the absorption according to the Beer-Lambert law. Based on the particular data for the investigated glasses [sch11], the ratio E_{SF5}/E_{N-BaK4} per ablated volume can be determined to amount to 1.8.

Further, the thermal loss mechanisms of the investigated glasses are represented by the particular thermal diffusivity α which is given by the quotient of the thermal conductivity k and the product of both the density ρ and the specific heat capacity c_p . For solid N-BaK4 and SF5, the proportionality factor $\alpha_{SF5}/\alpha_{N-BaK4}$ amounts to approximately 0.8. This implies that the applied laser energy does not fully contribute to the ablation process which could be explained by different amounts of attenuation of the incoming laser beam by the emerging debris cloud.



In comparison to pure laser ablation, the amount of ablated volume is increased by an average factor of 1.5 for N-BaK4 and 3.7 for SF5 in the case of laser-plasma ablation. This increase in ablated volume could be explained by de-excitation and related energy transfer of excited Ar and metastable Ar species, respectively. Regarding the generation of metastable Ar atoms (Ar^m), electron excitation in the bulk plasma and ion-impact excitation in the sheath region play a significant role for the population of the $^3\text{P}_2$ and $^3\text{P}_0$ metastable levels of Ar at 11.55 and 11.72 eV above the ground state [bag05]. Thus, the highest production rate of Ar^m is found at high electron densities, i.e., during the ignition of each plasma filament. Additionally, the Ar^m production is possible as a result of resonant neutralisation, where Ar^+ ions recombine with the negative surface charge on the dielectric substrate and form an Ar^m [nie12]. Due to the direct ignition on the substrate surface, a considerable Ar^m density can be assumed to exist in the near-surface area.

A dominant loss mechanism for Ar^m species at high pressures is the electron quenching, which is a collisional transfer of Ar from metastable to nearby radiative levels. Other loss processes under high pressure are given by two- and three-body collisions with Ar atoms [bel09]. Also, energy deposition due to Ar^m is possible by *Penning* ionization at the walls. However, the diffusion of Ar^m out of the plasma region (or to walls) can be considered to be negligible since in comparison to the Ar^m lifetime, diffusion is a slow process. Loss processes involving charge carriers occur only during the lifetime of the plasma which can be assumed to amount to a maximum of several tens of nanoseconds for each filament in the case of barrier discharges. In general, this leads to an additional energy deposition within the discharge gap and hence, close to the substrate. Since in the presented work, both the plasma and laser source were not synchronized, the residual Ar^m in between two plasma discharge events play the significant role in combination with the laser-induced plasma on the substrate surface. Laser-induced plasmas feature high gas temperature and thus, high collision frequency among heavy particles. In this context, two- and three-body de-excitation processes gain importance since the produced debris cloud features distinctive conditions for such collisions and the related de-excitation of Ar^m and energy deposition in the near-surface region.

Further, the above-described etching effect which was observed by the Ar plasma beam itself could contribute further material removal to the ablation process. However, this contribution can be expected to be rather small due to the marginal time frame for plasma etching between two laser pulses.

In addition to silicon dioxide (SiO_2), the main compounds of the investigated glasses are barium oxide (BaO) and zinc oxide (ZnO) for barite crown glasses and lead(II) oxide (PbO) for heavy flint glasses. Here, lead(II) oxide is the weakest of the involved compounds as shown by the comparison of the particular binding energies E_b in table 6.3.

Table 6.3: Binding energy E_b of main compounds of investigated glasses, calculated from standard enthalpies of formation ΔH_f^θ [mas83]

Compound	SiO_2	BaO	ZnO	PbO
E_b in eV	8.9	5.9	3.6	2.3



Conclusions

The atmospheric pressure Ar plasma treatment allows a significant surface smoothing and a simultaneous increase in both the strength and the surface energy of the investigated glass surfaces. Thus, it seems to be interesting for a finishing process of glasses in order to achieve higher stability. Such investigations will be done in further work. Even though no improvements in terms of form error, cracks, and debris were detected, both the ablation depth and the ablated volume were increased significantly with respect to pure laser ablation by introducing the presented hybrid laser-plasma ablation method. Thus, the presented plasma source features a cost-efficient and economic device in order to achieve higher ablation rates or reducing the laser energy required for a defined amount of ablation.

Discussion

As shown by the results presented in the articles embedded in chapter 5, sequential plasma-assisted ablation (seqPAA) allows enhanced laser ablation in terms of both energy requirement and machining results. These improvements are due to the plasma-induced modifications of the glass surfaces as presented in section 4.1, where the main mechanism is the increased absorption for the particular laser wavelength. Based on this effect, the required ablation threshold fluence is reduced. As a result, both the form error and the surface roughness of the ablated area are reduced since lower fluences imply a lower thermal impact on the glass surface, mitigating or even avoiding melting and the formation of laser-induced shock waves. The observed mitigation of debris can also be explained by an enhanced coupling of incoming laser irradiation and an accompanying (nearly) total vaporisation of the ablated volume instead of partial melting and ejection as in the case of pure laser ablation.

In comparison to other (hybrid) ablation techniques, the presented seqPAA method features a competitive and even higher ablation rate as listed in table 7.1. Since for LIPAA, LIBWE, LESAL and LIBDE (compare section 2.2) ablation is performed at the glass rear side, the particular values for sequential plasma-assisted rear side ablation are exclusively considered.

Table 7.1: Comparison of particular ablation rates of fused silica obtained by different ablation methods (rear side ablation) at an applied laser fluence of 1.3 J/cm²

method	absorbing medium	ablation rate in nm/pulse	reference
fs-ablation	none	65	[ute11]
LIPAA	tin (Sn)	60	[hop10]
LIBWE	tin (Sn)	150	[hop10]
LESAL	dichlorobenzene (C ₆ H ₄ Cl ₂)	1	[böh06b]
LIBDE-1	tin (Sn)	80	[hop10]
LIBDE-2	silicon monoxide (SiO)	150	[ihl08]
seqPAA	silicon suboxide (SiO_x), implanted hydrogen (H)	175	[brü12]

In comparison to pure laser ablation without any plasma pre-treatment, the ablation rate is notably increased by seqPAA on fused silica (factor 1.5 at 193 nm and 2.6 at 266 nm). This is also explained by the above-mentioned increase in absorption and the improved coupling of laser irradiation.

One has to consider that in the case of seqPAA on heavy flint glass, the plasma pre-treatment effected a comparatively low increase in absorption. However, a significant reduction of flaking around the ablation spots and an accompanying decrease in form error was achieved for this multi-component glass. This behaviour, i.e. a slight increase in absorption but a significant reduction in form error, was also observed in supplement-



tary, previously unreleased experiments where seqPAA was performed on photovoltaic cover glass, consisting of the network former SiO_2 (72.2 ma%) and, beyond this, different alkali oxides and divalent oxides. The low impact of the plasma pre-treatment on the absorption characteristics of such multi-component glasses can be explained by its dense network. In comparison to the “hollowed-out” silicon dioxide tetrahedrons of the fused silica network, the multi-component glass network generally offers less free space for the implantation of hydrogen.

Even though seqPAA allows improved laser machining results and an economisation of laser energy, a relative long-term plasma pre-treatment is necessary. This circumstance impedes an implementation of this method in industrial scale, at least for the production of bulk articles. Against this background, the process time can be shortened when employing simultaneous plasma-assisted laser ablation (simPAA).

Beside such economy of time, the main advantage of simPAA is the considerable increase in ablation rate as presented in chapter 6. The most probable underlying mechanism of this increase is the de-excitation of argon metastables due to collisions at laser-induced debris particles close to the glass surface. This assumption is confirmed by the fact that during simPAA, no mentionable plasma-induced change in ablation threshold was observed. This indicates the importance of the laser-induced debris cloud, emerging after the first laser shot, to the simPAA method. Since that plasma-physical mechanism is almost independent of the glass composition, an increased ablation rate was observed for all investigated glasses as shown in figure 7.1.

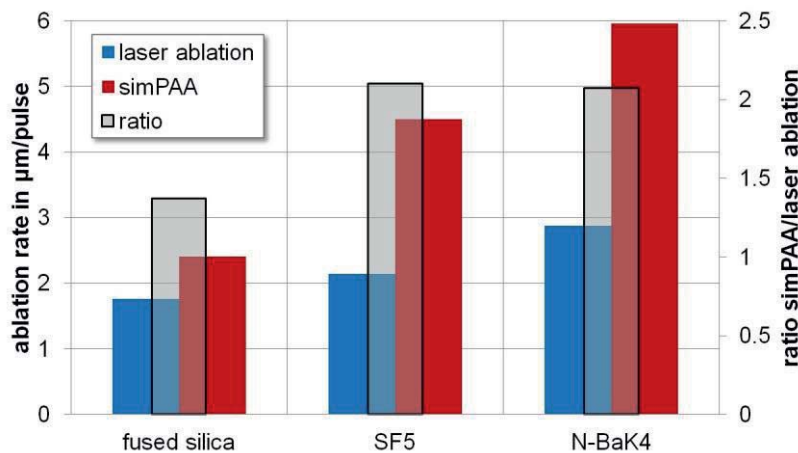


Fig. 7.1: Comparison of the ablation rates for fused silica, SF5, and N-BaK4, resulting from pure laser ablation and simPAA, including ratio

The material-independency was also confirmed by further work, where simPAA was performed on aluminium (AlMgSi 0.5) [ger12d] and aluminium oxide ceramic (Al_2O_3) [ger13d]. In all cases, the ablation rate was notably increased.

In addition to the observed increase in ablation rate and improvements of the machining quality, both presented atmospheric pressure plasma-assisted laser ablation methods allow a considerable economisation of laser energy. This was shown by the 4.6-fold reduction in ablation threshold in case of seqPAA and the doubling of the ablation rate during simPAA. From an energetic point of view, one has to consider the particular system effectiveness additionally: Typically, laser sources have a poor degree of efficiency, i.e. approx. 1% for excimer lasers and about 3-5% in the case of flash lamp-



pumped solid state (e.g. Nd:YAG) lasers. In contrast, dielectric barrier discharge-based atmospheric pressure plasma sources feature an effectiveness of approx. 50-70%, depending on the particular setup. Thus, two most outstanding advantages of DBD-APP-assisted laser ablation processes in terms of energetic considerations can be stated:

- The additional energy provided by the plasma is produced with much higher (at least 10-fold) efficiency than laser energy, in total resulting in lower costs and lower energy consumption.
- The advantageous effects arising from the sequentially or simultaneously applied plasmas allow suspending limitations of classical laser ablation processes. For achieving high ablation rates or ablation in the first place, the required laser energy is not arbitrarily upscalable. Especially in the case of glasses, high laser fluences cause thermally-induced disturbing effects (e.g. roughening, micro cracks, debris, and melt) on the substrate. As shown in the present work, such effects are mitigated or even avoided by the used assisting low-temperature plasmas.

To summarise it can be stated that the combination of both atmospheric pressure plasmas and laser irradiation represents a powerful and versatile tool for micro structuring of optical glasses. Based on the results discussed in the present work, further work on plasma-assisted laser ablation will be carried out in the near future as suggested in the following chapter.





Summary and Outlook

In the present work, two different approaches for atmospheric pressure plasma-assisted laser ablation of optical glasses were investigated. These approaches have notable potential and relevance for the development of novel techniques for the manufacture and improvement of micro optical components and systems.

In terms of sequential plasma-assisted ablation, it was shown that a plasma pre-treatment using a hydrogenous process gas results in a significant modification of the optical properties of the investigated glasses, i.e. the reflexion, the dispersion characteristics and the absorption. As ascertained by UV/VIS spectroscopic measurements, the last parameter was mainly increased in the near UV-wavelength range. This increase in absorption can be explained by plasma-chemically-induced modifications of the glass network. Beside the temporary formation of a near-surface suboxidial layer, the implantation of hydrogen into deeper regions of the glass bulk material turns out to be crucial for the observed modifications in optical properties. Further, a certain surface roughening and cleaning was resulting from the plasma pre-treatment. As a consequence of these plasma-induced effects, subsequent laser ablation of optical glasses was considerably enhanced. In addition to a reduction of the required energy threshold for ablation, the machining results were improved. Further, the ablation rate was increased with respect to pure laser ablation. In comparison to other conventional and hybrid laser ablation techniques, the ablation rate was in the same order of magnitude or even higher.

As regards simultaneous plasma-assisted laser ablation, a significant increase in ablation rate was achieved. This effect is based on plasma-physical mechanisms, i.e. most likely the de-excitation of metastable species at collision partners within the debris cloud during the ablation process. It was further shown that the plasma, which was applied for this method, allows a certain material removal and more precisely the smoothing of roughness peaks.

Given these results, continuing investigations on hybrid atmospheric pressure plasma-assisted ablation methods are to be performed. As a consequence of the numerous parameters involved in these methods, a multitude of possible topics can be defined. As an example, the impact of both the laser wavelength and pulse duration on sequential and simultaneous plasma-assisted ablation should be investigated in more detail. Regarding the used plasma, the influence of different discharge modes, working distances and process gases needs to be examined continuatively. The synchronisation of the laser and plasma pulse trains during simultaneous plasma-assisted ablation is furthermore of essential interest. Besides these topics, the underlying plasma-induced modification mechanisms and effects as well as different plasma-assisted hybrid ablation methods should be investigated for other materials of high technical relevance such as technical glasses, semiconductors and plastics.



Where optical glasses are concerned, the presented methods could be combined in order to provide an integrated plasma-assisted ablation and surface finishing process by benefiting from the reported effects. Such a possible process is schematically suggested in figure 8.1.

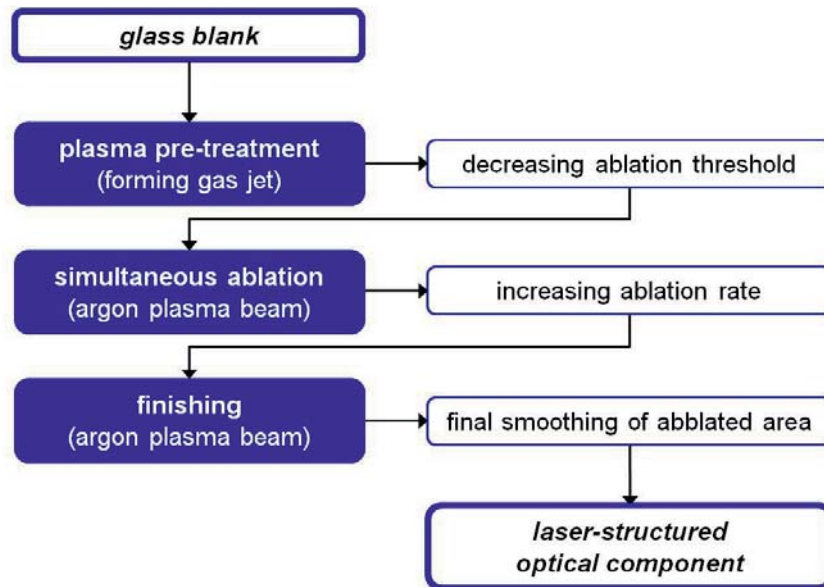


Fig. 8.1: Process chain of a possible integrated plasma-assisted ablation process, composed of the particular methods presented in this work

In addition to laser ablation of optical glasses, the observed plasma-induced phenomena could be applied for the finishing of optical surfaces, manufactured by classical production techniques. Against this background, the observed surface cleaning as a result of the plasma pre-treatment using forming gas is of great interest for a number of different applications. As an example, the laser-induced damage threshold (LIDT) is directly related to surface-adherent organic contaminations. By further development of a plasma cleaning process, the LIDT of high-energy laser optics could be increased. Further, the surface smoothing achieved by direct plasma treatment using argon as process gas turns out to be suitable for the finishing of high-quality UV optics. The combination of both techniques features a high technical relevance and is thus to be investigated in ongoing work.





References

References are given in alphabetic/chronological order, *indicates publications originating from the present work.

- [aka06] T. Akashi, Y. Yoshimura: Deep reactive ion etching of borosilicate glass using an anodically bonded silicon wafer as an etching mask, *Journal of Micromechanics and Microengineering* **16** (2006) 1051-1056
- [all81] W. Allison, J.W. Sheldon, E.E. Muschlitz: Collisional de-excitation of rare-gas metastable atoms Ar, Kr, Xe by molecular hydrogen and deuterium, *Journal of Physics B* **14** (1981) 4587-4594
- [als02] A. I. Al-Shamma'a, S. R. Wylie, J. Lucas, J. D. Yan: Atmospheric microwave plasma jet for material processing, *IEEE Transactions on Plasma Science* **30** (2002) 1863-1871
- [ard38] M. V. Ardenne: Das Elektronen-Rastermikroskop, *Zeitschrift für Physik* **109** (1938) 553-572
- [arn10] T. Arnold, G. Boehm, I.-M. Eichentopf, M. Janietz, J. Meister, A. Schindler: Plasma Jet Machining - A novel technology for precision machining of optical elements, *Vakuum in Forschung und Praxis* **22** (2010) 10-16
- [arn12] T. Arnold, G. Böhm: Application of atmospheric plasma jet machining (PJM) for effective surface figuring of SiC, *Precision Engineering* **36** (2012) 546-553
- [atk92] R. M. Atkins and P. J. Lemaire: Effects of elevated temperature hydrogen exposure on short-wavelength optical losses and defect concentrations in germanosilicate optical fibers, *Journal of Applied Physics* **72** (1992) 344-348
- [bag05] N. Bagger, A. Bogaerts, Z. Donko, R. Gijbels, N. Sadeghi: Study of the Ar metastable atom population in a hollow cathode discharge by means of a hybrid model and spectrometric measurements, *Journal of Applied Physics* **97** (2005) 123305 (12p)
- [bar05] A. Barranco, F. Yubero, J. P. Espinós, P. Groening, A. R. González-Elipé: Electronic state characterization of SiO_x thin films prepared by evaporation, *Journal of Applied Physics* **97** (2005) 113714 (8p)
- [beh97] G. Behrmann, M. Duignan: Excimer laser micromachining for rapid fabrication of diffractive optical elements, *Applied Optics* **36** (1997) 4666-4674
- [bel08] A. Belkind, S. Gershman: Plasma cleaning of surfaces, *Vacuum Technology and Coating* **11** (2008) 46-57
- [bel09] S. G. Belostotskiy, V. M. Donnelly, D. J. Economou, N. Sadeghi: Spatially resolved measurements of argon metastable (1s₅) density in a high pressure microdischarge using diode laser absorption spectroscopy, *IEEE Transactions on Plasma Science* **37** (2009) 852-858
- [bel12] M. Bellmann, C. Gerhard, C. Haese, S. Wieneke, W. Viöl: DBD plasma improved spot repair of automotive polymer surfaces, *Surface Engineering* **28** (2012) 754-758
- [ben61] H. E. Bennett, J. O. Porteus: Relation between surface roughness and specular reflectance at normal incidence, *Journal of the Optical Society of America* **51** (1961) 123-129
- [ben73] A. Benninghoven: Surface investigation of solids by the statical method of secondary ion mass spectroscopy (SIMS), *Surface Science* **35** (1973) 427-457
- [ben94] A. Benninghoven: Surface analysis by Secondary Ion Mass Spectrometry (SIMS), *Surface Science* **299-300** (1994) 246-260
- [ben04] M. Bente, G. Avramidis, S. Förster, E. G. Rohwer, W. Viöl: Wood surface modification in dielectric barrier discharges at atmospheric pressure for creating water repellent characteristics, *Holz als Roh- und Werkstoff* **62** (2004) 157-163



- [bie13] T. Bieber, X. Glad, L. de Poucques, R. Hugon, J.-L. Vasseur, J. Bougdira: Argon ion and neutral metastable levels destruction in a magnetically enhanced inductively coupled plasma reactor, *The Open Plasma Physics Journal* **6** (2013) 32-43
- [bin86] G. Binnig, C.F. Quate: Atomic force microscope, *Physical Review Letters* **56** (1986) 930-933
- [bli08] J. Bliedner, G. Gräfe: *Optiktechnologie*, 1st edition (2008), Carl Hanser Verlag, München
- [boh02] Böhme R., Braun A. and Zimmer K. Backside etching of UV-transparent materials at the interface to liquids, *Applied Surface Science* **186** (2002) 276-281
- [boh04] R. Böhme, K. Zimmer: Low roughness laser etching of fused silica using an adsorbed layer, *Applied Surface Science* **239** (2004) 109-116
- [boh06a] R. Böhme, K. Zimmer, B. Rauschenbach: Laser backside etching of fused silica due to carbon layer ablation, *Applied Physics A* **82** (2006) 325-328
- [boh06b] R. Böhme, K. Zimmer, D. Ruthe, B. Rauschenbach: Backside etching at the interface to diluted medium with nanometer etch rates, *Journal of Laser Micro/Nanoengineering* **1** (2006) 190-194
- [bok80] Z. Boksay, G. Bouquet: The pH dependence and an electrochemical interpretation of the dissolution rate of a silicate glass network, *Physics and Chemistry of Glasses* **21** (1980) 110-113
- [bol83] Y. Boliang, D.H. Ryan, J. M. D. Coey, Z. Altounian, J. O. Ström-Olsen, F. Razavi: Hydrogen-induced change in magnetic structure of the metallic glass Fe₈₉Zr₁₁, *Journal of Physics F* **13** (1983) L217-L222
- [bou29] P. Bouguer: *Essai d'optique, sur la gradation de la lumière*, 1st edition (1729), Claude Jombert, Paris
- [brü11] S. Brückner, S. Rösner, C. Gerhard, S. Wieneke, W. Viöl: Plasma-based ionisation spectroscopy for material analysis, *Materials Testing* **53** (2011) 639-642
- [brü12]* S. Brückner, J. Hoffmeister, J. Ihlemann, C. Gerhard, S. Wieneke, W. Viöl: Hybrid laser-plasma micro-structuring of fused silica based on surface reduction by a low-temperature atmospheric pressure plasma, *Journal of Laser Micro/Nanoengineering* **7** (2012) 73-76
- [buc08] A. Buček, T. Homola, M. Aranyosiová, D. Velič, T. Plecenik, J. Havel, P. Šťáhel, A. Zahoranová: Atmospheric pressure nonequilibrium plasma treatment of glass surface, *Chemické Listy* **102** (2008) S1459-S1462
- [bue90] C. Buerhop, B. Blumenthal, R. Weissmann: Glass surface treatment with excimer and CO₂ lasers, *Applied Surface Science* **46** (1990) 430-434
- [cer09] M. Černák, L. Černáková, I. Hudec, D. Kováčik, A. Zahoranová: Diffuse coplanar surface barrier discharge and its applications for in-line processing of low-added-value materials, *The European Physical Journal - Applied Physics* **47** (2009) 1-6
- [cha58a] R. J. Charles: Static Fatigue of Glass I, *Journal of Applied Physics* **29** (1958) 1549-1553
- [cha58b] R. J. Charles: Static Fatigue of Glass II, *Journal of Applied Physics* **29** (1958) 1554-1560
- [che05] J. Cheng, M. Yen, C. Wei, Y. Chuang, T. Young: Crack-free direct-writing on glass using a low-power UV laser in the manufacture of a microfluidic chip, *Journal of Micromechanics and Microengineering* **15** (2005) 1147-1156
- [che10] S. Cheruthazhekatt, M. Černák, P. Slaviček, J. Havel: Gas plasmas and plasma modified materials in medicine, *Journal of Applied Biomedicine* **8** (2010) 55-66
- [cob79] J. W. Coburn, H. F. Winters: Ion- and electron-assisted gas-surface chemistry - An important effect in plasma etching, *Journal of Applied Physics* **50** (1979) 3189-3196
- [coo90] L. M. Cook: Chemical processes in glass polishing, *Journal of Non-Crystalline Solids* **120** (1990) 152-171

- [dah12] S. Dahle, R. Gustus, W. Viöl, W. Maus-Friedrichs: DBD plasma treatment of titanium in O₂, N₂ and air, *Plasma Chemistry and Plasma Processing* **32** (2012) 1109-1125
- [din02] X. Ding, Y. Kawaguchi, H. Niino, A. Yabe: Laser-induced high-quality etching of fused silica using a novel aqueous medium, *Applied Physics A* **75** (2002) 641-645
- [dou08] J. Dou, J. Li, P. Herman, J. Aitchison, T. Fricke-Begemann, J. Ihlemann, G. Marowsky: Laser machining of micro-lenses on the end face of single-mode optical fibers, *Applied Physics A* **91** (2008) 591-594
- [ehl11] J. Ehlbeck, U. Schnabel, M. Polak, J. Winter, T. von Woedtke, R. Brandenburg, T. von dem Hagen, K.-D. Weltmann: Low temperature atmospheric pressure plasma sources for microbial decontamination, *Journal of Physics D* **44** (2011) 013002 (18pp)
- [emm13] S. Emmert, F. Brehmer, H. Hänßle, A. Helmke, N. Mertens, R. Ahmed, D. Simon, D. Wandke, W. Maus-Friedrichs, G. Däschlein, M. P. Schön, W. Viöl: Atmospheric pressure plasma in dermatology: Ulcus treatment and much more, *Clinical Plasma Medicine* **1** (2013) 24-29
- [fan06a] C. Fanara, P. Shore, J. R. Nicholls, N. Lyford, J. Kelley, J. Carr, P. Sommer: A new Reactive Atom Plasma Technology (RAPT) for precision machining: the etching of ULE[®] surfaces, *Advanced Engineering Materials* **8** (2006) 933-939
- [fan06b] Z. Fang, X. Qiu, Y. Qiu, E. Kuffel: Dielectric barrier discharge in atmospheric air for glass-surface treatment to enhance hydrophobicity, *IEEE Transactions on Plasma Science* **34** (2006) 1216-1222
- [för05] S. Förster, C. Mohr, W. Viöl: Investigations of an atmospheric pressure plasma jet by optical emission spectroscopy, *Surface and Coatings Technology* **200** (2005) 827-830
- [frü05] J. Frühauf: *Werkstoffe der Mikrotechnik*, 1st edition (2005), Carl Hanser Verlag München
- [gat08] R. R. Gattass, E. Mazur: Femtosecond laser micromachining in transparent materials, *nature photonics* **2** (2008) 219-225
- [ger08] C. Gerhard, F. Druon, P. Blandin, M. Hanna, F. Balembois, P. Georges, F. Falcoz: Efficient versatile-repetition-rate picosecond source for material processing applications, *Applied Optics* **47** (2008) 967-974
- [ger12a]* C. Gerhard, D. Tasche, S. Brückner, S. Wieneke, W. Viöl: Near-surface modification of optical properties of fused silica by low-temperature hydrogenous atmospheric pressure plasma, *Optics Letters* **37** (2012) 566-568
- [ger12b]* C. Gerhard, S. Roux, S. Brückner, S. Wieneke, W. Viöl: Low-temperature atmospheric pressure argon plasma treatment and hybrid laser-plasma ablation of barite crown and heavy flint glass, *Applied Optics* **51** (2012) 3847-3852
- [ger12c]* C. Gerhard, M. Kretschmer, W. Viöl: Plasma meets glass - Plasma-based modification and ablation of optical glasses, *Optik & Photonik* **7** (2012) 35-38
- [ger12d]* C. Gerhard, S. Roux, S. Brückner, S. Wieneke, W. Viöl: Atmospheric pressure argon plasma-assisted enhancement of laser ablation of aluminum, *Applied Physics A* **108** (2012) 107-112
- [ger13a]* C. Gerhard, J. Heine, S. Brückner, S. Wieneke, W. Viöl: A hybrid laser-plasma ablation method for improved nanosecond laser machining of heavy flint glass, *Lasers in Engineering* **24** (2013) 391-403
- [ger13b]* C. Gerhard, T. Weihs, D. Tasche, S. Brückner, S. Wieneke, W. Viöl: Atmospheric pressure plasma treatment of fused silica, related surface and near-surface effects and applications, *Plasma Chemistry and Plasma Processing* **33** (2013) 895-905
- [ger13c]* C. Gerhard, T. Weihs, A. Luca, S. Wieneke, W. Viöl: Polishing of optical media by dielectric barrier discharge inert gas plasma at atmospheric pressure, *Journal of the European Optical Society: Rapid Publications* **8** (2013) 13081 (5pp)
- [ger13d]* C. Gerhard, S. Roux, F. Peters, S. Brückner, S. Wieneke, W. Viöl: Hybrid laser ablation of Al₂O₃ applying simultaneous argon plasma treatment at atmospheric pressure, *Journal of Ceramic Science and Technology* **4** (2013) 19-24



- [gib96] P. Gibbon, E. Forster: Short-pulse laser-plasma interactions, *Plasma Physics and Controlled Fusion* **38** (1996) 769-793
- [gre13] A. Gredner, C. Gerhard, S. Wieneke, K. Schmidt, W. Viöl: Increase in generation of poly-crystalline silicon by atmospheric pressure plasma-assisted excimer laser annealing, *Journal of Materials Science and Engineering B* **3** (2013) 346-351
- [ham82] D. K. Hamilton, T. Wilson: Surface profile measurement using the confocal microscope, *Journal of Applied Physics* **53** (1982) 5320-5322
- [han06] Y. Hanada, K. Sugioka, K. Obata, S. V. Garnov, I. Miyamoto, K. Midorikawa: Transient electron excitation in laser-induced plasma-assisted ablation of transparent materials, *Journal of Applied Physics* **99** (2006) 043301 (6p)
- [hel09] A. Helmke, D. Hoffmeister, N. Mertens, S. Emmert, J. Schuette, W. Viöl: The acidification of lipid film surfaces by non-thermal DBD at atmospheric pressure in air, *New Journal of Physics* **11** (2009) 115025 (11pp)
- [her10] Heraeus Quarzglas GmbH & Co. KG: *Spectrosil®2000*, data sheet (2010)
- [her11] Heraeus Quarzglas GmbH & Co. KG: *Quarzglas für die Optik - Daten und Eigenschaften*, data sheet (2011)
- [hic60] T. W. Hickmott: Interaction of Atomic Hydrogen with Glass, *Journal of Applied Physics* **31** (1960) 128-136
- [hof12]* J. Hoffmeister, C. Gerhard, S. Brückner, J. Ihlemann, S. Wieneke, W. Viöl: Laser microstructuring of fused silica subsequent to plasma-induced silicon suboxide generation and hydrogen implantation, *Physics Procedia* **39** (2012) 613-620
- [hom13] T. Homola, J. Matoušek, M. Kormunda, L. Y. L. Wu, M. Černák: Plasma treatment of glass surfaces using diffuse coplanar surface barrier discharge in ambient air, *Plasma Chemistry and Plasma Processing* **33** (2013) 881-894
- [hon06] S. M. Hong, S. H. Kim, J. H. Kim, H. I. Hwang: Hydrophilic surface modification of PDMS using atmospheric RF plasma, *Journal of Physics: Conference Series* **34** (2006) 656-661
- [hop06] B. Hopp, C. Vass, T. Smausz, Z. Bor: Production of submicrometre fused silica gratings using laser-induced backside dry etching technique, *Journal of Physics D* **39** (2006) 4843-4847
- [hop07] B. Hopp, T. Smausz, M. Bereznai: Processing of transparent materials using visible nanosecond laser pulses, *Applied Physics A* **87** (2007) 77-79
- [hop08] B. Hopp, T. Smausz, T. Csizmadia, J. Budai, A. Oszkó, G. Szabó: Laser-induced backside dry etching: wavelength dependence, *Journal of Physics D* **41** (2008) 175501 (6pp)
- [hop10] B. Hopp, T. Smausz, T. Csizmadia, C. Vass, T. Csákó, G. Szabó: Comparative study of different indirect laser-based methods developed for microprocessing of transparent materials, *Journal of Laser Micro/Nanoengineering* **5** (2010) 80-85
- [hua07] Z. Q. Huang, M. H. Hong, K. S. Tiaw, Q. Y. Lin: Quality glass processing by laser induced backside wet etching, *Journal of Laser Micro/Nanoengineering* **2** (2007) 194-199
- [hüb80] K. Hübner: Chemical bond and related properties of SiO₂ VII: Structure and electronic properties of the SiO_x region of Si-SiO₂ interfaces, *Physica Status Solidi A* **61** (1980) 665-673
- [ihl92a] J. Ihlemann, B. Wolff, P. Simon: Nanosecond and femtosecond excimer laser ablation of fused silica, *Applied Physics A* **54** (1992) 363-368
- [ihl92b] J. Ihlemann: Excimer laser ablation of fused silica, *Applied Surface Science* **54** (1992) 193-200
- [ihl03] J. Ihlemann, S. Müller, S. Puschmann, D. Schäfer, M. Wei, J. Li, P.R. Herman: Fabrication of submicron gratings in fused silica by F₂-laser ablation, *Applied Physics A* **76** (2003) 751-753

- [ihl07] J. Ihlemann, M. Schulz-Ruhtenberg, T. Fricke-Begemann: Micro patterning of fused silica by ArF- and F₂-laser ablation, *Journal of Physics: Conference Series* **59** (2007) 206-209
- [ihl08] J. Ihlemann: Micro patterning of fused silica by laser ablation mediated by solid coating absorption, *Applied Physics A* **93** (2008) 65-68
- [iwa06] M. Iwasaki, M. Ito, T. Uehara, M. Nakamura, M. Hori: Ion attachment mass spectrometry of nonequilibrium atmospheric-pressure pulsed remote plasma for SiO₂ etching, *Journal of Applied Physics* **100** (2006) 093304 (5pp)
- [iwa08a] M. Iwasaki, H. Inui, Y. Matsudaira, H. Kano, N. Yoshida, M. Ito, M. Hori: Nonequilibrium atmospheric pressure plasma with ultrahigh electron density and high performance for glass surface cleaning, *Applied Physics Letters* **92** (2008) 081503 (3p)
- [iwa08b] M. Iwasaki, Y. Matsudaira, K. Takeda, M. Ito, E. Miyamoto, T. Yara, T. Uehara, M. Hori: Roles of oxidizing species in a nonequilibrium atmospheric-pressure pulsed remote O₂/N₂ plasma glass cleaning process, *Journal of Applied Physics* **103** (2008) 023303 (7p)
- [jah10] M. Jahn, J. Richter, R. Weichenhain-Schriever, J. Meinertz, J. Ihlemann: Ablation of silicon suboxide thin layers, *Applied Physics A* **101** (2010) 533-538
- [jeo98] J. Y. Jeong, S. E. Babayan, V. J. Tu, J. Park, I. Henins, R. F. Hicks, G. S. Selwyn: Etching materials with an atmospheric-pressure plasma jet, *Plasma Sources Science and Technology* **7** (1998) 282-285
- [jin10] H. L. Jin, B. Wang, F. H. Zhang: Effect on surface roughness of zerodur material in atmospheric pressure plasma jet processing, *Proceedings of the 5th International Symposium on Advanced Optical Manufacturing and Testing Technologies: Advanced Optical Manufacturing Technologies (SPIE 7655)* (2010) 76552X
- [joh66] I. T. Johansen: Electrical conductivity in evaporated silicon oxide films, *Journal of Applied Physics* **37** (1966) 499-507
- [kae69] D. H. Kaelble: Peel adhesion: influence of surface energies and adhesive rheology, *Journal of Adhesion Science and Technology* **1** (1969) 102-123
- [kaw06] D. Kawamura, A. Takita, Y. Hayasaki, N. Nishida: Method for reducing debris and thermal destruction in femtosecond laser processing by applying transparent coating, *Applied Physics A* **82** (2006) 523-527
- [kim05] Y. Kim, D. Bae, Y. Kim: LCD glass cleaning by atmospheric pressure glow discharge plasma. *Key Engineering Materials* **297-300** (2005) 2351-2355
- [kim11] S. Kim, V. Dao, H. Choi: One atmospheric pressure plasma treatment of FTO glass for improving the efficiency of DSSC, *Proceedings of the 219th Meeting of the Electrochemical Society* (2011) C1
- [kit62] I. I. Kitaigorodskii, D. I. Mendeleev, E. A. Fainberg, L. A. Grechnik: The influence of certain oxides on reduction of lead silicate glasses in hydrogen, *Glass and Ceramics* **19** (1962) 645-647
- [kle06] J.-H. Klein-Wiele, J. Békési, P. Simon, J. Ihlemann: Fabrication of SiO₂ phase gratings by UV laser patterning of silicon suboxide layers and subsequent oxidation, *Journal of Laser Micro/Nanoengineering* **1** (2006) 211-214
- [kog04] U. Kogelschatz: Atmospheric-pressure plasma technology, *Plasma Physics and Controlled Fusion* **46** (2004) B63-B75
- [kol08] K. Kolari, V. Saarela, S. Franssila: Deep plasma etching of glass for fluidic devices with different mask materials, *Journal of Micromechanics and Microengineering* **18** (2008) 064010 (6pp)
- [lac03] J. M. Lackner, W. Waldhauser, R. Ebner, W. Lenz, C. Suess, G. Jakopic, G. Leising, H. Hutter: Pulsed laser deposition: a new technique for deposition of amorphous SiO_x thin films, *Surface and Coatings Technology* **163-164** (2003) 300-305
- [lad02] F. Ladieu, P. Martin, S. Guizard: Measuring thermal effects in femtosecond laser-induced breakdown of dielectrics, *Applied Physics Letters* **81** (2002) 957-959



- [lan18] I. Langmuir: The adsorption of gases on plane surfaces of glass, mica and platinum, *Journal of the American Chemical Society* **40** (1918) 1361-1403
- [lan23] I. Langmuir: Positive ion currents from the positive column of mercury arcs, *Science* **58** (1923) 290-291
- [law99] J. Lawrence, L. Li: Wettability characteristics of an Al₂O₃/SiO₂-based ceramic modified with CO₂, Nd:YAG, excimer and high-power diode lasers, *Journal of Physics D* **32** (1999) 1075-1082
- [lee99] P. W. Leech: Reactive ion etching of quartz and silica-based glasses in CF₄/CHF₃ plasmas, *Vacuum* **55** (1999) 191-196
- [lev85] I. M. Levin, V. S. Khotimchenko, G. M. Sochivkin: Concentration of hydrogen and water in fused silica blanks, *Glass and Ceramics* **42** (1985) 359-361
- [li01] X. Li, T. Abe, M. Esashi: Deep reactive ion etching of Pyrex glass using SF₆ plasma, *Sensors and Actuators A* **87** (2001) 139-145
- [li03a] L. Li, T. Abe, M. Esashi: Smooth surface glass etching by deep reactive ion etching with SF₆ and Xe gases, *Journal of Vacuum Science & Technology B* **21** (2003) 2545-2549
- [li03b] X. Li, L. Ling, X. Hua, M. Fukasawa, G.S. Oehrlein: Effects of Ar and O₂ additives on SiO₂ etching in C₄F₈-based plasmas, *Journal of Vacuum Science & Technology A* **21** (2003) 284-293
- [lid91] D. R. Lide (ed.): *CRC Handbook of Chemistry and Physics*, 72nd edition (1991), CRC Press, Boca Raton Ann Arbor Boston
- [lyu00] V. A. Lyubochko, V. V. Malikov, O. G. Parfenov, N. V. Belousova: Reduction of aluminium oxide in a nonequilibrium hydrogen plasma, *Journal of Engineering Physics and Thermophysics* **73** (2000) 568-572
- [mai07] N. Mainusch, C. Pflugfelder, J. Ihlemann, W. Viöl: Plasma jet coupled with Nd:YAG laser: new approach to surface cleaning: *Plasma Processes and Polymers* **4** (2007) 4, S33-S38
- [mai08] T. Mai: Toward debris-free laser micromachining, *Industrial Laser Solutions* **23** (2008) 16-18
- [man43] T. C. Manley: The Electric Characteristics of the Ozonator Discharge, *Transactions of the Electrochemical Society* **84** (1943) 83-96
- [mar12] M. Marschewski, J. Hirschberg, T. Omairi, O. Höfft, W. Viöl, S. Emmert, W. Maus-Friedrichs: Electron spectroscopic analysis of the human lipid skin barrier: cold atmospheric plasma-induced changes in lipid composition, *Experimental Dermatology* **21** (2012) 921-925
- [mas83] W. Masterton, E. Slowinski, C. Stanitski: *Chemical Principles*, 5th edition (1983), Saunders College Publishing, Philadelphia
- [men06] E. Mendez, K. M. Nowak, H. J. Baker, F. J. Villarreal, D. R. Hall: Localized CO₂ laser damage repair of fused silica optics, *Applied Optics* **45** (2006) 5358-5367
- [nak84] M. Nakamura, Y. Mochizuki, K. Usami, Y. Itoh, T. Nozaki: Infrared absorption spectra and compositions of evaporated silicon oxides (SiO_x), *Solid State Communications* **50** (1984) 1079-1081
- [nie12] B. Niermann, R. Reuter, T. Kuschel, J. Benedikt, M. Böke, J. Winter: Argon metastable dynamics in a filamentary jet micro-discharge at atmospheric pressure, *Plasma Sources Science and Technology* **21** (2012) 034002 (8p)
- [nik05] S. Nikumb, Q. Chen, C. Li, H. Reshef, H. Y. Zheng, H. Qiu, D. Low: Precision glass machining, drilling and profile cutting by short pulse lasers, *Thin Solid Films* **477** (2005) 216-221
- [nog85] K. Noguchi, N. Shibata, N. Uesugi, Y. Negishi : Loss increase for optical fibers exposed to hydrogen atmosphere, *Journal of Lightwave Technology* **3** (1985) 236-243

- [nus97] P. Nussbaum, R. Völkel, H. P. Herzig, M. Eisner, S. Haselbeck: Design, fabrication and testing of microlens arrays for sensors and microsystems, *Pure and Applied Optics* **6** (1997) 617-636
- [oh10] J. S. Oh, J. B. Park, E. Gil, G. Y. Yeom: High-speed etching of SiO₂ using a remote-type pin-to-plate dielectric barrier discharge at atmospheric pressure, *Journal of Physics D: Applied Physics* **43** (2010) 425207 (6pp)
- [owe69] D. K. Owens, R. C. Wendt: Estimation of the surface free energy of polymers, *Journal of Applied Polymer Science* **13** (1969) 1741-1747
- [pae13] H. Paetzelt, G. Böhm, T. Arnold: Plasma jet polishing of rough fused silica surfaces, *Proceedings of euspen 13th International Conference*, (2013) 19-22
- [pal85] E.D. Palik: *Handbook of Optical Constants of Solids*, 1st edition (1985), Academic Press, Boston
- [par05] J. H. Parka, N.-E. Lee, J. Lee, J. S. Park, H. D. Park: Deep dry etching of borosilicate glass using SF₆ and SF₆/Ar inductively coupled plasmas, *Microelectronic Engineering* **82** (2005) 119-128
- [pau80] L. Pauling: The nature of silicon oxygen bonds, *American Mineralogist* **65** (1980) 321-323
- [pau91] A. Paul: *Chemistry of glasses*, 2nd edition (1991), Chapman and Hall, London
- [ped87] L. R. Pederson: Comparison of sodium leaching rates from a Na₂-3SiO₂ glass in H₂O and D₂O, *Physics and Chemistry of Glasses* **28** (1987) 17-21
- [pen27] F. M. Penning: Über Ionisation durch metastabile Atome, *Die Naturwissenschaften* **15** (1927) 818
- [per99] M. D. Perry, B. C. Stuart, P. S. Banks, M. D. Feit, V. Yanovsky, A. M. Rubenchik: Ultrashort-pulse laser machining of dielectric materials, *Journal of Applied Physics* **85** (1999) 6803-6810
- [pfo93] H. Pforte: *Der Optiker - Band 1: Werkstoffe*, 1st edition (1993), Verlag Gehlen, Bad Homburg vor der Höhe
- [phi71] H. R. Philipp: Optical properties of non-crystalline Si, SiO, SiO_x, and SiO₂, *Journal of Physics and Chemistry of Solids* **32** (1971) 1935-1945
- [rai70] R. K. Rains, R. H. Kadlec: The reduction of Al₂O₃ to aluminum in a plasma, *Metallurgical Transactions B* **1** (1970) 1501-1506
- [rud99] P. Rudolph, J. Bonse, J. Krüger, W. Kautek: Femtosecond and nanosecond-pulse laser ablation of bariumaluminumborosilicate glass, *Applied Physics A* **69** (1999) S763-S766
- [rus02] R. E. Russo, X. Mao, J. J. Gonzalez, S. S. Mao: Femtosecond laser ablation ICP-MS, *Journal of Analytical Atomic Spectrometry* **17** (2002) 1072-1075
- [sai05] Y. Saito, H. Hirayama, M. Suzaki, Y. Tsuda: Dry cleaning process of glass substrate surfaces by atmospheric plasma, *Proceedings of the International Conference on Electrical Engineering* (2005) PS3-01, ICEE-F0127
- [sat10] T. Sato, R. Kurosaki, Y. Kawaguchi, A. Narazaki, H. Niino: Fabrication of multiple slanted microstructures on silica glass by laser-induced backside wet etching, *Journal of Laser Micro/Nanoengineering* **5** (2010) 256-262
- [sat11] T. Sato, Y. Kawaguchi, R. Kurosaki, A. Narazaki, W. Watanabe, H. Niino: Laser-induced backside wet etching employing green DPSS laser and liquid metallic absorber, *Journal of Laser Micro/Nanoengineering* **6** (2011) 204-208
- [sch82] L. Schumann, A. Lehmann, H. Sobotta, V. Riede, U. Teschner, K. Hübner: Infrared studies of reactively sputtered SiO_x films in the composition range 0.2 ≤ x ≤ 1.9, *Physica Status Solidi B* **110** (1982) K69-K73
- [sch88] H. Scholze: *Glas - Natur, Struktur und Eigenschaften*. 3rd edition (1988), Springer Verlag, Berlin Heidelberg New York



- [sch05a] A. Schindler, T. Hänsel, F. Frost, G. Böhm, W. Frank, A. Nickel, T. Arnold, R. Schwabe, S. Gürtler, S. Görsch, B. Rauschenbach: Modern methods of highly precise figuring and polishing, *Glass Science and Technology* **78**, Suppl. C (2005) 111
- [sch05b] M. Schulz-Ruhtenberg, J. Ihlemann, J. Heber: Laser patterning of SiO_x-layers for the fabrication of UV diffractive phase elements, *Applied Surface Science* **248** (2005) 190-195
- [sch09] A. Schweikart, A. Fery: Controlled wrinkling as a novel method for the fabrication of patterned surfaces, *Microchimica Acta* **165** (2009) 249-263
- [sch11] Schott AG: *Optical Glass Catalogue*, data sheet (2011)
- [sch14] Schott AG: *Optisches Glas - Eigenschaften*, data sheet (2014)
- [sel01] G. S. Selwyn, H. W. Herrmann, J. Park, I. Henins: Materials processing using an atmospheric pressure, RF-generated plasma source, *Contributions to Plasma Physics* **6** (2001) 610-619
- [sha83] A. L. Shabalov, M. S. Feldman: Optical and dielectric properties of thin SiO_x films of variable composition, *Thin Solid Films* **110** (1983) 215-224
- [sha01] L. Shah, J. Tawney, M. Richardson, K. Richardson: Femtosecond laser deep hole drilling of silicate glasses in air, *Applied Surface Science* **183** (2001) 151-164
- [shu07] E. V. Shun'ko, V. S. Belkin: Cleaning properties of atomic oxygen excited to metastable state 2s²2p⁴(¹S₀), *Journal of Applied Physics* **102** (2007) 083304 (14p)
- [shu12] E. V. Shun'ko, V. S. Belkin: Treatment surfaces with atomic oxygen excited in dielectric barrier discharge plasma of O₂ admixed to N₂, *AIP Advances* **2** (2012) 022157 (24p)
- [sug01] K. Sugioka, K. Midorikawa: Novel technology for laser precision microfabrication of hard materials, *RIKEN Review* **32** (2001) 36-42
- [ten06] C. Tendero, C. Tixier, P. Tristant, J. Desmaison, P. Leprince: Atmospheric pressure plasmas: a review, *Spectrochimica Acta B* **61** (2006) 2-30
- [thö09] T. Thöniss, G. Adams, C. Gerhard: Optical system design - Software tools cover envelope calculations to the final engineering drawings, *Optik & Photonik* **4** (2009) 30-33
- [tso82] S. T. Tso, J. A. Pask: Reaction of fused silica with hydrogen gas, *Journal of the American Ceramic Society* **65** (1982) 457-460
- [ute10] O. Utéza, N. Sanner, B. Chimier, M. Sentis, P. Lassonde, F. Légaré, J. C. Kieffer: Surface ablation of dielectrics with sub-10 fs to 300 fs laser pulses: crater depth and diameter, and efficiency as a function of laser intensity, *Journal of Laser Micro/Nanoengineering* **5** (2010) 238-241
- [ute11] O. Utéza, N. Sanner, B. Chimier, A. Brocas, N. Varkentina, M. Sentis, P. Lassonde, F. Légaré, J. C. Kieffer: Control of material removal of fused silica with single pulses of few optical cycles to sub-picosecond duration, *Applied Physics A* **105** (2011) 131-141
- [vei01] V. Veiko: Laser microshaping: Fundamentals, practical applications, and future prospects, *RIKEN Review* **32** (2001) 11-18
- [viö11] W. Viöl, S. Wieneke, S. Brückner, R. Damm: Hollow funnel-shaped plasma generator, Patent Application WO 2011/095245 (2011)
- [vog65] W. Vogel, K. Gerth, W. Heindorf: Zur Entwicklung der optischen Gläser, *Jenaer Rundschau* 1/1965, 75-76
- [wan99] J. Wang, H. Niino, A. Yabe: One-step microfabrication of fused silica by laser ablation of an organic solution, *Applied Physics A* **68** (1999) 111-113
- [wan06] B. Wang, Q. Zhao, L. Wang, S. Dong: Application of atmospheric pressure plasma in the ultrasmooth polishing of SiC optics, *Materials Science Forum* **532-533** (2006) 504-507
- [yam04] T. Yamamoto, M. Okubo, N. Imai, Y. Mori: Improvement on hydrophilic and hydrophobic properties of glass surface treated by nonthermal plasma induced by silent corona discharge, *Plasma Chemistry and Plasma Processing* **24** (2004) 1-12

- [yao10] Y. X. Yao, B. Wang, J. H. Wang, H. L. Jin, Y. F. Zhang, S. Dong: Chemical machining of Zerodur material with atmospheric pressure plasma jet, *CIRP Annals - Manufacturing Technology* **59** (2010) 337-340
- [yas02] Y. Yasui, H. Niino, Y. Kawaguchi, A. Yabe: Microetching of fused silica by laser ablation of organic solution with XeCl excimer laser, *Applied Surface Science* **186** (2002) 552-555
- [yen06] M.-H. Yen, J.-Y. Cheng, C.-W. Wei, Y.-C. Chuang, T.-H. Young: Rapid cell-patterning and microfluidic chip fabrication by crack-free CO₂ laser ablation on glass, *Journal of Micromechanics and Microengineering* **16** (2006) 1143-1153
- [zha98a] J. Zhang, K. Sugioka, K. Midorikawa: Direct fabrication of microgratings in fused quartz by laser-induced plasma-assisted ablation with a KrF excimer laser, *Optics Letters* **23** (1998) 1486-1488
- [zha98b] J. Zhang, K. Sugioka, K. Midorikawa: Laser-induced plasma-assisted ablation of fused quartz using the fourth harmonic of a Nd⁺:YAG laser, *Applied Physics A* **67** (1998) 545-549
- [zha99a] J. Zhang, K. Sugioka, K. Midorikawa: High-quality and high-efficiency machining of glass materials by laser-induced plasma-assisted ablation using conventional nanosecond UV, visible, and infrared lasers, *Applied Physics A* **69** (1999) S879-S882
- [zha99b] Y.-P. Zhao, G.-C. Wang, T.-M. Lu: Surface-roughness effect on capacitance and leakage current of an insulating film, *Physical Review B* **60** (1999) 9157-9164
- [zha08a] J. Zhang, B. Wang, S. Dong: Application of atmospheric pressure plasma polishing method in machining of silicon ultra-smooth surfaces, *Frontiers of Electrical and Electronic Engineering in China* **3** (2008) 480-487
- [zha08b] J. Zhang, B. Wang, S. Dong: The design of an atmospheric pressure plasma torch used for polishing ultra-smooth surfaces, *Key Engineering Materials* **364-366** (2008) 340-345
- [zim02] K. Zimmer, R. Böhme, A. Braun, B. Rauschenbach, F. Bigl: Excimer laser-induced etching of sub-micron surface relief gratings in fused silica using phase grating projection, *Applied Physics A* **74** (2002) 453-456
- [zim03] K. Zimmer, A. Braun, R. Böhme: Etching of fused silica and glass with excimer laser at 351 nm, *Applied Surface Science* **208-209** (2003) 199-204
- [zim04] K. Zimmer, R. Böhme, B. Rauschenbach: Laser etching of fused silica using an adsorbed toluene layer, *Applied Physics A* **79** (2004) 1883-1885
- [zim06a] K. Zimmer, R. Böhme, B. Rauschenbach: Enhancing the etch rate at backside etching of fused silica, *Journal of Laser Micro/Nanoengineering* **1** (2006) 292-296
- [zim06b] K. Zimmer, R. Böhme, B. Rauschenbach: Laser backside etching of fused silica due to carbon layer ablation, *Applied Physics A* **82** (2006) 325-328
- [zim06c] K. Zimmer, D. Hirsch, F. Bigl: Excimer laser machining for the fabrication of analogous microstructures, *Applied Surface Science* **96-98** (2006) 425-429
- [zim09] K. Zimmer, R. Böhme, C. Vass, B. Hopp: Time-resolved measurements during backside dry etching of fused silica, *Applied Surface Science* **255** (2009) 9617-9621





Table of Symbols and Abbreviations

Symbols and abbreviations are given in alphabetic order. Within the running text, symbols are further specified by prefixes, suffixes and/or sub-/superscripts where required.

<u>symbol</u>	<u>meaning</u>	<u>unit</u>
$2w$	laser beam diameter	m (and subunits)
A	absorption, area	% m ² (and subunits)
α	absorption coefficient, angle, thermal diffusivity	- degrees m ² /s (and subunits)
AOI	angle of incidence	degrees
C	elementary concentration	%
c_p	heat capacity	W/K (and subunits)
\emptyset	diameter	m (and subunits)
d	distance, depth	m (and subunits)
δ	roundness form error	m (and subunits)
ΔH_f^0	standard enthalpy of formation	J/mole (and subunits)
D	diameter	m (and subunits)
ΔT	change in transmission	%
Δt	pulse duration	s (and subunits)
E	energy, modulus of elasticity	J (and subunits) N/m ² (and subunits)
ϵ	permittivity	F/m (and subunits)
F	fluence	J/m ² (and subunits)
f	focal length	m (and subunits)
f_{rep}, f_{pulse}	pulse repetition rate	Hz (and subunits)
γ_s	solid surface energy	J/m ² (and subunits)
h	height	m (and subunits)
HK	<i>Knoop</i> hardness	-
I	intensity	W/cm ² (and subunits)
κ	extinction coefficient	-
k	absorption coefficient, thermal conductivity	- W/mK (and subunits)
l	length	m (and subunits)
λ	wavelength	m (and subunits)
M^2	laser beam quality factor	-
N	complex index of refraction	-
n	index of refraction (real part of N)	-
v_e, v_d	<i>Abbe</i> number	-
P	power, polarity	W (and subunits) -
Φ	fluence	J/cm ² (and subunits)



R	reflexion	%
r	radius, distance	m (and subunits)
Ra	arithmetic mean roughness	m (and subunits)
R_{etch}	etch rate	m/s (and subunits)
ρ	density	kg/m ³ (and subunits)
Rq	root mean squared roughness	m (and subunits)
Rz	peak-to-valley height	m (and subunits)
σ	strength	N/m ² (and subunits)
T	transmission	%
t	duration, thickness	s (and subunits) m (and subunits)
τ	pulse duration	s (and subunits)
T_e	electron temperature	eV
T_{gas}	gas temperature	K
Θ	bond angle	degree (°)
θ	full angle of divergence	mrads
TIS	total integrated scatter	-
$U, u(t)$	voltage	V
w	waviness	m (and subunits)
x	stoichiometry factor O/Si	-
z	thickness	m (and subunits)
z_R	<i>Rayleigh</i> -length	m (and subunits)

abbreviationmeaning

AFM	atomic force microscopy
APP	atmospheric pressure plasma
DBD	dielectric barrier discharge
EDX	energy dispersive X-ray spectroscopy
FTIR	<i>Fourier</i> transform infrared (spectroscopy)
LESAL	laser etching at a surface adsorbed layer
LIBDE	laser-induced backside dry etching
LIBWE	laser-induced backside wet etching
LIDT	laser-induced damage threshold
LIPAA	laser-induced plasma-assisted ablation
MZC	minimum zone circle (method)
NBO	non-bridging oxygen
RATP [®]	reactive atomic plasma technology
RIE	reactive ion etching
RSF	relative sensitivity factor
SEM	scanning electron microscopy
seqPAA	sequential plasma-assisted ablation
simPAA	simultaneous plasma-assisted ablation
SIMS	secondary ion mass spectroscopy
slm	standard litres per minutes
ULE [®]	ultra low expansion (glass)
XPS	X-ray photoelectron spectroscopy







Acknowledgements

My special thank is dedicated to the doctoral advisers and reviewers of the present dissertation, Prof. Dr. Wolfgang Maus-Friedrichs and Prof. Dr. Wolfgang Viöl, for fruitful discussions, advice and for supervising my doctoral project.

I thank my co-workers and co-authors of the articles embedded in the present work Stephan Brückner, Jörn Heine, Jennifer Hoffmeister, Dr. Jürgen Ihlemann, Dr. Alfonz Luca, Sophie Roux, Daniel Tasche, Tobias Weihs, Prof. Dr. Stephan Wieneke and Prof. Dr. Wolfgang Viöl for our successful teamwork.

I further thank Augusto Cardenas, Benedikt Ernst, René Gustus, Marcus Kretschmer, Gesa Pähler, Marc Sailer, Kirsten Schiffmann, Rika Unkelbach and Hendrik von Hörsten for their help during the experiments and measurements.

Many thanks also to my colleagues and friends Dr. Geoffrey Adams, Georg Avramidis, Dr. Benjamin Bahr, Dr. Pierre Blandin, Stephan Brückner, Dr. Frédéric Druon, Dr. Patrick Georges, Edgar Roddewig and Prof. Dr. Stephan Wieneke for their help and for fruitful discussion.

The support by the European Regional Development Funds (EFRE) and the Workgroup Innovative Projects of Lower Saxony (AGiP) in the frame of the Lower Saxony Innovation Network for Plasma Technology (NIP), project funding reference number W2-80029388, is gratefully acknowledged.

I particularly thank my companion Martina Lüders for her patience and sympathy during the preparation of the present dissertation and our son Benjamin for brightening up daily grind.





Appendix

A - Curriculum Vitae of the Author

Christoph GERHARD, M.Sc. Dipl.-Ing. (FH), born on the 18th of June 1977 in Lich

Work Experience

- since 01/2013: Scientific Coordinator, *Hochschule für angewandte Wissenschaft und Kunst*, Göttingen
- since 07/2012: Research Associate, *Fraunhofer Anwendungszentrum für Plasma und Photonik*, Göttingen
- 10/2010-12/2012: Research Associate, *Niedersächsischer Innovationsverbund Plasmatechnik*, alternating employment at:
- *Technische Universität Clausthal*, Clausthal-Zellerfeld (10/2011-12/2012)
 - *Hochschule für angewandte Wissenschaft und Kunst*, Göttingen (4/2011-9/2011)
 - *Laser Laboratorium Göttingen e.V.*, Göttingen (10/2010-3/2011)
- 7/2009-9/2010: Technical Staff Member and Research Associate, *Bremer Institut für angewandte Strahltechnik GmbH*, Bremen
- 10/2006-6/2009: Product Manager for Optics, *Linos Photonics GmbH & Co. KG*, Göttingen
- 3/2006-8/2006: Graduant, *Laboratoire Charles Fabry de l'Institut d'Optique*, Orsay/France
- 7/2000-8/2002: Skilled Labour/Training Officer, *Linos Photonics GmbH*, Gießen

Education

- 10/2010-9/2014: PhD Studies (Physical Technologies), *Technische Universität Clausthal*, Clausthal-Zellerfeld
- 9/2008-3/2010: Master Studies (Optical Engineering/Photonics), *Hochschule für Angewandte Wissenschaft und Kunst*, Göttingen
- 9/2002-9/2006: Diploma Studies (Precision Manufacturing Technology), *Hochschule für angewandte Wissenschaft und Kunst*, Göttingen
- 8/1998-6/2000: Apprenticeship (Precision Optician), *Feinoptische Fabrik Karl-Heinz Kratz*, Mücke
- 1997: University-Entrance Diploma, *Laubach-Kolleg*, Laubach

Honours

- 2009: Georg-Simon-Ohm-Award (*Deutsche Physikalische Gesellschaft*)



B - Statutory Declarations (*Eidesstattliche Erklärungen*)

Hiermit erkläre ich an Eides Statt, dass ich die bei der Fakultät für Natur-und Materialwissenschaften der Technischen Universität Clausthal eingereichte Dissertation selbstständig und ohne unerlaubte Hilfe verfasst und die benutzten Hilfsmittel vollständig angegeben habe.

Hiermit erkläre ich an Eides Statt, dass die eingereichte Dissertation weder in Teilen noch in Ihrer Gesamtheit einer anderen Hochschule zur Begutachtung vorliegt oder vorgelegen hat und dass ich bisher noch keinen Promotionsversuch unternommen habe.

C. Gerhard



